Summary Report

on

Evaluation of Fabrication Related Indications in Reactor Upper Head Penetrations

to

U.S. Nuclear Regulatory Commission
Washington, DC

by

F. W. Brust, T. Zhang, D. J. Shim, and G. Wilkowski
Engineering Mechanics Corporation of Columbus
3518 Riverside Drive
Suite 202
Columbus, OH 43221

David L. Rudland
Office of Nuclear Regulatory Research
U.S. Nuclear Regulatory Commission

March 24, 2011

Table of Contents

List of Figures

1. Background and Overview

In February and April 2001, the occurrence of circumferential cracks above the J-weld in control-rod- drive-mechanism (CRDM) nozzles at operating nuclear power plants raised a significant safety concern in the nuclear power industry. In some instances, cracks up to 165-degrees of the circumference of the weld were found even though there was very little leakage at the top of the reactor pressure vessel (RPV) head. This cracking occurrence led to the issuance of US Nuclear Regulatory Commission (NRC) Bulletin 2001-01 requesting that the industry supply additional information regarding these indications in order to assess the significance of the cracking problem in CRDM nozzles. This NRC request resulted in many of these utilities choosing to inspect their RPV heads for signs of leakage. The immediate key question of concern for the industry was that if leakage was detected, how long the plant could operate until an insufficient margin against failure was reached. These actions helped plants plan detailed volumetric inspections, and initiate repairs or replacements of whole RPV heads. Upper head replacements by utilities has begun and is well underway with at least 36 of the 69 US Pressurized Water Reactor (PWR) pressure vessel upper heads being replaced using Alloy 52/152 materials for their penetration nozzle J-groove welds by the end of 2009. Analyses were conducted on the remaining RPV heads estimated to be further away from failure than RPV heads of immediate concern to determine failure probabilities, i.e., how much time exists from crack initiation to leakage, as well as from leakage to failure.

In July of 2001, the NRC organized an independent panel on CRDM cracking to review the NRC's CRDM efforts. Numerous meetings were held with industry and the Advisory Committee on Reactor Safeguards (ACRS) since that time. From discussions at these meetings and reviews of the industry efforts underway, it became apparent that some technical aspects related to solving this problem were either unknown or unclear. As more information became available because of these meetings and industry reviews, the complexity of this problem became better understood. This report extends the work that has been performed at Engineering Mechanics Corporation of Columbus (Emc^2) since 2001. The main focus of the current work was to assess the impact on CRDM operations of the indications observed in replacement heads fabricated with A52/152 weld metal. Essentially, the research focused on whether such indications could lead to reduced lifetimes in the RPV head assembly.

In PWR pressure vessels, the reactor pressure vessel head contains numerous penetrations so that control-rod-drive mechanism nozzles can be inserted to allow control rods to move up-and-down as needed for reactor operation (Figure 1-1.) The holes through the head permit the reactor pressure vessel control-rod-drive-mechanism (CRDM) nozzles or control-element-drive-mechanism (CEDM) nozzles to be inserted through the head. As shown in Figure 1-2, the nozzle consists of an Alloy 600 pipe (or tube) that goes through the head and has a partial penetration weld to the vessel at the ID surface of the head. This weld is referred to as the J-weld and the weld material at the time of plant construction (circa 1960's and 1970's) was Alloy 82/182. Alloy 600 and Alloy 82/182 were originally chosen for their excellent resistance to general corrosion and because their coefficients of thermal expansion closely matched that of the RPV head low alloy steel (either A508 or A533 steel). The nozzle tube typically has a 101.6 mm outside diameter with a thickness of 15.875 mm.

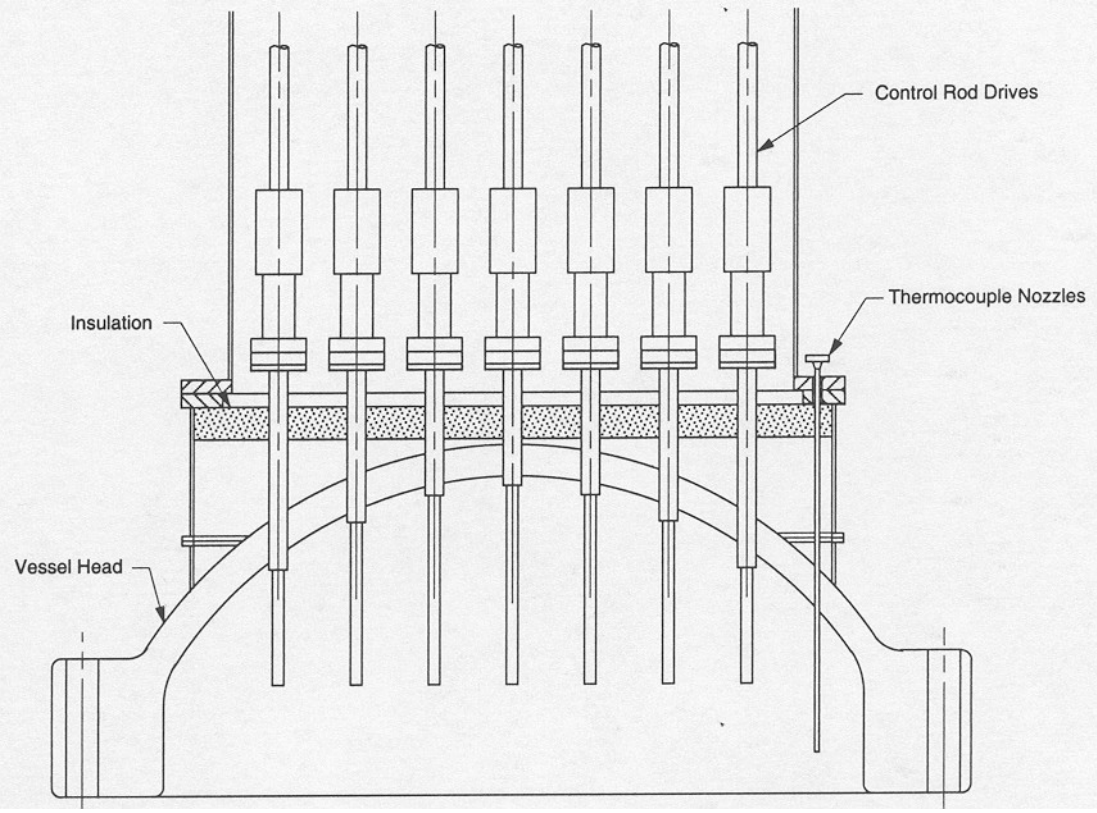

Figure 1-1 Control rod drive mechanism

In 1989, cracks were first detected in CRDM nozzle Alloy 600 tubes in France. Alloy 600 was found to be susceptible to stress-corrosion cracking in the PWR water environment with the residual stresses from the J-weld. This stress-corrosion cracking mechanism is now referred to as primary water stress-corrosion cracking (PWSCC). At the time of plant construction, PWSCC was an unknown, and thus unexpected, aging mechanism in this material. It is now known that these originally chosen materials will deteriorate with age when conditions of stress, water, and material create an environment that will lead to PWSCC. A significant amount of effort was spent back in the early 1990's in calculating and experimentally measuring residual stresses for CRDM nozzles, primarily in the hoop direction in the Alloy 600 tube. Some of that work was documented in Electric Power Research Institute (EPRI) conference proceedings [1]. US plants have begun to replace the heads with Alloy 690 using Alloy 52/152 weld metal. Upper head replacements by US utilities is well underway with at least 36 of the 69 US PWR pressure vessel upper heads being replaced using Alloy 52/152 materials for their penetration nozzle J-groove welds by the end of 2009. Alloy 690 and Alloy 52/152 both have a higher chromium content compared to the original alloys which leads to improved PWSCC resistance.

However, construction-related indications have been found in some US replacement reactor pressure vessel heads (RPVH) being fabricated from Alloy 690 material and compatible weld metals, Alloy 52/152. These indications were found in every single nozzle/head weld ranging

from 5 to as many as 22 indications per nozzle in a recent plant RPVH replacement. The sources of these fabrication-related indications are believed to be slag inclusions in the weld metal along with micro-fissuring and possible hot cracking during the weld deposition process. The numerous construction-related indications in these RPVHs could be more than 50 mm in length. Hot cracking during the weld fabrication is generally due to the difficulty of welding with Alloy 52/152. Hot cracking includes solidification cracking in the weld, liquidation cracking at the heat affected zone (HAZ), and ductility dip cracking (DDC). The indications were mostly circumferential in orientation but there were some axial indications observed as well.

Emc^2 has divided the description of this study and its results into three parts. The first part of the study includes the welding residual stress analysis conducted using elastic-plastic finite element analysis procedures and A52/152 material data. These results are compared to companion results using Alloy 82/182 material data. Alloy 82/182 was the material used to construct the original dissimilar metal welds in these heads. PWSCC tends to occur in Alloy 82/182 material due to its lower chromium content compared with the replacement Alloy 52/152. While there are many angles that RPVH nozzles are inserted through the RPV, the work presented in this report provides results for both center-hole (0 degree) and greatest side-hill (53 degree) nozzles (See Figure 1-1) in order to bound the problem.

The second part of the study deals with assessment of flaws in the reactor pressure vessel head penetration nozzles. In common flaw analysis, a representation of physical cracks needs to be placed into the system model in order to conduct the evaluation. The insertion of these representational cracks could result in prohibitive computational expense. In this report, the finite element alternating method (FEAM) was used for calculating stress intensity factors for cases where multiple cracks exist. More than twenty cracks, inserted with sizes and locations based on field measurements of indications, are considered in the analyses for both center-hole and side-hill nozzles. The overall stress trends observed are similar to the trends without adding cracks. However, cracks introduce more local stress fluctuations around the indications. The magnitude of the local fluctuation could be around 100 MPa. Moreover, the actual values of the stress intensity factors are in the range where PWSCC could occur.

In the final part of this report, limit analysis was conducted. A new finite element model with a voided-out weld region was used to simulate loss of structural capacity due to multiple flaws and the void-out volume effects on the structural integrity and future performance of RPVH were evaluated. Discussions based on weld residual stress, multiple flaw analysis and limit analysis conclude the report.

The FE residual stress or K-solution analysis methods discussed in the current study have been well documented in other reports [2, 3]. These reports do not address comparisons of the weld residual stresses in the RPVH assemblies. However, the side-hill and center-hole weld residual stresses are compared in Reference 4. In addition to the comparison between the Emc^2 K-solution results, the results of the current study are also compared to the MRP Report 105 K-solution results of Reference 5.

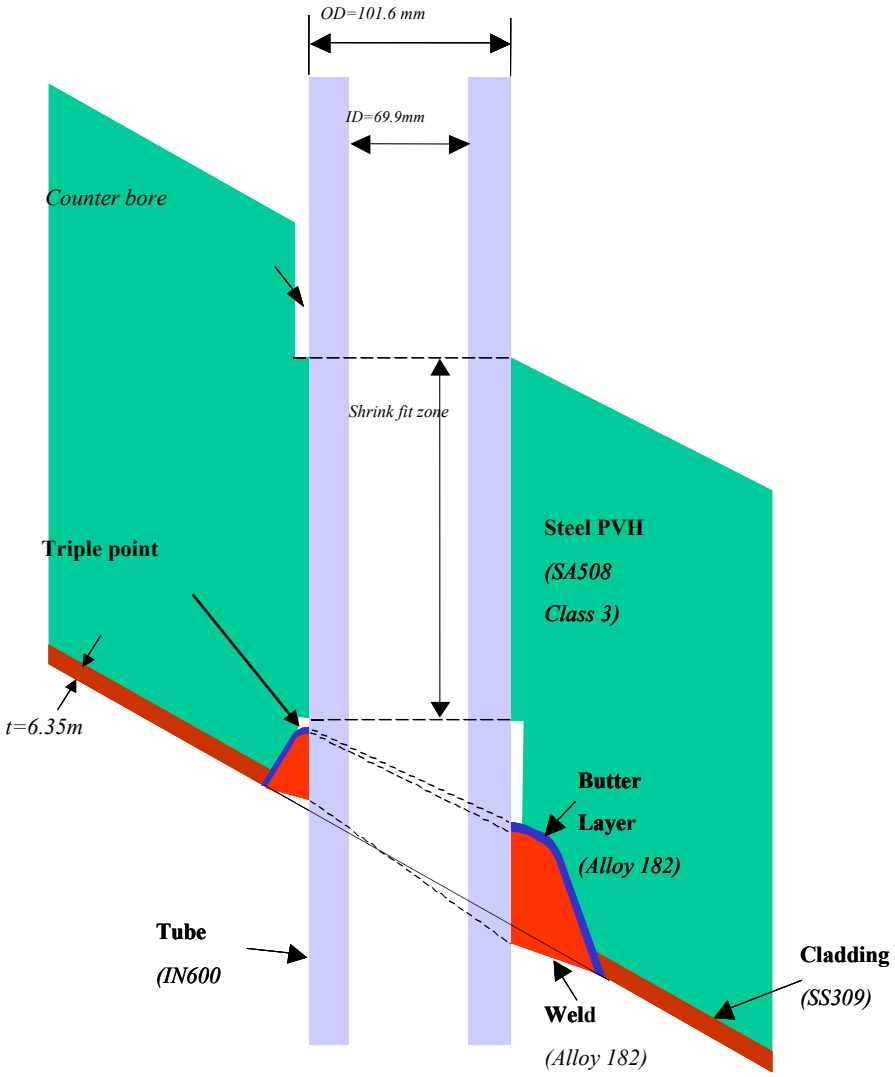

Figure 1-2 Typical reactor vessel head J-groove weld

2. Introduction

With Alloy 52/152 introduced as weld metal for the replacement of reactor pressure vessel heads (RPVH), fabrication-related indications have been found in some nozzle/head welds ranging from 5 to as many as 22 indications per nozzle. The sources of these weld fabrication indications are believed to be slag inclusions in the weld metal along with micro-fissuring and possible hot cracking during the weld deposition process. However, since there are numerous indications and

some are quite long (more than 50 mm in length) it is believed that some of these indications may be caused by additional mechanisms such as hot cracking. Hot cracking includes solidification cracking (weld), liquidation cracking (HAZ), and ductility dip cracking (DDC). It is also difficult to perform welding with Alloy 52/152 (the newer Alloy 52M is less difficult to weld). Large grains could be produced in the welds and micro-cracks tend to develop in such material. Therefore, micro-cracking in Alloy 52/152 is a potential concern. The observed indications were mostly circumferential in orientation but some axial indications were observed as well. Many studies and research work show that welding residual stress is the critical driving force in crack growth and propagation. Hence the first part of this report discusses the welding residual stress analysis for Alloy 52/152 RPVH J-welds and includes a thorough comparison of residual stress fields between the original Alloy 82/182 material and Alloy 52/152. Both center-hole (0 degree) and the largest side-hill (53 degree) nozzles were analyzed. Results are presented in detail in the following sections.

In most commonly used finite element methods for fracture problems, it is necessary to use very fine meshes around the crack tip. The creation of these fine meshes requires significant human effort in developing the mesh and also demands tremendous computation time. The finite element alternating method [6] has proven to be a very efficient and accurate method for the analysis of fracture mechanics problems. The major advantage of the method is that a finite element mesh of *the un-cracked geometry* is all that is needed. The most important aspect of FEAM is that the same mesh can be used to obtain solutions for many different crack sizes, locations, and for multiple cracks. Because the finite element stiffness matrix only needs to be reduced once, regardless of the crack size, crack location, crack orientation, crack number (mixed mode conditions can be handled as well), etc., the method is extremely efficient. In addition, Mode I, II, and III stress intensity factors are computed without recourse to contour or surface integrals or to other means for indirectly computing stress intensity factors from energy release rates. Here, FEAM will be used to solve multiple crack (up to 25 cracks) problems for center-hole (0 degree) and side-hill (53 degree) nozzles.

In addition, the weld residual stress redistributions caused by the cracking are discussed. It is these stresses that are used for a PWSCC analysis of a dominant flaw. Finally, a limit analysis of the micro-cracking is performed. The purpose of the limit load assessment is to determine the safety margins which exist in the RPV replacement heads if the cracking is assumed to be linked.

3. Weld Residual Stress Analysis

The RPVH geometry analyzed was a Westinghouse design, fabricated by Combustion Engineering for the Pressure Vessel Research User's Facility (PVRUF) at the US Department of Energy's Oak Ridge National Laboratory (ORNL). Figure 1-1 shows the basic dimensions of this RPV head. The geometric features and materials surrounding the nozzle penetration are depicted in Figure 1-2. For this geometry, the term "nozzle" is used to represent the entire penetration (tube and welds) shown in Figure 1-2, while the term "tube" is used to represent just the Alloy 600 or 690 tube. In the original manufacture of the nozzle, the Alloy 600 tube is inserted in the RPV head with shrink fit where the head is at room temperature and the tube is

cooled to liquid nitrogen temperature. The initial degree of interference fit when both the head and the tube are at room temperature may range from 0 to 0.11 mm on radius. Once the tube is in place, it is welded from the inside of the head using a J-weld procedure. Also in the J-weld groove, a butter layer is deposited on the steel-head side, before the final J-weld is completed using multiple passes of filler metal. The buttered layer is machined and stress relieved with the rest of the vessel prior to shrink-fitting the tube and making the J-weld.

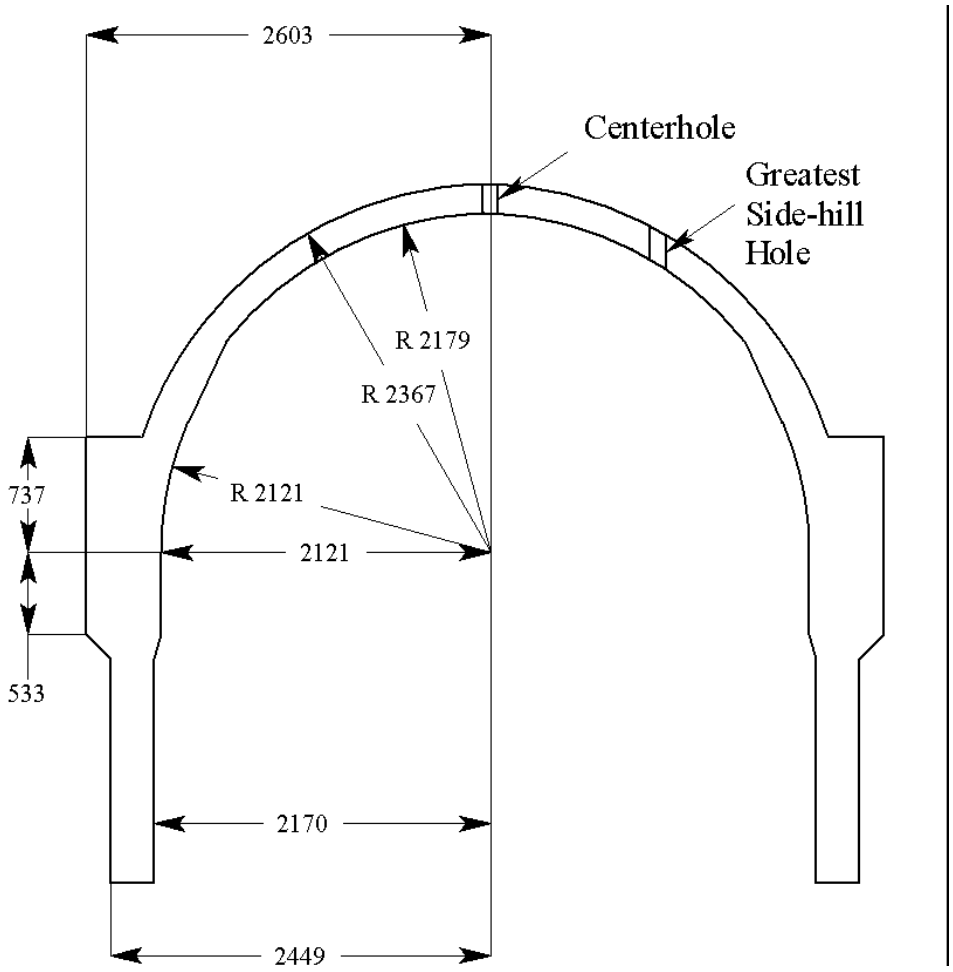

Figure 3-1 Typical reactor pressure vessel head (dimensions in mm)

There are 78 upper head penetration nozzles on the reactor head in the Westinghouse design (other RPVs may have more or less CRDM nozzles). The center-hole and steepest side-hill nozzle were chosen for this investigation. The nozzles have angles that are identified as 0 degree and 53 degrees to the reactor head and are located as shown in Figure 1-1 and Figure 3-1. Original filler metal was Alloy 82/182 while the new filler material is Alloy 52/152. Since temperature dependent material properties were not yet available for the Alloy 52/152 weld material, for the purpose of this initial study, it was assumed that the Alloy 82/182 material data

could be scaled up by 20% on stress at each plastic strain point to approximate the temperature dependent material properties of Alloy 52/152. This is conservative since higher weld residual stresses will be predicted and used for flaw assessment later. Elastic properties for Alloy 52/152 are assumed to be identical to Alloy 82/182. After these analyses were completed, test data became available (see Figure 3-2). It is now known that the tensile properties of Alloy 52/152 are quite close to those of Alloy 82/182, except at room temperature. However, these analyses were not redone using the actual Alloy 52/152 properties since the results are conservative.

Figure 3-2 shows the plots of the true stress and true strain for Alloy 52M/152 (top). The bottom part of Figure 3-2 compares the true stress/true strain curves for both Alloy 52M/152 and Alloy 82/182 up to 538 C. The curves compare very closely, except at room temperature, where the Alloy 52M/152 data are about 15% higher. The comparison for higher temperatures is likewise very close. Since operating temperature stresses (about 318 C) are used for PWSCC predictions, the analyses performed in this report, and the corresponding weld residual stresses and stress intensity factors are over predicted and thus conservative at operating temperature.

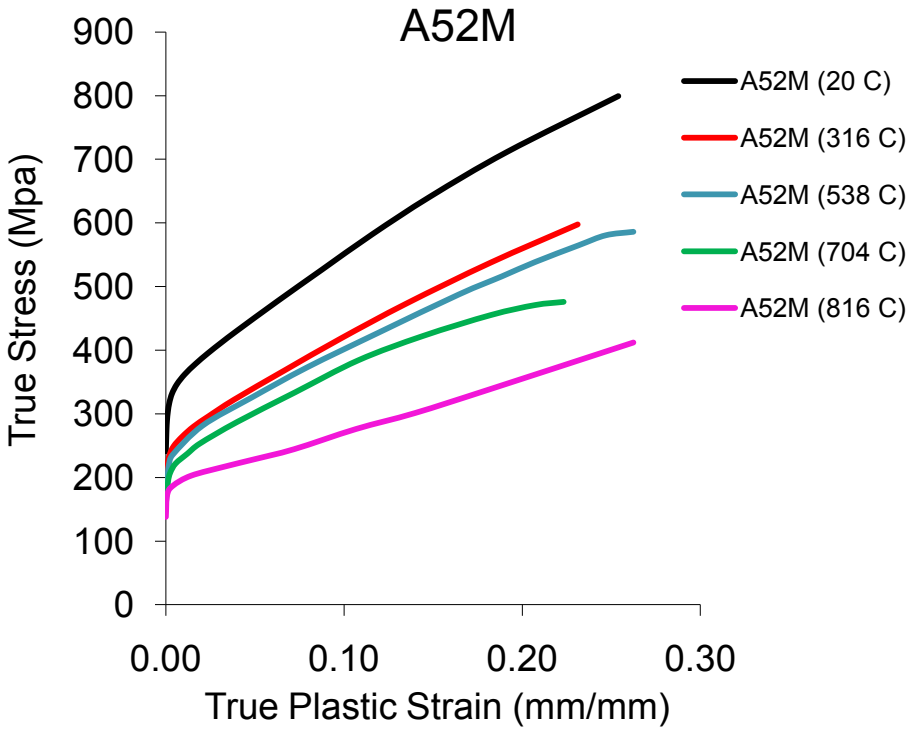

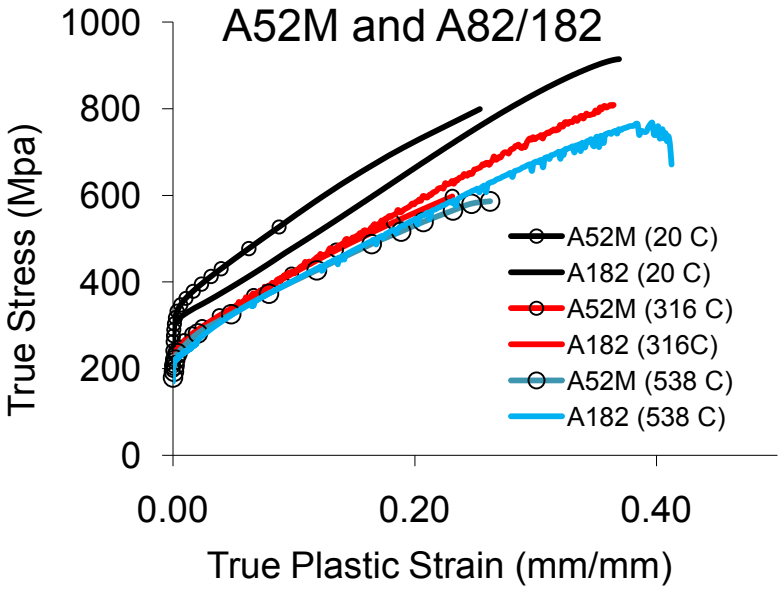

Figure 3-2 True stress strain curve comparisons for Alloy 52M/152 and Alloy 82/182

3.1 Computational Weld Model

To evaluate the residual stress distribution, thermo-elastic-plastic FEM analyses of the welding and cooling processes were conducted to simulate welding the J-weld in the CRDM nozzles. The heat flow and mechanical deformation during welding were simulated using a sequentially coupled approach [7, 8, 9, 10, 11]. With such an approach, the transient heat-transfer analysis was conducted to solve the temporal and spatial distribution of the temperature in the model, and then the computed thermal history was used as thermal loading input in the subsequent mechanical analysis calculating the residual stress field. Temperature-dependent mechanical properties were utilized and isotropic hardening was assumed. The effects of melting, solidification, and annealing were simulated in the analysis. The justifications for using the sequentially coupled modeling approach were provided elsewhere [7, 12]. The formation of the welding residual stress was a result of the thermo-mechanical deformation process during welding.

The welding heat flow in the tube was modeled as a heat-conduction problem. Temperature-dependent thermal conductivity and specific heat values were used. The welding simulation was performed on a pass-by-pass basis, following the weld pass deposition sequence as required. A weld pass was activated only when it was deposited. The weld simulation process first requires application of sufficient heat to melt the weld metal (up to 1,700 K) and a small layer of the base metal. Typically, the welding arc is treated as a volumetric moving heat source, taking the double-ellipsoidal distribution proposed by Goldak, et al. [13]. However, such moving source analyses can be very computationally intense. Therefore a uniform heat distribution was used across the weld bead cross-section. This approach, compared to other methods such as Goldak's double-elliptical heat flux model, has been proven to be easier to implement and more robust for irregular shapes of weld metal. As a matter of fact, Emc^2 experience in separate sensitivity studies was that the difference in the final distortion or residual stresses is insignificant between Goldak's model and the current approach [14]. This method effectively ignores the motion of the welding arc, allows for heat transfer radially away from the centerline of the weld path with no heat transfer ahead or behind the weld bead, and "shortens" the welding time. To do this, a uniform energy density is added to the whole weld pass in an exponential function form:

$$q = \frac{\sqrt{3}Q}{\sqrt{\pi}VT} e^{\left[-3(t-t_o)^2/T^2\right]} \qquad (1)$$

Where q is the energy density (W/mm^3) from the weld arc, V is the total volume of the weld pass, t is a starting time, T is the characteristic time of the traveling arc, inversely proportional to the welding speed, and Q is the total heat input during the time of welding. For this heat source, every material point in the weld will experience the same heat source cycle and hence similar temperature histories. Therefore, at any time, there is no heat flux gradient and therefore minimum temperature gradients over the entire weld pass. Since the actual weld metal is deposited continuously, the uniform source approach described above should produce conservative results from a practical industrial point of view [15,16,17].

The simulations were performed with the commercial software ABAQUS 6.8-1 [18]. The temperature dependent material properties were input with a piece-wise linear approximation. A set of user subroutines was used to deal with the special issues associated with welding heat flow and stress analysis which cannot be readily handled by the general purpose FE packages in ABAQUS. The analysis procedure included not only the pass-by-pass welding steps, but also other essential fabrication steps expected to have strong effects on the stresses in the nozzle penetration region: hydro-testing, pressure, and temperature loading during operation. Furthermore, the deformation of the contact surface between the tube and the RPV head and the changes in contact area and pressure during the welding process were simulated. Temperature-dependent material properties were used for simulating welding residual stress, including the thermo-physical and mechanical properties of the materials involved in the CRDM nozzle fabrication. Great care was taken to ensure that the material properties used in the weld simulation analysis were as realistic as possible. The material properties necessary for the CRDM weld stress analysis were collected from various sources in the open literature and through data exchanges with industry. In addition, the temperature-dependent stress-strain curves for Alloy 82/182 weld metal [up to 1,255 K (1,800 F)] and carbon steel SA-508 [up to 1,033 K (1,400 F)] were estimated and experimentally determined at ORNL [19]. The Alloy 52/152 weld metal was modeled using Alloy 82/182 stress-strain curves scaled up by 20%. Table 1 shows a summary of the elastic mechanical properties at the operating temperature of 318 C.

For the case of center-hole nozzle, the mesh is shown in Figure 3-3, Figure 3-3(a) shows the overall mesh and Figure 3-3(b) shows the magnified view of the weld region. There were thirteen passes modeled. Since this tube structure is symmetrical, an axis-symmetric model was developed. The 3-D model was actually performed using the axis-symmetric finite element model and the results were then rotated by an ABAQUS visualization routine. This rotation of results is convenient since one can alter the rotation angles to permit more or less angular refinement in certain areas for the subsequent crack analysis. In this axis-symmetrical model, the total number of nodes is 2,400 and the total number of elements is 2,200.

For the side-hill nozzle, the complex geometry of the nozzle penetration was simulated with a 3D model. The model was a 22.5-degree solid section as shown in Figure 3-4 using fourteen lumped passes. Figure 3-4(a) is the overall mesh and Figure 3-4(b) is the local view of the weld region.

Table 1 Mechanical properties for Emc^2 CRDM analyses at 318 C

Material	Use	Elastic Modulus, MPa	Poisson's Ratio	σ_y, MPa
Low Yield Alloy 600	CRDM tube	203,165	0.32	214.2
SA-508	RPV head	183,150	0.30	268.9
Alloy 52/152	Weld and butter	203,165	0.32	195.4
SS309	Cladding	176,290	0.30	148.8

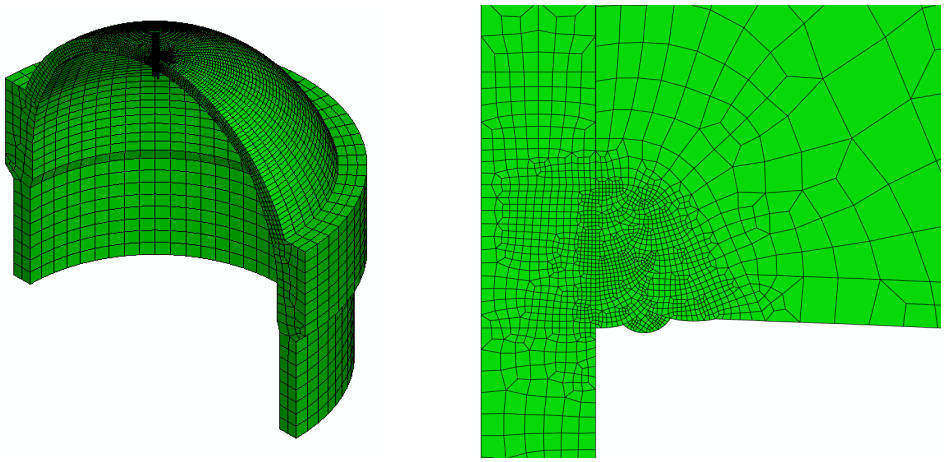

(a) (b)

Figure 3-3 Center-hole nozzle model (a) overall mesh (b) magnified view

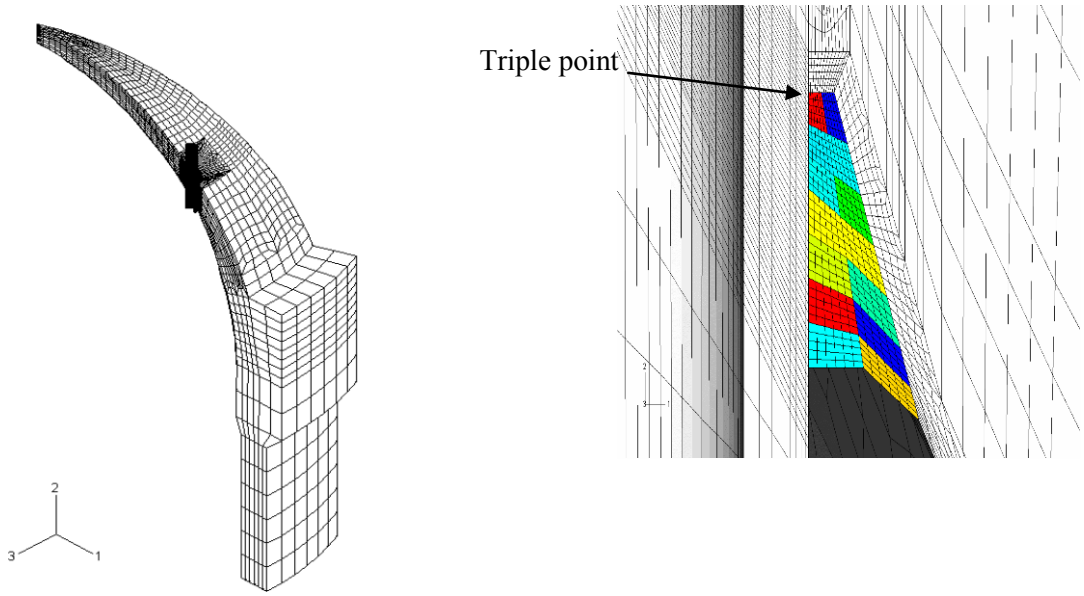

(a) (b)

Figure 3-4 Steepest side-hill nozzle model (a) overall mesh (b) magnified view

There are approximately 70,000 nodes and 64,000 8-node linear brick elements in the side-hill model. This model has a symmetry plane through the center of the CRDM nozzle and the head.

3.2 Center-hole Weld Residual Stress Results

A center-hole RPVH case with the estimated weld material of Alloy 52/152 (i.e. 20% higher than Alloy 82/182, as discussed above) was analyzed. Elastic and physical properties for Alloy 52/152 are assumed to be identical to Alloy 82/182. Figure 3-5 illustrates the model geometry. This analysis was performed using an axis-symmetric finite element model and the results were then rotated by an ABAQUS routine onto a 3D mesh. This rotation of results is convenient since one can alter the rotation angles to permit more or less angular refinement in certain areas for the subsequent crack analysis. This is not possible for the side-hill angle cases since the geometry is not axis-symmetric. This is the reason that the center-hole case was analyzed first since it is very easy to vary mesh refinement during the crack analysis phase. This helped to define the 3D refinement necessary for crack analysis accuracy for the side-hill cases.

Figure 3-6, Figure 3-7, and Figure 3-8 show the contour plots for axial, hoop and von Mises stresses with service pressure of 17.24 MPa at operating temperature (318 C). Among the figures, the left illustration indicates the stress contour**s** using Alloy 52/152 and on the right are the stress contour plots with Alloy 82/182. For axial stress, the difference between the two materials is quite small in both the tube and the weld region. For hoop and von Mises stress**es** in Figure 3-7 and Figure 3-8, the stresses in the tube are similar overall while the stress in the weld using Alloy 52/152 is a little higher than that using Alloy 82/182. This is expected because the strength of Alloy 52/152 is 20% higher than Alloy 82/182 (based on the assumptions used here). Again, it is noted that using the scaled up properties for the Alloy 52/152 produce conservatively higher weld residual stress results.

To have a quantitative comparison of stress for the center-hole cases, line plots along tube ID and OD with path definition as in Figure 3-5 were developed and presented in Figure 3-9 to Figure 3-14. The blue solid lines are the results for Alloy 52/152 and the dashed lines are the results for original Alloy 82/182. Figure 3-9 and Figure 3-10 plot the axial stress along tube ID and OD, respectively; Figure 3-11 and Figure 3-12 show the hoop stress along tube ID and OD. These plots show that the weld residual stresses change little using either the Alloy 82/182 material or the estimated Alloy 52/152 material. The Alloy 52/152 material gives slightly higher results. For reference, the bottom of the weld is shown on these figures with the red line.

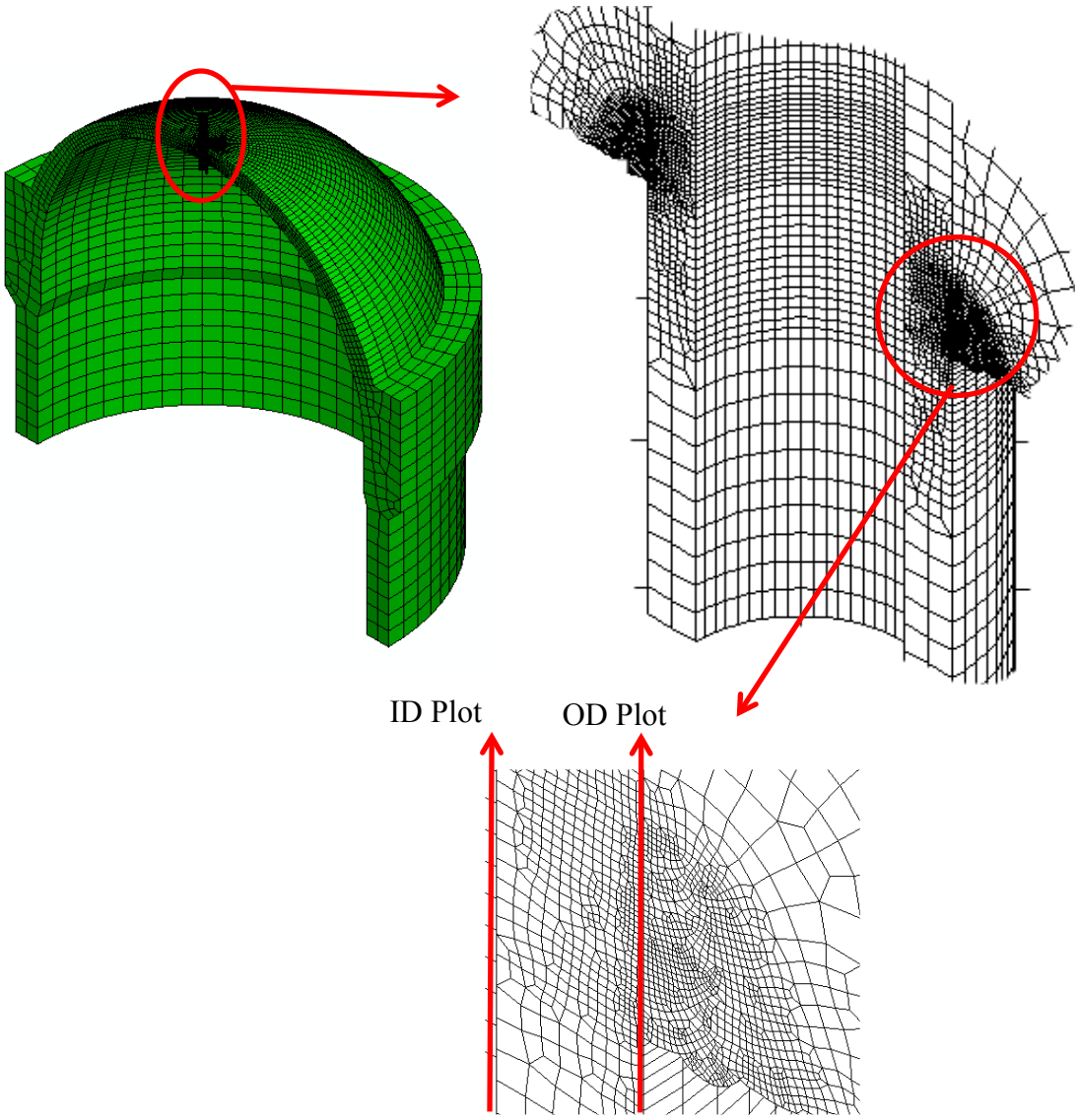

Figure 3-5 Three-dimensional model of center-hole CRDM case

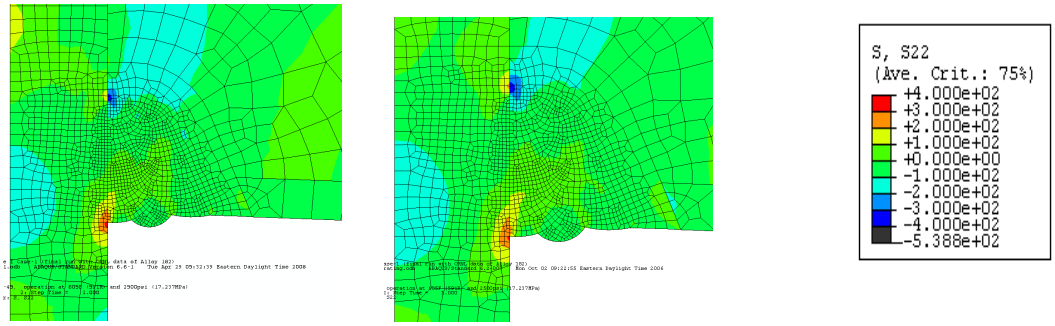

Figure 3-6 Contour plot comparison of axial stress with Alloy 52/152 (Left) and Alloy 82/182 (Right)

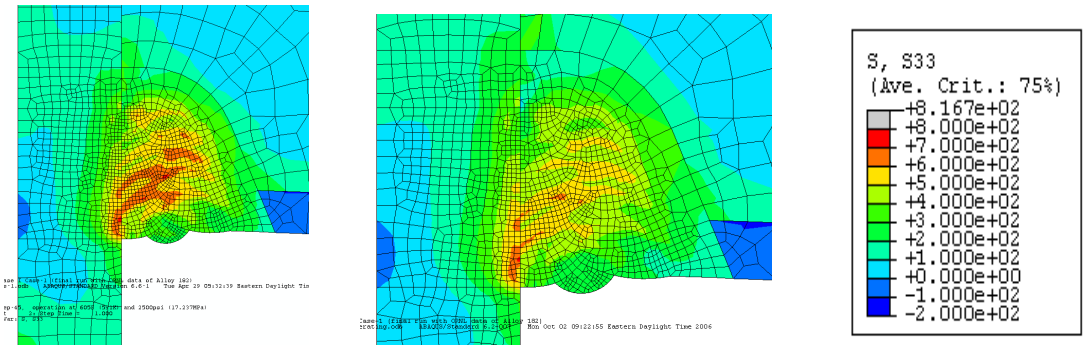

Figure 3-7 Contour plot comparison of hoop stress with Alloy 52/152 (Left) and Alloy 82/182 (Right)

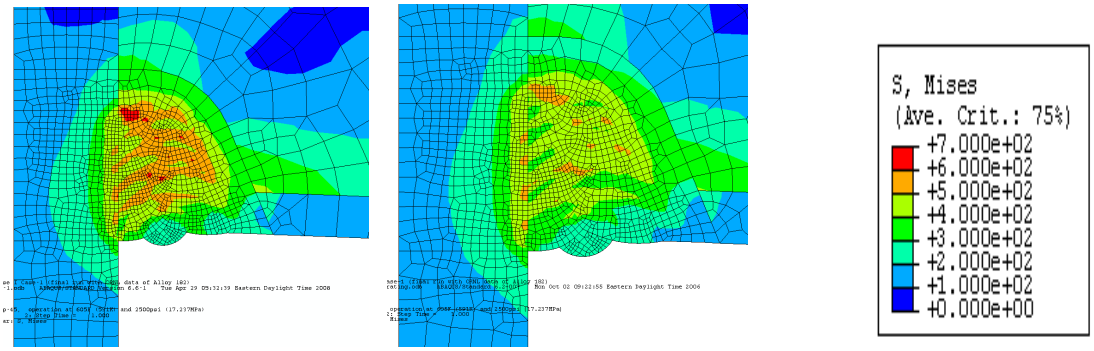

Figure 3-8 Contour plot comparison of von Mises stress with Alloy 52/152 (Left) and Alloy 82/182 (Right)

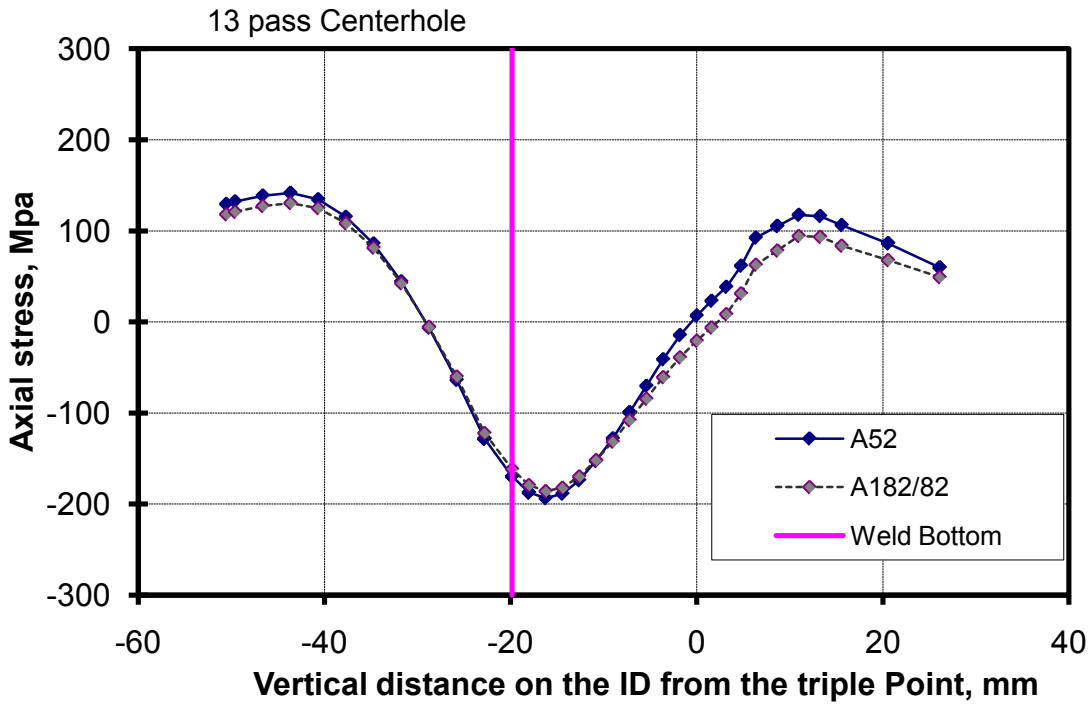

Figure 3-9 Axial stress comparison on ID with Alloy 52/152 and Alloy 82/182 materials.

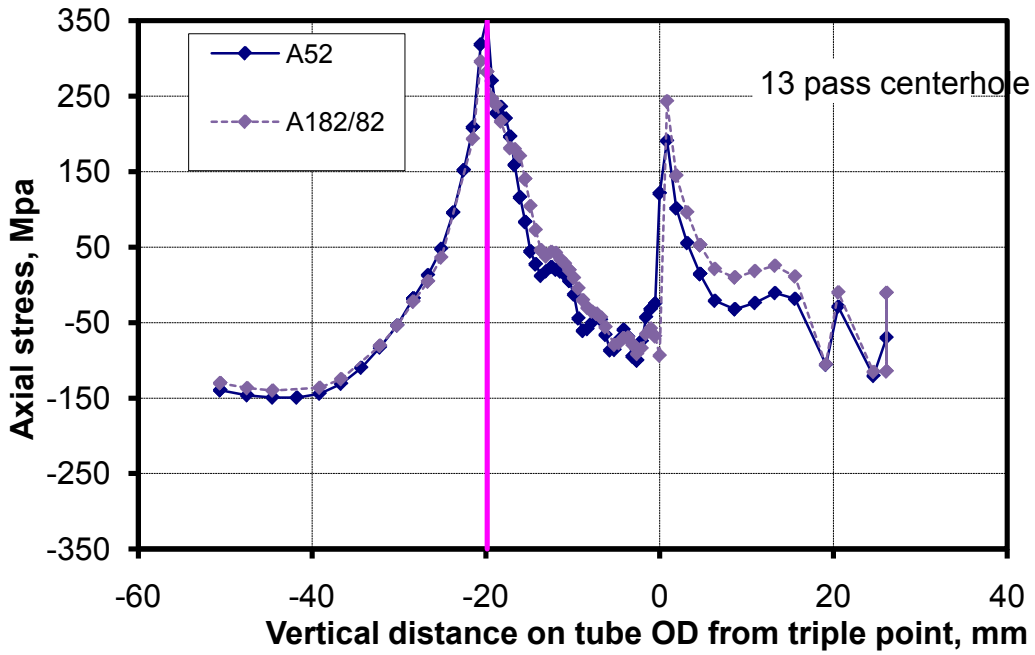

Figure 3-10 Axial stress comparison on OD with Alloy 52/152 and Alloy 82/182 materials.

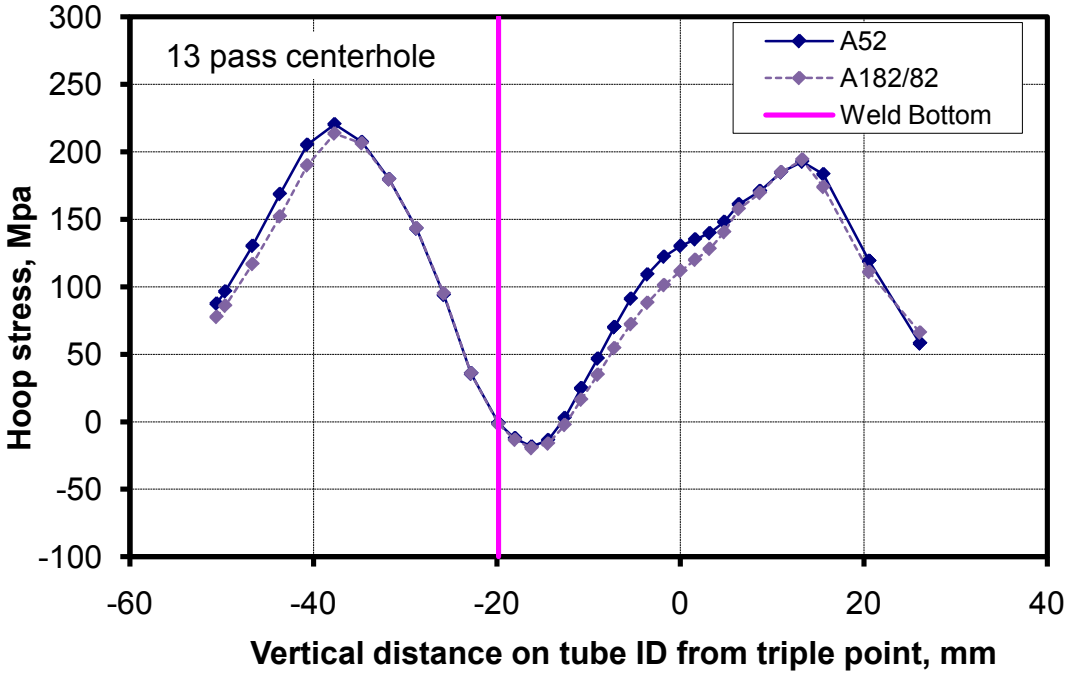

Figure 3-11 Hoop stress comparison on ID with Alloy 52/152 and Alloy 82/182 materials.

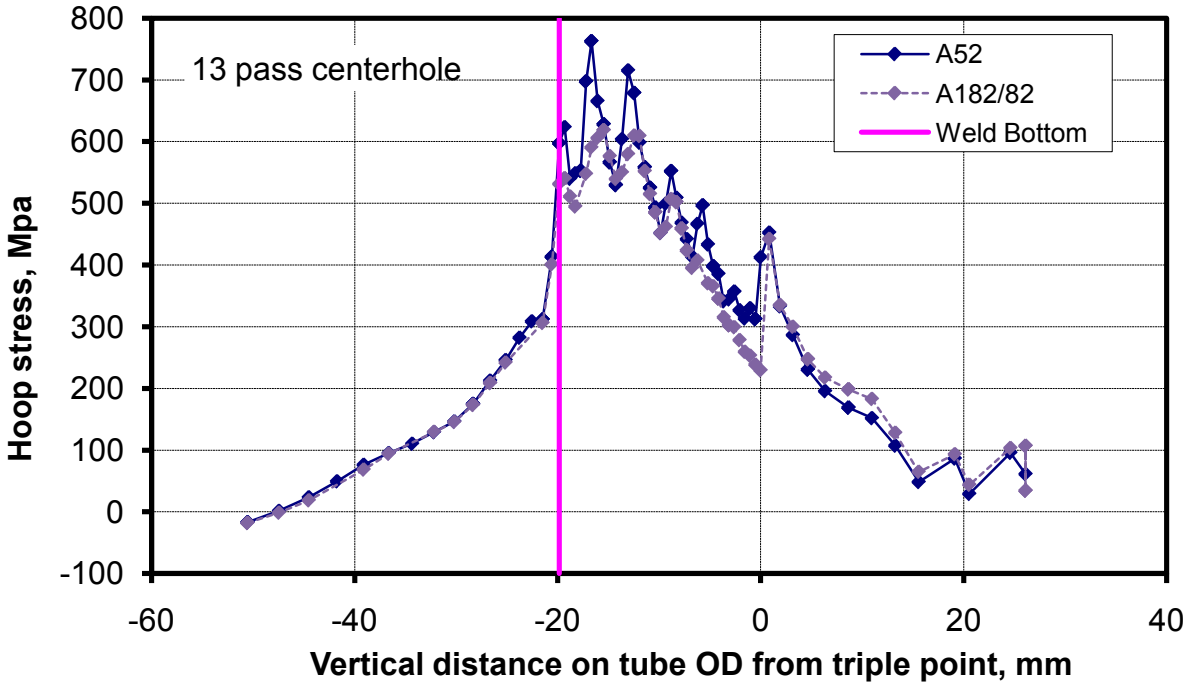

Figure 3-12 Hoop stress comparison on OD with Alloy 52/152 and Alloy 82/182 materials.

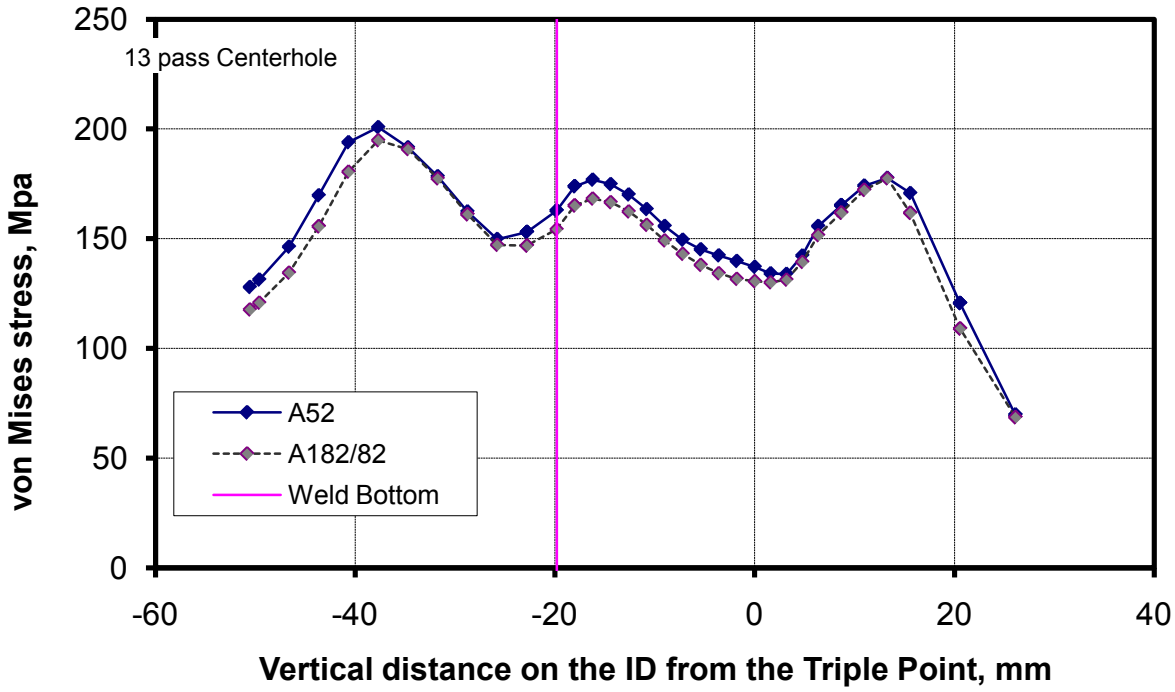

Figure 3-13 Von Mises stress comparison on ID with Alloy 52/152 and Alloy 82/182 materials.

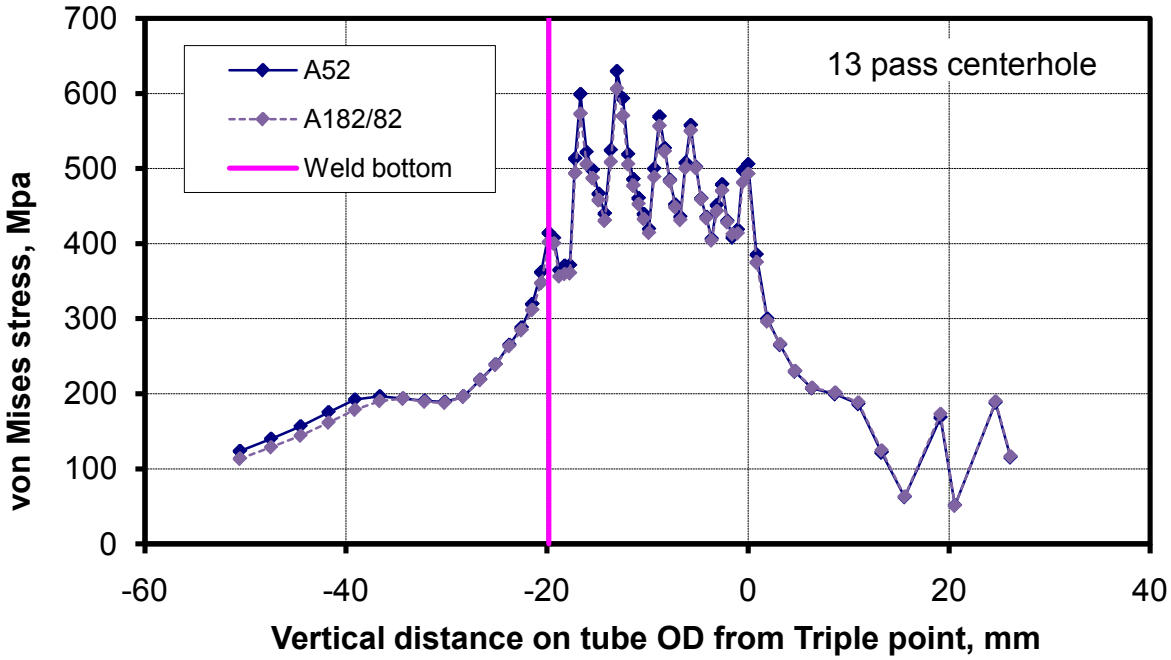

Figure 3-14 Von Mises stress comparison on OD with Alloy 52/152 and Alloy 82/182 materials.

3.3 53-Degree Side-hill Weld Residual Stress Results

A 53-degree side-hill RPVH case with the estimated weld material properties for Alloy 52/152 was analyzed for weld residual stresses and results presented here. As with the center-hole case, these results were obtained by multiplying the stress data for Alloy 82/182 by 1.2 while keeping the plastic strains the same since material data for Alloy 52/152 was not available at the time these analyses were performed. As discussed above, these results should be conservative compared with using the actual material data shown in Figure 3-2. Elastic and physical properties for Alloy 52/152 are assumed to be identical to Alloy 82/182.

Figure 3-15 shows the FEA model and magnified view of the weld and tube. The tube inner diameter (ID) and outer diameter (OD) are shown along with the welds on the uphill and downhill sides of the tube. Note that the weld on the downhill side looks larger than that on the uphill side. In reality it is only slightly larger. Comparison of stress predictions (weld residual stress with service pressure of 17.24 MPa at operating temperature (318 C)) are presented in the following sections.

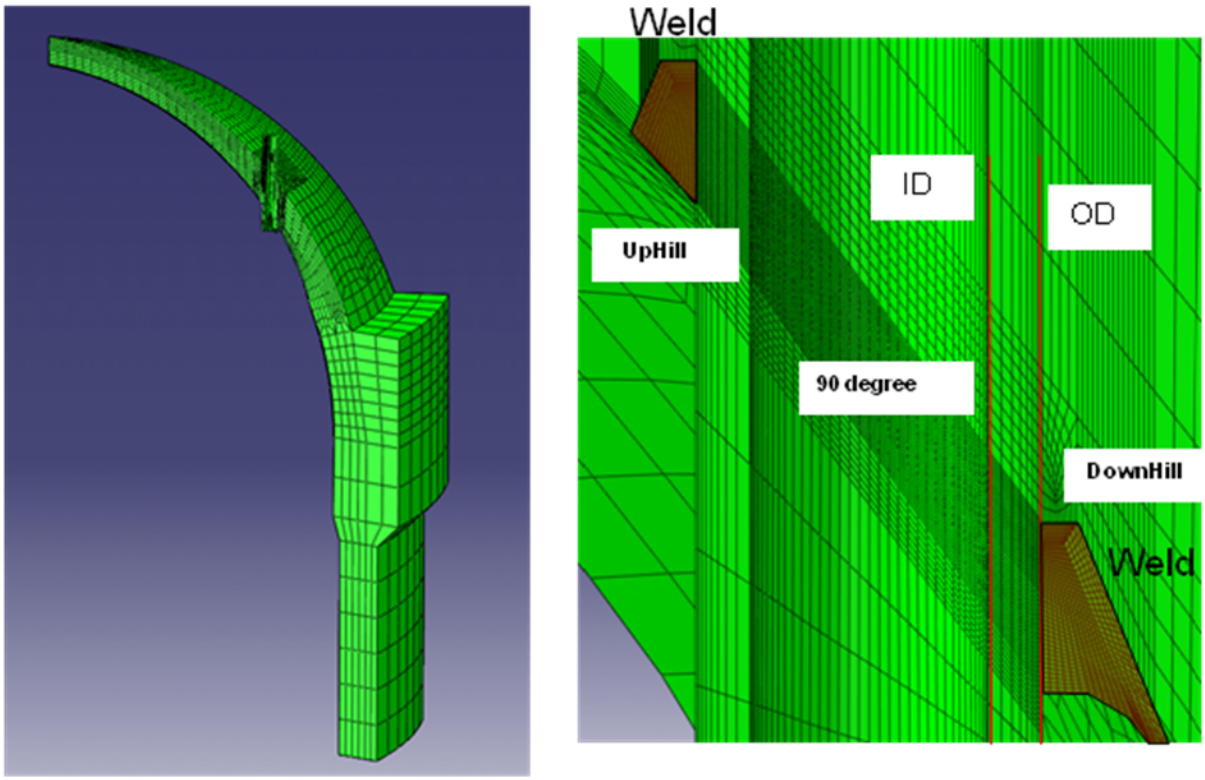

Figure 3-15 Finite element model of the 53-degree side-hill nozzle

Figure 3-16 shows von Mises stress contour plot comparisons using both Alloy 82/182 weld metal (left side) and Alloy 52/152 weld metal (right side). The overall stress contour plots are quite similar but the stress level of Alloy 52/152 is higher and spread over a larger area.

Figure 3-17 and Figure 3-18 show comparisons of hoop and axial residual stresses, respectively. Here hoop and axial stress definitions are defined with reference to the tube coordinates. For instance, axial stresses would lead to circumferential cracks in the tube and hoop stresses would lead to axial cracks in the tube. In general, all components of stress are largest on the uphill side (compared to the downhill side) and the stresses in the Alloy 52/152 welds are larger than those in the Alloy 82/182 welds.

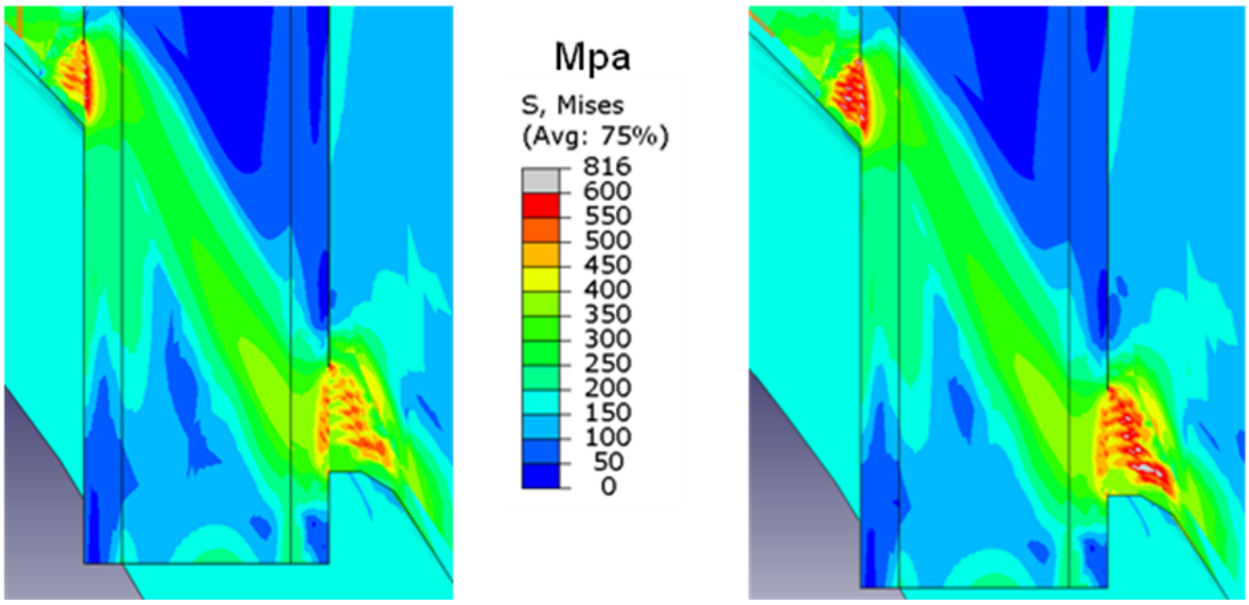

Figure 3-16 Von Mises stress contour plots (left) Alloy 82/182 and (right) Alloy 52/152

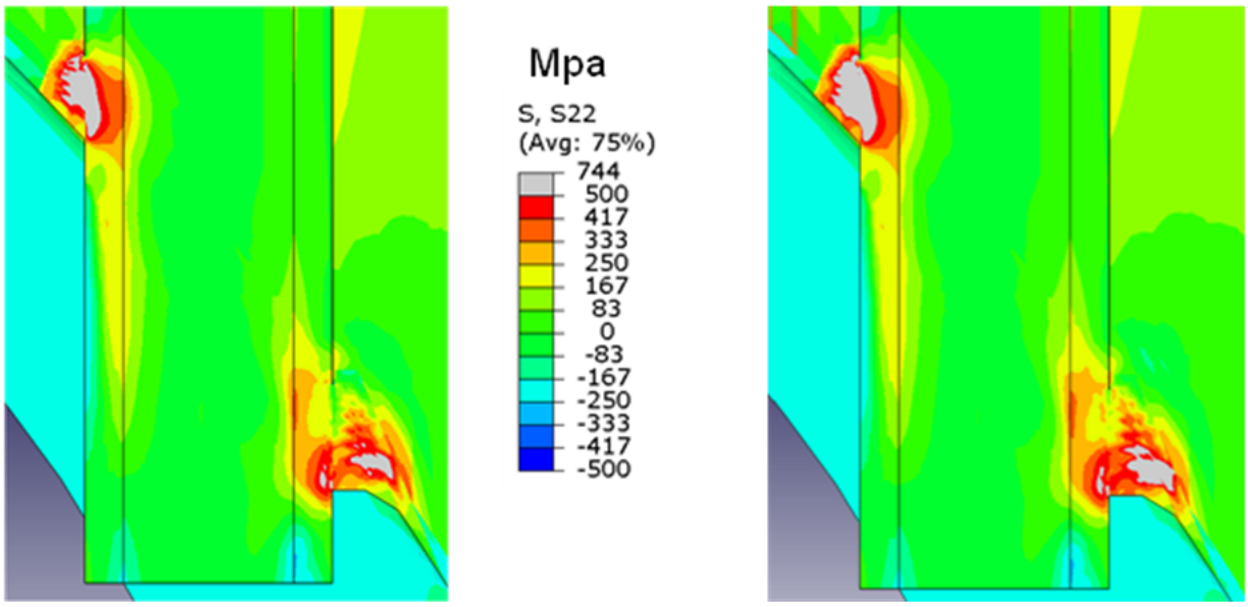

Figure 3-17 Hoop stress contour plots (left) Alloy 82/182 and (right) Alloy 52/152

Later, it will be seen that indications in the welds is dominated on the downhill side of the joint, i.e. most of the fabrication related indications occur near the downhill weld. This is important since the axial stresses are lower at the downhill locations so PWSCC would be less likely. If the bulk of the weld process cracking was on the uphill side, things may be worse. It is also convenient to compare line stress plots in order to illustrate differences between the two weld metals. Figure 3-19 illustrates the definitions of the locations of the line plots for comparison. In Figure 3-19, the weld and butter regions are shown for the up-hill weld location. The triple

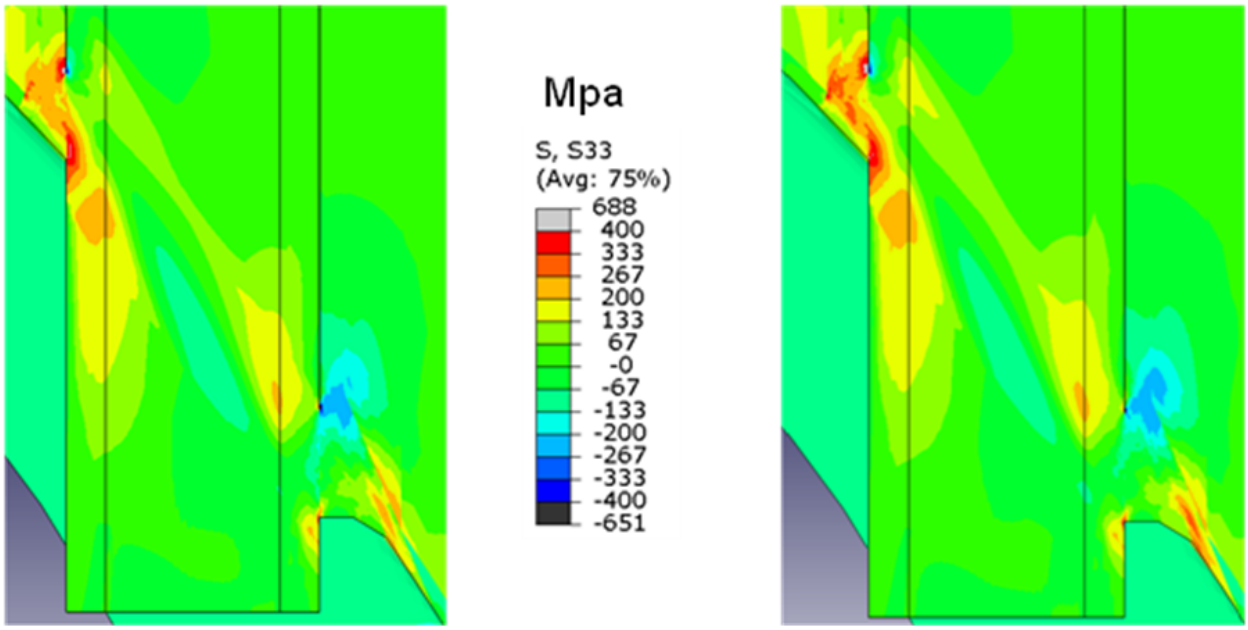

Figure 3-18 Axial stress contour plots (left) Alloy 82/182 and (right) Alloy 52/152

point is defined as the intersection of the weld and the OD of the tube. Three axial lines (A1, A2, and A3) are also defined. Line A1 is along the OD of the tube and lines A2 and A3 are 5- and 10-mm from the tube OD, respectively. All axial line plots of stress shown later begin at the bottom and proceed upwards. In addition, line plots are also presented along horizontal lines (H1, H2) as shown in Figure 3-19, with H2 going through the triple point of the weld. These plots all begin at the tube ID and proceed to the left.

Figure 3-20(a) illustrates the comparison of axial stresses along the vertical line (A1) which is at the tube OD for the uphill weld location. From Figure 3-19, these line plots start at the bottom of the tube and proceed vertically. The zero (or '0') point on the horizontal axis represents the triple point shown in Figure 3-19. For reference, Figure 3-20(a) (and all other line plots) identify where the weld is first reached, the weld end is reached, and the butter end is reached. It is seen that the axial stresses are almost identical between the two material cases away from the weld. Within the weld, the axial stresses differ by as much as 60%, with the Alloy 82/182 stresses higher than the Alloy 52/152 material. The axial stresses in the butter oscillate somewhat for the Alloy 52/152 material and for the Alloy 82/182. These oscillations are due to the pass-by-pass nature of the solution and the use of isotropic hardening. Axial stresses would lead to circumferential cracking if a fluid path existed to establish PWSCC at the tube OD, which could

presumably lead to tube ejection. The fact that the axial stresses in the Alloy 52/152 material are lower is advantageous from a residual stress standpoint. Similarly, Figure 3-20(b) shows hoop stress line plots along vertical line A1 at the tube OD. Interestingly, very little difference in stress occurs between the materials, with the Alloy 52/152 results slightly higher. Since hoop stress magnitudes are high, axial crack growth should dominate at this location if a fluid path existed for PWSCC growth.

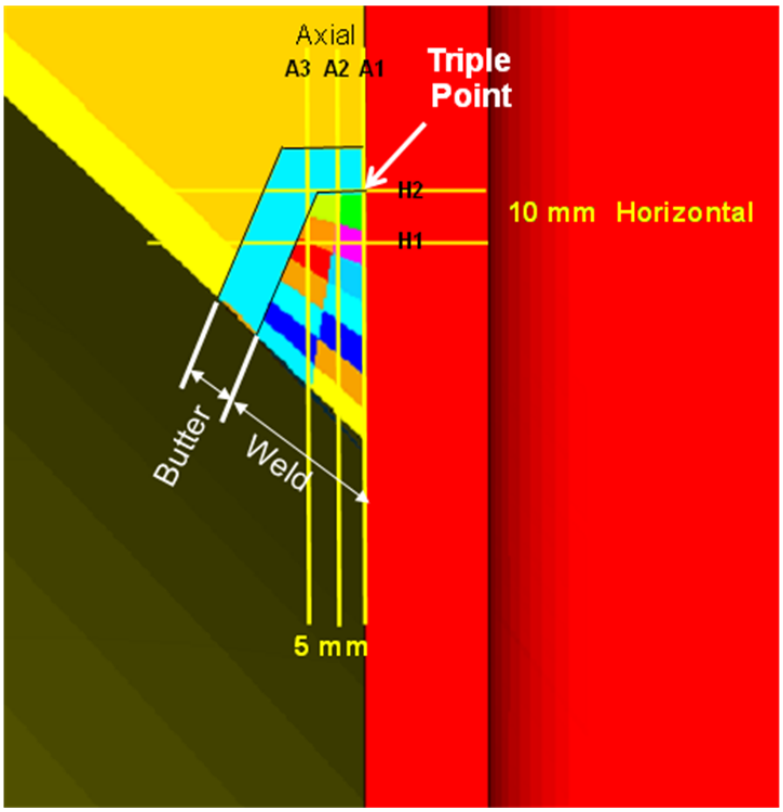

Figure 3-19 Definition of lines for plotting (uphill side).

Figure 3-21 shows axial stress line plots along the vertical lines A2 and A3 (Figure 3-19) which are 5 and 10-mm from the tube, respectively. The results for the Alloy 52/152 material are higher than those for Alloy 82/182 (in contrast to that along the tube OD (line A1)). However, these differences are mainly in the lower portion of the weld and are less than 25% at most. Note that these plots start at the weld bottom location since they are away from the tube (Figure 3-19). Figure 3-22 shows axial stresses plotted along horizontal lines (H2 and H1 in Figure 3-19). Again, very little difference in axial stress magnitudes between the two different weld materials is observed.

Comparison of line plots of axial and hoop stresses at other locations such as the downhill or 90-degree location (between the uphill and downhill locations) show little differences as well. In general the maximum difference of stresses between the two materials is about 25%, and this is only at very local locations. As discussed earlier, we used estimated material properties (1.2 times the known properties for Alloy 82/182) since the material test data for Alloy 52/152 were not yet available at the time these analyses were done. However, as seen in Figure 3-2 there is

about a 15% room temperature increase in stress in Alloy 52/152 compared to Alloy 82/182, with little difference at higher temperatures. As such, it is anticipated that the weld residual stresses from the fracture assessments (performed next) will be conservative and there is no need to re-do the analyses with the correct Alloy 52/152 properties.

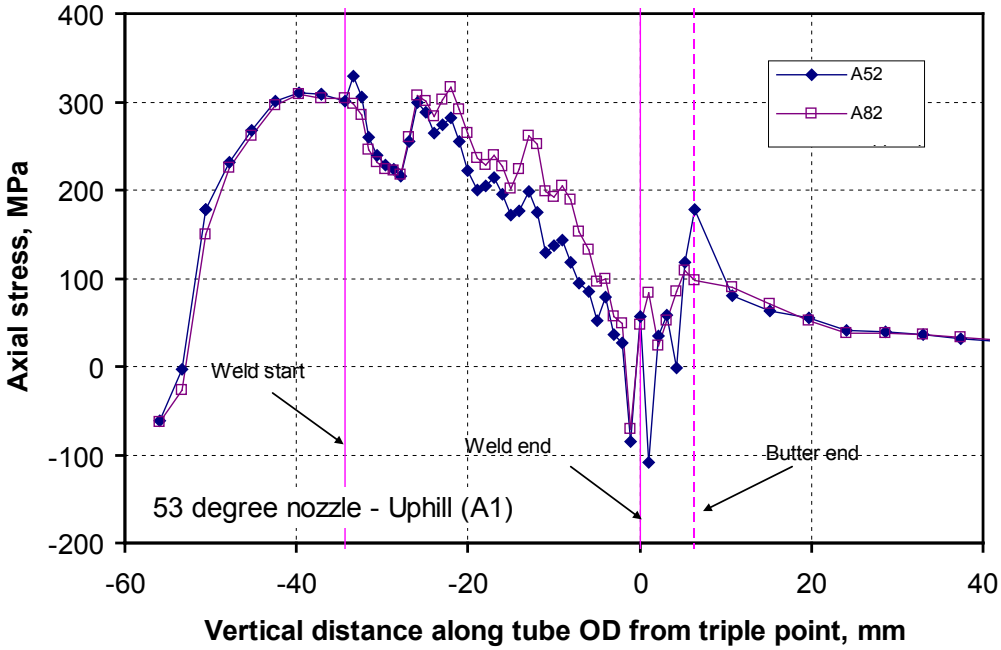

(a) Axial Stress

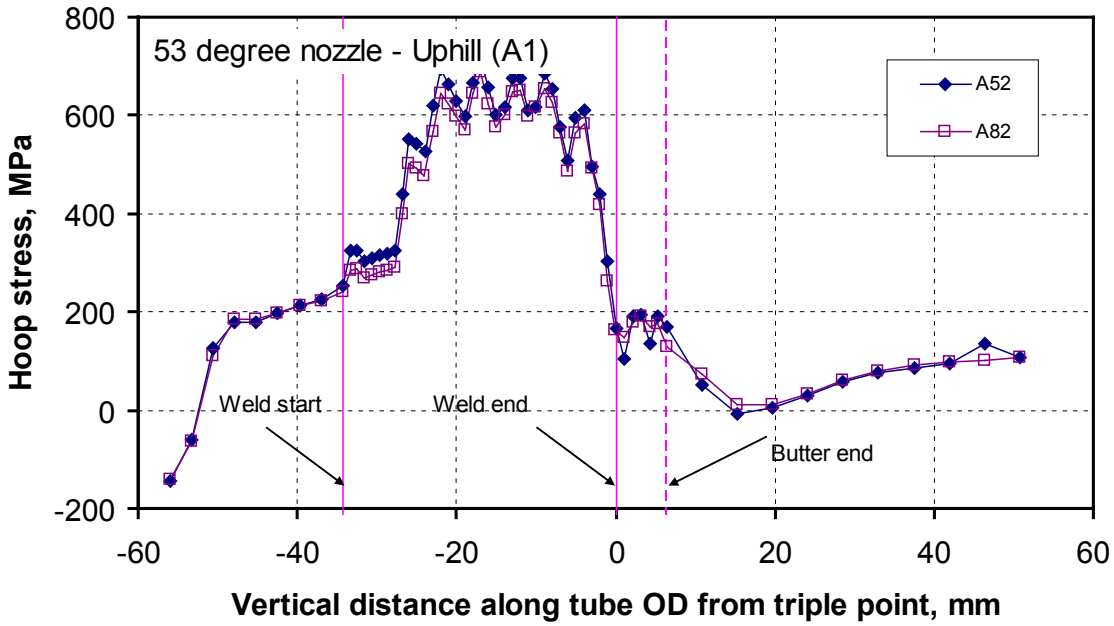

(b) Hoop Stress

Figure 3-20 Stress line plots along axial line A1 along tube OD for uphill side.

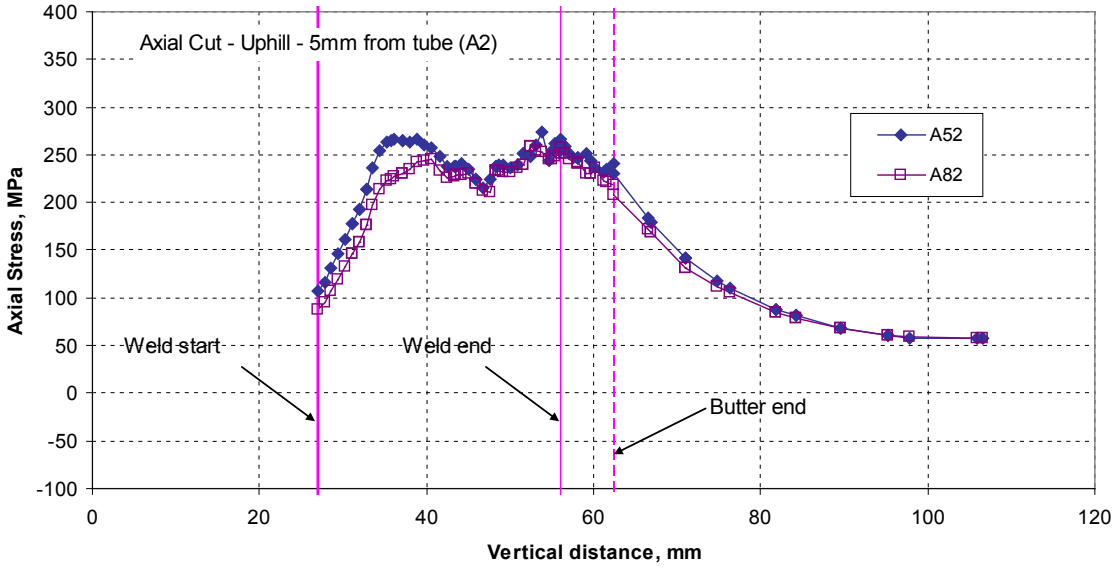

(a) Line A2 5-mm from tube

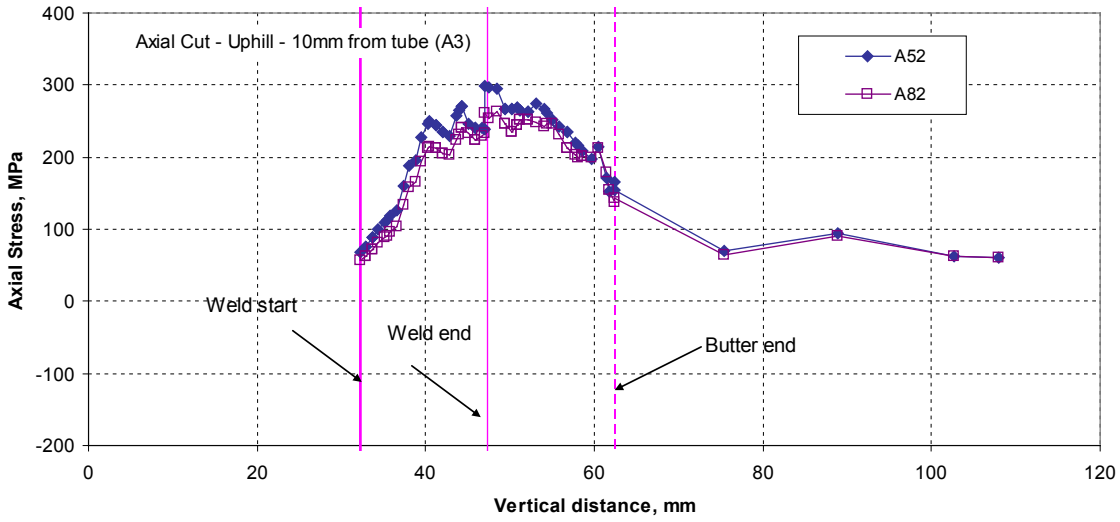

(b) Line A3 10-mm from tube

Figure 3-21 Axial stress line plots along axial lines A2 and A3.

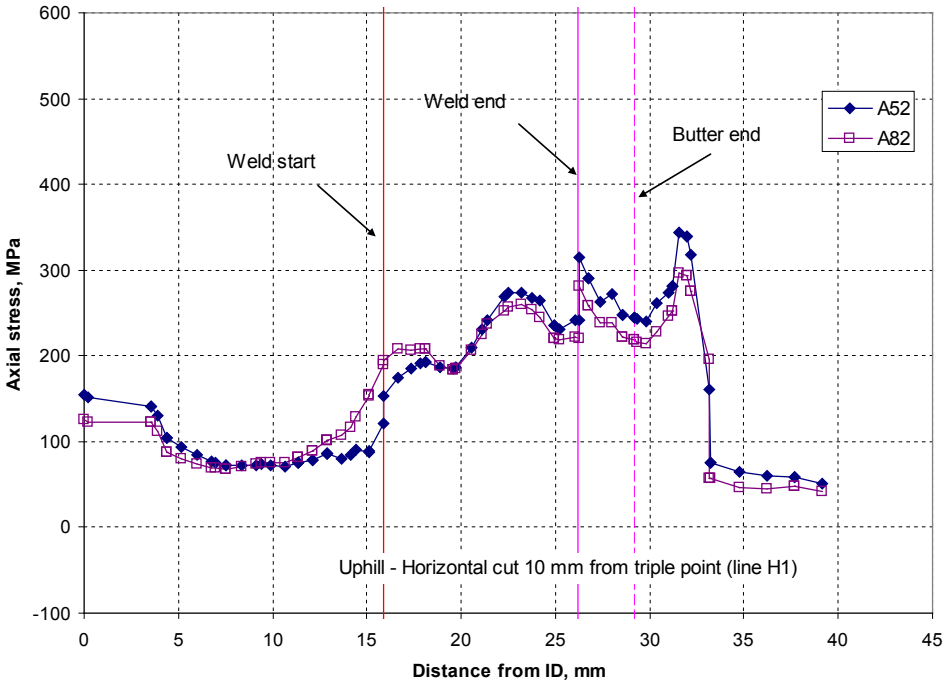

(a) H2 at triple point (see Figure 5)

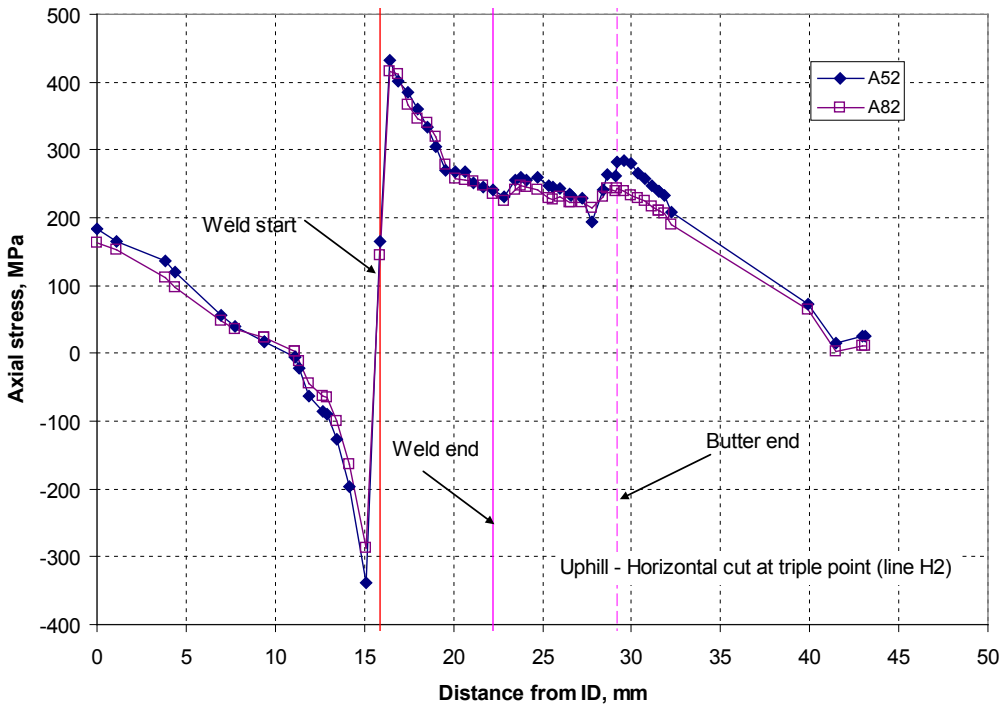

(b) H1 5-mm below triple point (Figure 5)

Figure 3-22 Axial stress line plots along horizontal line

4. Fracture Assessment and the Finite Element Alternating Method

The objective of this effort was to conduct flaw evaluations for simulated flaws in the welds of reactor pressure vessel head penetration nozzles. Indications have been found in some replacement heads being fabricated from Alloy 690 material and compatible weld metals, Alloy 52/152. In one recent investigation, flaws were found in every single nozzle/head weld ranging from 5 to as many as 22 cracks per nozzle. The sources of these weld fabrication indications are believed to be slag inclusions in the weld metal along with micro-fissuring and possible hot cracking during the weld deposition process. However, since there are numerous indications and some are quite long (more than 50 mm in length), it is believed that some of these indications may be caused by additional mechanisms such as hot cracking. The observed indications were mostly circumferential in orientation but some axial indications were observed as well.

The volumetric UT scans of the one particular replacement head were able to document the crack length, location, but not the crack depths. Since the width of the embedded defect was not recorded, it was difficult to determine if the crack front was into the weld, or along the weld/tube interface. Therefore, analyses of a 53-degree nozzle welded with Alloy 52/152 filler metal with multiple cracks were performed. Because there are potentially many cracks in the welds, it is important to determine if these cracks are critical and if multiple crack interactions can cause problems. The methods to perform crack assessment for as many as 24 cracks in a J-weld using the finite element alternating method are summarized here.

The stress intensity factors, K_I, K_{II}, and K_{III} must be determined in order to perform PWSCC assessment. There are many methods for obtaining the stress intensity factors for given crack geometries including:

1. *Closed form solutions*. There are a number of fracture handbooks which list formulae for stress intensity factors for different crack geometries obtained from classical methods of elasticity theory. Due to the mathematical complexity of these solutions, they are only available for rather simple geometries.
2. *Numerical or finite element methods*. Today finite element methods are often used to obtain stress intensity factors for crack geometries which are outside the range of handbook solutions. There are many handbooks which compile stress intensity factors for a large number of cracks in specific geometries from finite element solutions. Some handbooks and computer codes combine libraries of closed form solutions and numerical solutions for use in a fatigue assessment. For instance, K solutions are compiled for surface cracks in pipes for pressure, tension, and bend type loads for cracks of many different sizes. For complex geometries that exist in the RPVH, finite element methods of some type specific to the unique geometry must be used.
3. *Finite element alternating methods (FEAM)*. FEAM represents a combination of finite element methods (for an un-cracked body) and analytical methods to obtain K. The finite element alternating method is very convenient for obtaining K for problems where multiple cracks must be assessed. Using classical finite element methods to calculate K for multiple cracks is quite tedious. FEAM details are discussed next.

4.1 The Finite Element Alternating Method

It is useful to provide a discussion of the finite element alternating method (FEAM). FEAM, developed in the aerospace industry, is a convenient method for calculating stress intensity factors for cases where multiple cracks are present. FEAM is an efficient and accurate method to solve multiple crack problems. The finite element mesh does not include the crack geometry, thus simplifying mesh generation and allowing one mesh to be used for a variety of crack sizes and orientations. Three-dimensional embedded elliptical cracks and part-elliptical surface cracks can be modeled as well as two-dimensional embedded and surface cracks. By incorporating the analytical solution for an elliptical crack in an infinite body, Mode I, II, and III stress intensity factors are computed without recourse to contour or surface integrals. For this study, the focus is stress re-distribution after putting multiple cracks in the weld. The method itself is efficient because the finite element stiffness matrix needs to be decomposed only once even if the crack geometry changes. Multiple crack analyses were conducted for both center-hole and side-hill nozzles. Sensitivity analyses of different crack numbers and mesh refinement studies were thoroughly studied for the center-hole case. Extensive research work was performed to develop the FEAM method and it is now used with confidence in the aerospace community [20, 21 and 22].

The fundamental mathematical concept of the alternating method has been known for more than one hundred years. The method is quite general in that it can be applied to a wide range of elasticity problems. Schwartz's [23] original solution for two overlapping domains (or geometries) involves using known solutions for two separate geometries to obtain the solution for the more complex geometry obtained by partially overlaying the two regions. One may consider this as the solution for the union of the two original regions and the overlay region (Figure 4-1(a)). Neumann [24] modified this concept to obtain the solutions for the intersection of the two geometries (Figure 4-1(b)). Neumann's observation is particularly useful since one of the domains can be an infinite domain where many closed form solutions exist (Figure 4-1(c)). With the finite element alternating method, the solution for a crack in an infinite solid loaded via arbitrary crack face tractions (Figure 4-1(c), left) serves as the infinite domain solution (the so called "VNA solution", which is quite complicated mathematically) while the finite domain solution is represented by the finite element portion of the solution (Figure 4-1(c), middle). This is the source of the name Schwartz-Neumann finite element alternating method. It is noted that most current applications of the alternating method are for solving crack problems, although other difficult problems could be considered as well.

The current finite element alternating method (FEAM), which is summarized in References 25, 26, and 27 is the state of the art method for obtaining stress intensity factors for three dimensional surface and embedded crack problems and for two dimensional problems. Early versions of the method emerged in the late 1960's through the work of Kobayashi and co-workers [27]. However, the method was somewhat limited because the analytic solution was incomplete until Vijayakumar and Atluri [28] developed the complete solution for an elliptic crack in an infinite solid subjected to *arbitrary order surface tractions*. During the last twenty years the method has been completely accepted as a practical computational tool to investigate fatigue and fracture problems in industry. The method has recently been extended to handle two and three-dimensional elastic-plastic and creep problems where the J-Integral and other fracture parameters may be evaluated for both stationary and growing cracks. All of these features are

present in the version of the software program ALT3D used here [30], but only the calculation of elastic stress intensity factors, re-distributed stresses, and crack opening displacements were calculated here.

Figure 4-2 schematically illustrates the FEAM method. The finite element portion of the solution, Figure 4-2 (top left) illustrates a bimetal pipe. Weld residual stresses combined with service loads (which could be displacement loading, thermal gradients, etc.) represents the first (finite element) solution for the un-cracked body. From this solution, crack face tractions are automatically calculated. These then serve as the loading for the closed form infinite body problem with an elliptical crack. The infinite domain solution is actually the complete closed form solution for an elliptic crack in an infinite solid subjected to arbitrary order surface polynomials. The major advantage of the method, as seen in Figure 4-2 is that a finite element mesh of *the un-cracked geometry* is all that is needed. The mixed mode stress intensity factors are obtained naturally from this procedure. The upper right illustrates the crack growth solution for a fan blade. The lower left illustrates solutions for crack growth in a turbine blade. The

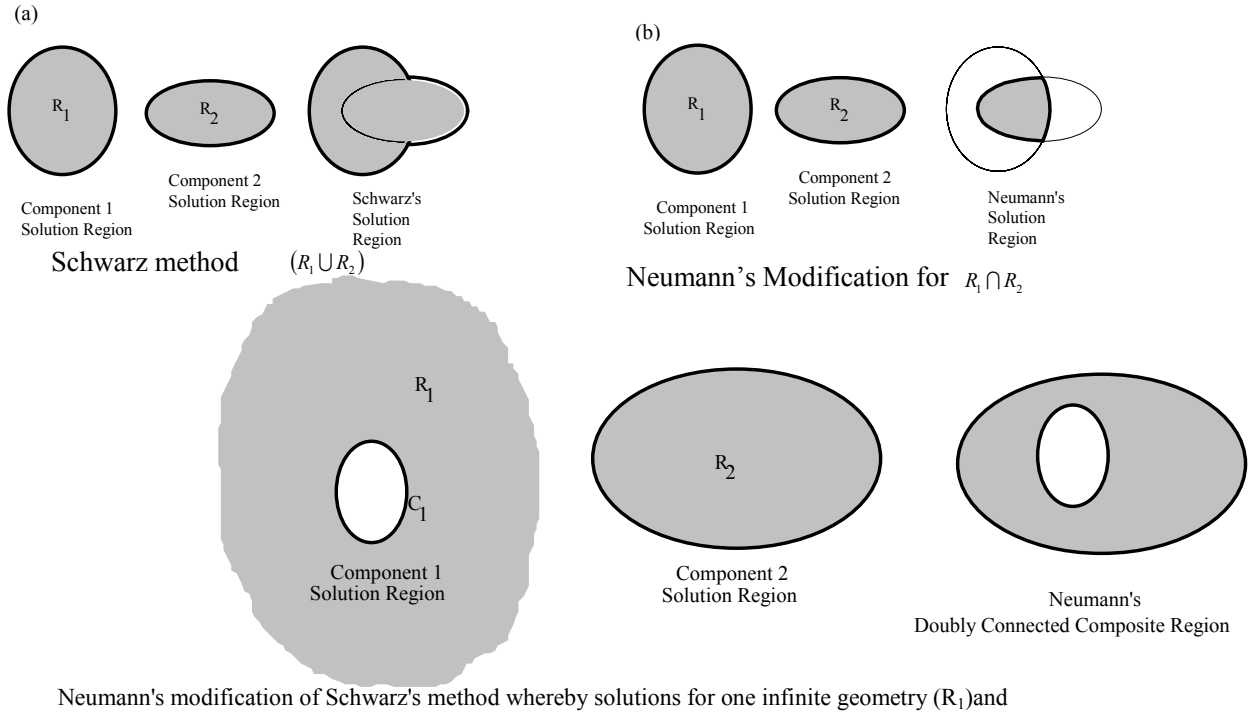

Figure 4-1 Alternating Method (Theory Based In Elasticity Theory (see for instance Krylov-Kantoravich [29]))

intersection of the ellipse with the structure defines the crack. As such, arbitrary crack shapes are possible. This is illustrated further in the lower right hand illustration in Figure 4-2.

The most important aspect of FEAM is that the same mesh can be used to obtain solutions for many different crack sizes, locations, and for multiple cracks. Because the finite element stiffness matrix only needs to be reduced once regardless of the crack size, crack location, crack

orientation, crack number (mixed mode conditions can be handled as well), etc., the method is extremely efficient.

Some attractive features of FEAM include:

- The finite element mesh does not include the crack geometry; thus simplifying mesh generation and allowing one mesh to be used for a variety of crack sizes and orientations.
- 3D embedded elliptical cracks and part-elliptical surface cracks can be modeled as well as 2D embedded and surface cracks. In fact, any arbitrary portion of the ellipse only needs to intersect the component permitting quite arbitrary crack shapes to be considered.
- Mode I, II, and III stress intensity factors are computed without recourse to contour or surface integrals or to other means for indirectly computing stress intensity factors from energy release rates.

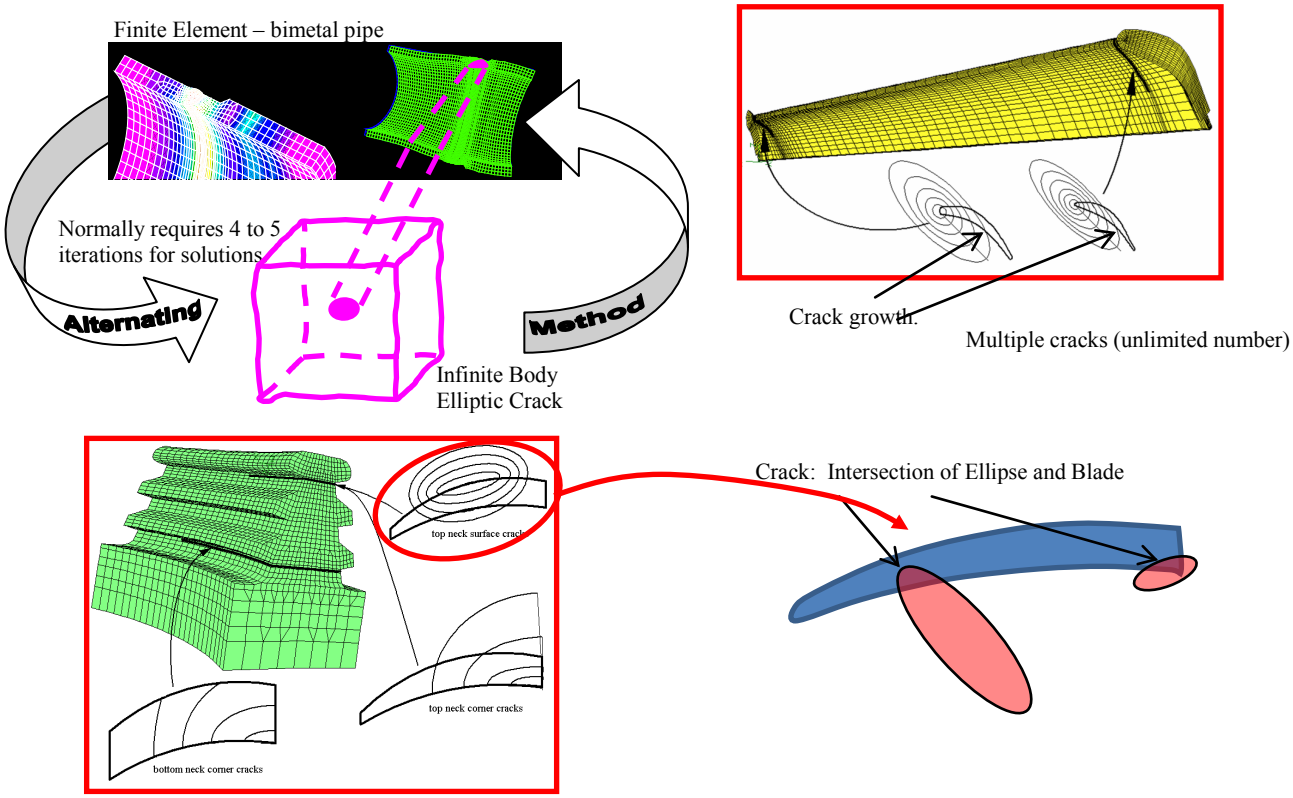

Figure 4-2 Illustration of the FEAM method.

- The finite element stiffness matrix needs to be decomposed only one time (even if the crack geometry changes) thus making the method computationally efficient.
- Loading can include nodal forces, displacements, and temperatures, normal and shear element surface tractions, angular velocity, linear acceleration, initial/residual stress.

- Multiple cracks can be defined and thus problems and interacting cracks can be solved.
- Multiple materials can be defined so that solutions for cracks near a material interface can be obtained.
- Penalty function methods are provided for modeling complex boundary conditions and constraints.
- For weld residual stress crack growth prediction, redistribution of the stresses is automatically accounted for when evaluating K for growing cracks.

In this study, the developed FEAM software ALT3D [30], which has many attractive features, was used.

5. Analysis of Indications in RPVH

The fabrication indications in the RPVH nozzles were modeled as a series of cracks in this section. Certainly, if the indication is a slag inclusion this is a conservative assumption since a crack would be a 'worse case' indication. The analyses were performed by simulating cracks occurring at different locations and by varying the number of cracks. The locations of the indications are defined from recent typical plant measurements that were made as part of a RPVH replacement. An example of the type of indications found in heads from ultrasonic testing (UT) scans is shown in Figure 5-1. The indications were considered to be cracks as shown in Figure 5-1 for the specified Penetration 59 are typical of what can be found and were used here to illustrate the effect. The cracks are numbered, with the 0- and 360-degree positions at the bottom of the penetration. Because of the symmetrical nature of the FEA model, only the cracks in the range of 180 degree to 360 degree are considered, in which there are 12 cracks, i.e. Crack 7 to Crack 18. This means that there were actually 23 cracks in the full model due to this assumption of symmetry (Crack 18 is an embedded one symmetrical to mesh symmetry plane). The crack locations from typical measurements are for different types of nozzle configurations. The crack orientation is defined such that the circumferential crack is opened by axial stress and the axial crack is opened by hoop stress. Some cracks are not ideally circumferential, i.e., a slight angle exists between the crack plane and the circumferential direction. However, for convenience sake, these cracks will be referred to as circumferential cracks. All cracks of Penetration 59 are circumferential cracks. Table 2 lists all of the cracks and their locations. Among those Crack 18, Crack 17, Crack 16 and Crack 15 are embedded cracks defined from 0 to 360 degrees. Crack 13, Crack 14, Crack 10, Crack 12, Crack 11, Crack 9, Crack 8, and Crack 7 are referred to as circumferential cracks, defined from 0 to 180 degrees.

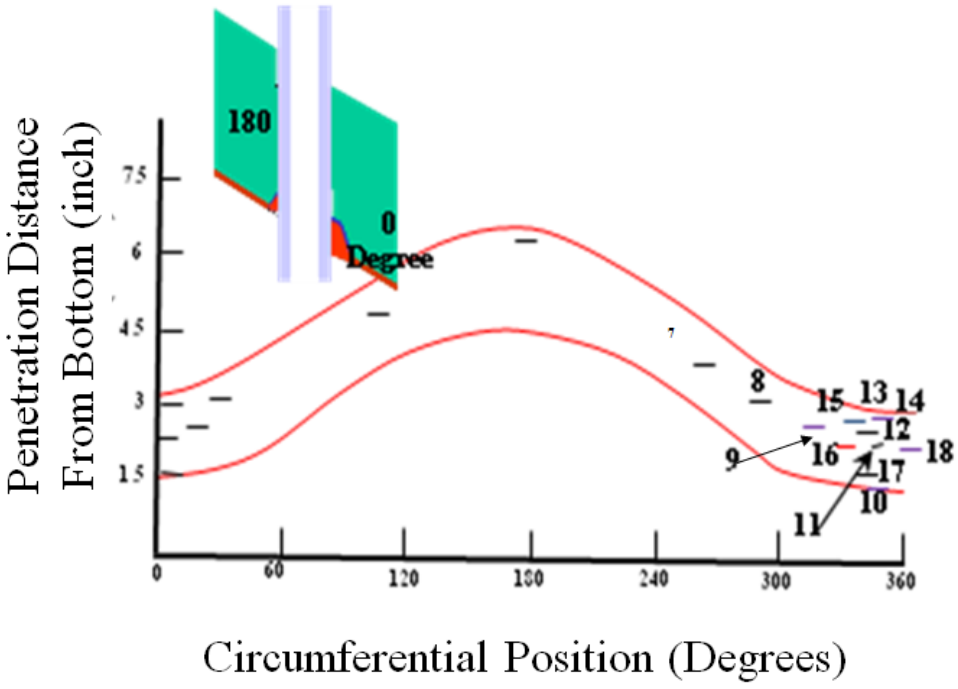

Figure 5-1 Weld profile and crack distribution of Penetration 59

Table 2 Crack distribution of Penetration 59

Crack #	Crack length (mm)	Crack depth (mm)	Type	Crack center position	
				Disp. from weld bottom (mm)	Disp. from weld ID (mm)
18	11.53	3.0	Circ. (embed)	9.83	3.52
17	4.46	2.0	Circ. (embed)	9.83	6.16
16	4.55	2.27	Circ. (embed)	7.38	3.66
15	7.26	3.0	Circ. (embed)	15.68	4.44
14	2.67	0.667	Circ.	16.72	0
13	6.3	2.06	Circ.	9.83	0
12	6.452	3.0	Circ.	15.68	0
11	4.7	1.68	Circ.	12.83	0
10	16.0	1.9	Circ.	9.97	0
9	14.22	3.556	Circ.	14.38	0
8	7.1628	3.0	Circ.	15.16	0
7	4.446	2.0	Circ.	10.49	0

5.1 Preliminary FEAM Assessments

To begin the crack assessments of the RPVH using FEAM, several preliminary analyses were performed to determine proper mesh definition and for initial validation. A center-hole RPVH

case with the estimated weld material Alloy 52/152 was analyzed as a preliminary example prior to modeling several cases with the measured crack distributions discussed above. This analysis was actually performed using an axis-symmetric finite element model and the stress results are then rotated by an ABAQUS routine. This rotation of results is convenient since one can alter the rotation angles to permit more or less angular refinement in certain areas for the subsequent crack analysis. This will not be possible for other cases with other side-hill angles.

Figure 5-2 is the 3-D center-hole model and weld mesh (also refer to Figure 3-5). This model was generated by revolving the axis-symmetrical mesh used to perform the weld analysis in a circumferential direction. The revolving interval is 5 degrees. The total number of nodes is 89,910 and the total number of elements is 80,388. Performing a full three dimensional weld analysis of this case using the geometry shown in Figure 5-2 would be time consuming and the axis-symmetric model for the center-hole case is a reasonable approximation. Multiple crack cases were studied using the finite element alternating method (FEAM), which was discussed in Section 4. It is important to transfer the stress components from cylindrical coordinate system produced by ABAQUS during mesh revolution to a Cartesian coordinate system, which is required in the FEAM code [30].

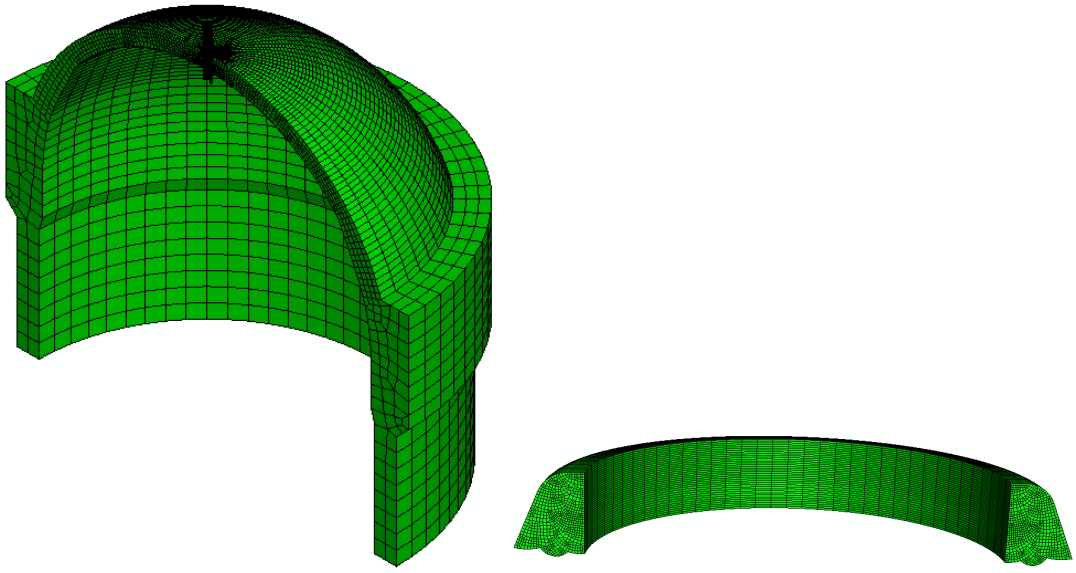

Figure 5-2 3-D model and weld mesh

5.1.1 Two Crack Case.

The first case studied is a two-crack case. The two surface cracks (defined from 0 to 180 degrees) are shown in Figure 5-3(a). Figure 5-3(b) and Figure 5-3(c) show the definition of crack dimensions and the crack ellipse in the global model. The FEAM method introduces elliptical or part-elliptical cracks into the mesh and then calculates the mixed mode stress intensity factors along the length of the crack. For the crack (half-ellipse) shown in Figure 5-3(b), the stress intensity factors are reported as a function of angle from 0 to 180-degrees. (In all cases, the long ellipse direction is 0 degrees.) For embedded cracks, the results are reported

for angles ranging from 0 to 360-degrrees. For other cases, the results are shown for the actual physical dimension of the crack as the ellipse intersects the actual body. Many of the cracks of interest here are embedded cracks, where K will be reported from 0 to 360-degrees. For this case, the crack length is 6-mm and the crack depth is 4-mm. These two cracks are put in symmetrical locations in the model because the stress intensity factors for both cracks must be identical. This verifies the accuracy of the code. At first, the K values were not identical during the early analyses. After extensive study, it was found that this was due to the difference in coordinate definitions for the stress components between ABAQUS (cylindrical) and FEAM (Cartesian). From a theoretical point of view, the stress intensity factors of two cases have to be identical. Figure 5-4 shows the plots, which are identical. It verifies the FEAM software can capture the symmetrical nature of the solution and helped FEAM validation efforts.

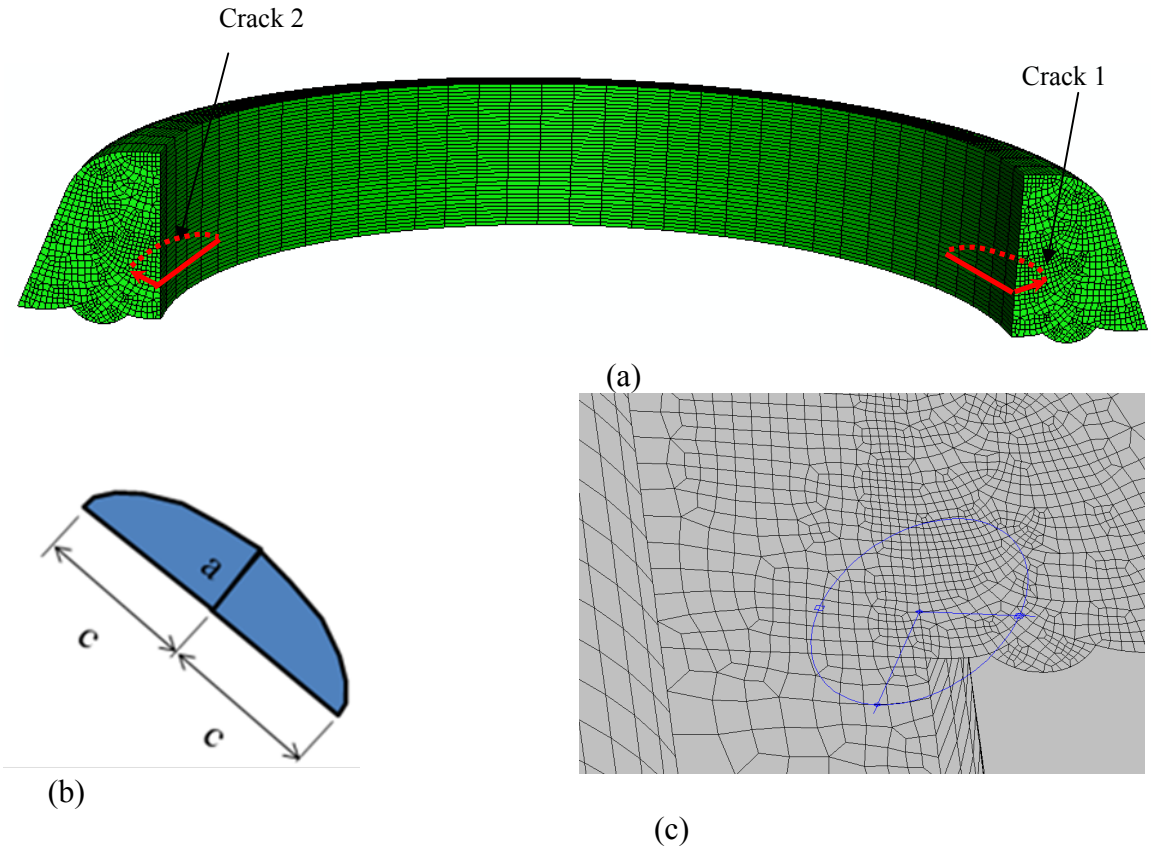

Figure 5-3 Two surface crack locations

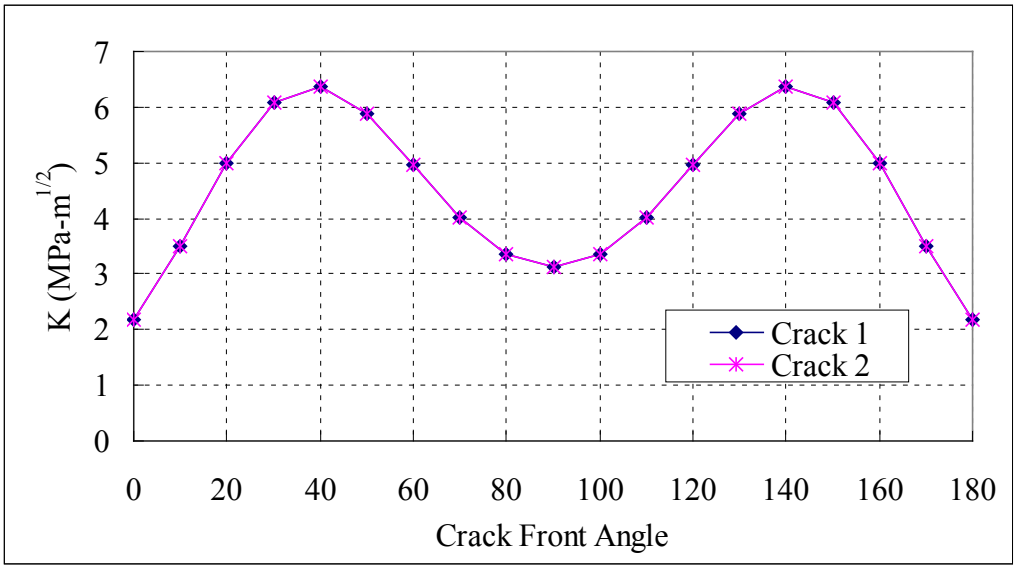

Figure 5-4 Stress intensity factors (K_I) for different crack front angles

5.1.2 Four Crack Case.

Several examples with 4 cracks were also studied as part of the validation effort. The four are defined as embedded cracks. Figure 5-5 is the top view of weld mesh. In this case the axial cracks are defined along the radial direction. The length of each of the circumferential cracks (Crack 1 and Crack 3) is 6-mm and the depth is 4-mm; the length of each of the axial cracks (Crack 2 and Crack 4) is 8-mm and the depth is 6-mm. Figure 5-6 shows the plots of results. The K-values of axial cracks are larger than those of circumferential cracks. Again, as seen by the identical results shown in Figure 5-6, the symmetrical property is maintained. It is also seen that, for this case and crack location, the stress intensity factors for the 'radial' cracks, Cracks 2 and 4, driven by the hoop stresses, are much larger than those for Cracks 1 and 3, where crack closure is occurring since the radial weld residual stresses are slightly less than zero at these locations.

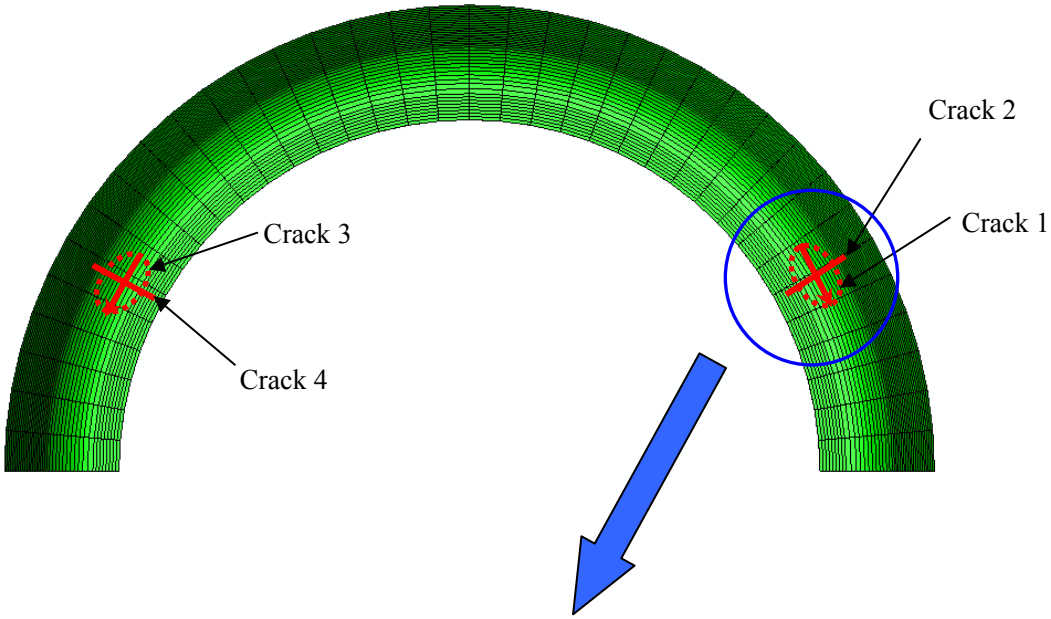

(a)

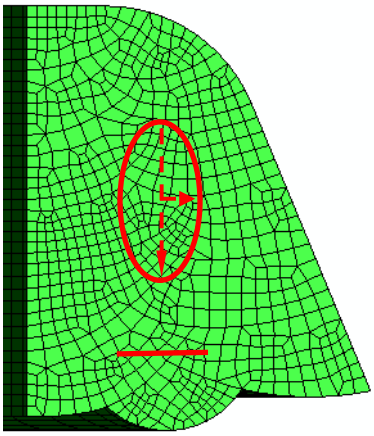

(b)

Figure 5-5 Four symmetrical embedded cracks (top view, axial cracks along radial directions)

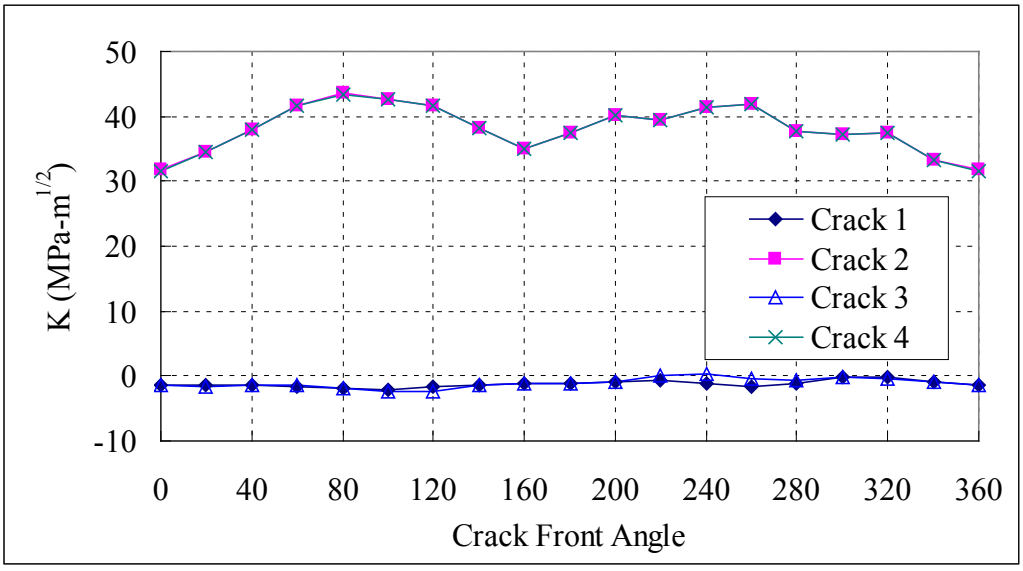

Figure 5-6 Stress intensity factors (K_I) for different crack front angles

The above studied cracks can also be distributed along a Cartesian coordinate direction, defined in Figure 5-7. For this case, K_I, K_{II}, K_{III} and K_{eq} are plotted in Figure 5-8 , Figure 5-9 and Figure 5-10. From these figures, K_I is larger than K_{II} and K_{III}; but the K_{II} and K_{III} are not negligible. Because Mode-II and Mode-III are due to shear stresses and shear stresses are symmetrical in the model, K_{II} and K_{III} are also symmetrical with different sign. As such, the comparisons in Figure 5-9 and Figure 5-10 are perfect, further verifying the FEAM procedure.

It is also important to point out that the magnitudes of the stress intensity factors are not small. For K_I in the range greater than 20 Mpa-$m^{1/2}$, PWSCC will occur in Alloy 82/182 weld material. For Alloy 52/152 replacement weld material, PWSCC can also occur, although at a much slower rate compared to Alloy 82/182. Hence, if a fluid path did exist to the cracks examined here, PWSCC could indeed occur.

It is also important to note that PWSCC is assumed to occur for cracks growing in Mode I, or opening mode, conditions. Mixed mode crack growth has not been examined in developing the PWSCC crack growth rate data, although for real welds, mixed mode conditions will exist because weld residual stresses produce shear stresses as well as normal stresses. When cracks interact, as for multiple cracks, mixed mode will occur. For mixed mode conditions, the normalized equivalent stress intensity factor is postulated. Figure 5-11 shows a plot of the equivalent stress intensity factors for these cracks. The equivalent stress intensity factor is defined as the square root of the sum of the squares of the component stress intensity factors, or:

$$K_{eq} = (K_I^2 + K_{II}^2 + K_{III}^2)^{1/2}$$

and is assumed to characterize PWSCC for mixed mode cracks.

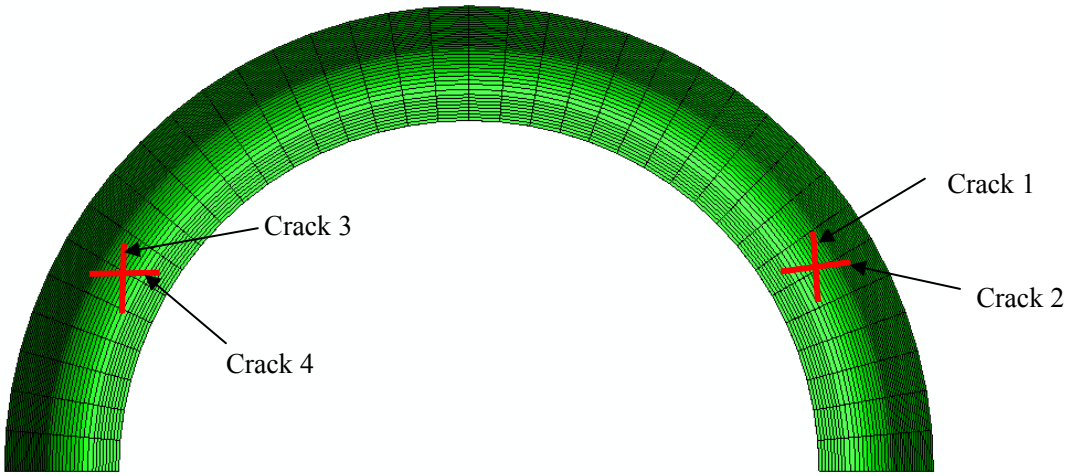

Figure 5-7 Four symmetrical embedded cracks (top view, axial cracks along radial directions)

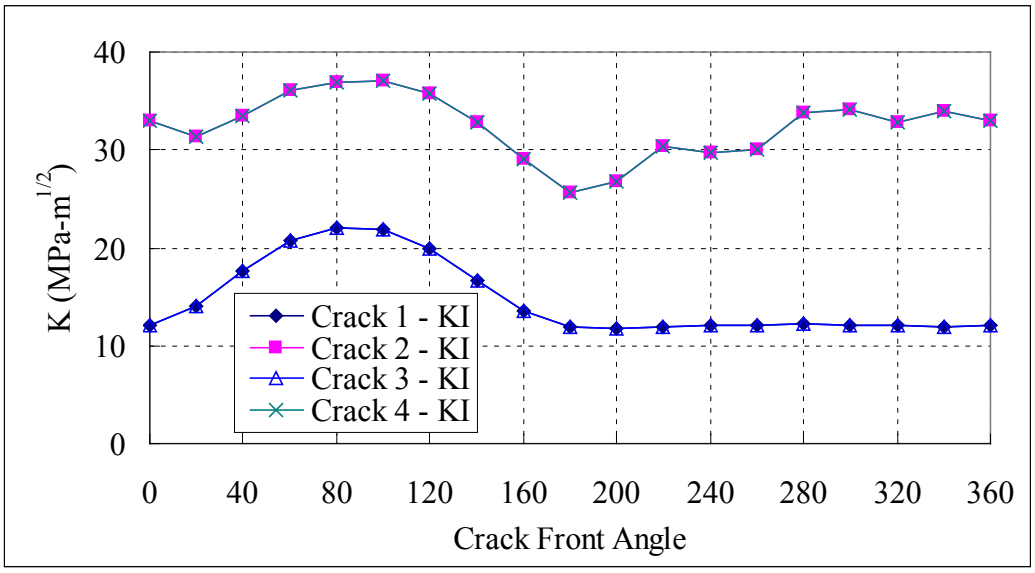

Figure 5-8 Stress intensity factors (K_I) for different crack front angles

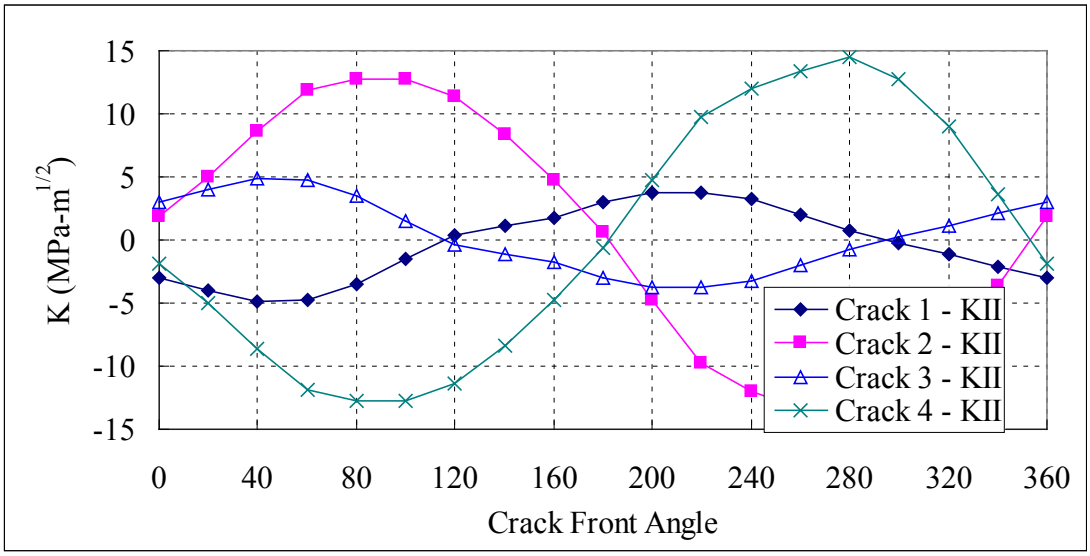

Figure 5-9 Stress intensity factors (K_{II}) for different crack front angles

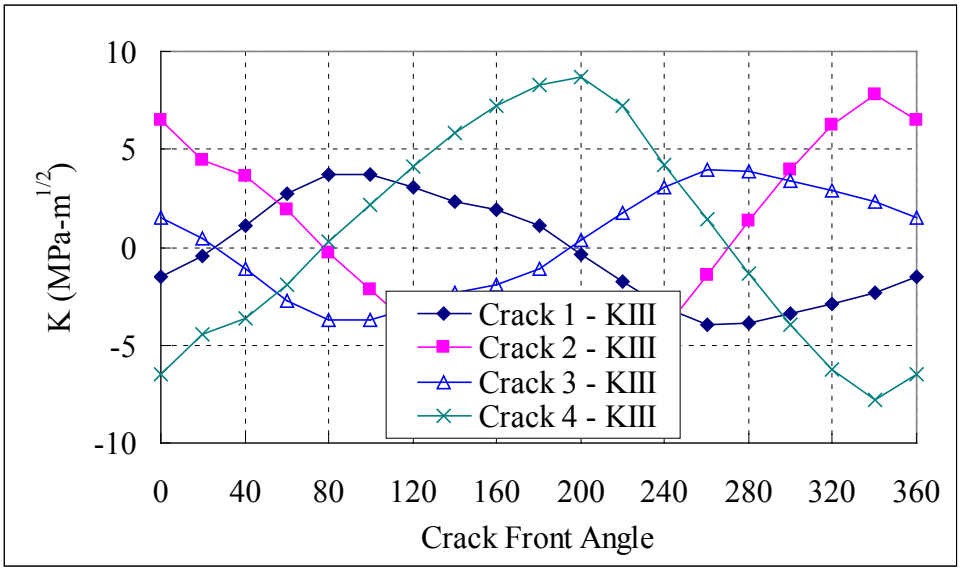

Figure 5-10 Stress intensity factors (K_{III}) for different crack front angles

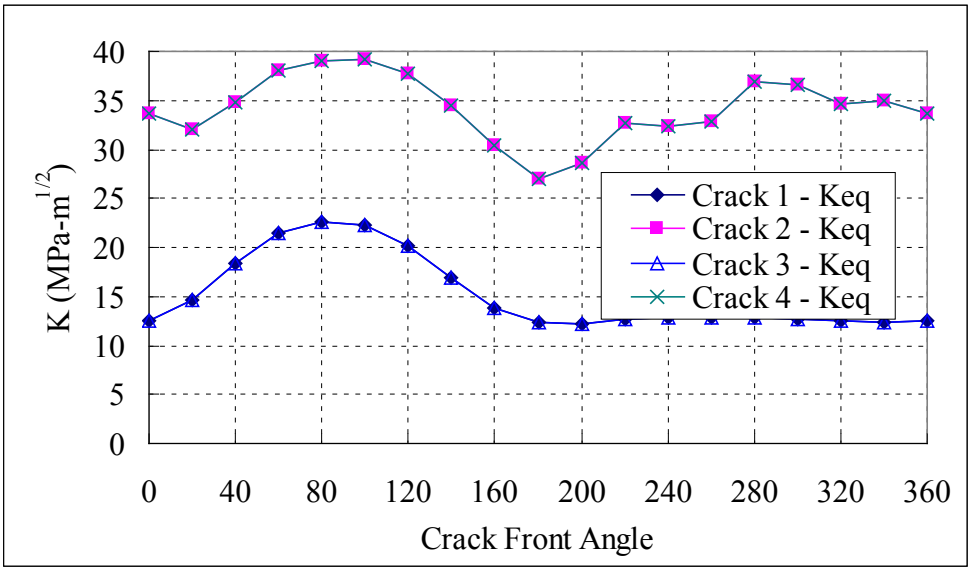

Figure 5-11 Stress intensity factors (K_{eq}) for different crack front angles

A more general case was also studied. The four surface cracks (defined from 0 to 180 degrees) are defined in Figure 5-12. In this case, Cracks 1 and 3 are not ideally circumferential, i.e., a slight angle exists between the crack plane and the circumferential direction. However, for convenience sake, these cracks will be referred to as circumferential cracks. The length and depth of each circumferential crack is 6-mm and 4-mm; the length and depth of each axial crack is 8-mm and 6-mm. For this case, K_I, K_{II}, K_{III} and K_{eq} are plotted in Figure 5-13, Figure 5-14, Figure 5-15 and Figure 5-16. Again, because the cracks are input symmetrically, the original solution was axis-symmetric and the weld residual stresses were mapped to the full 3D solution. For the FEAM assessment, Cracks 1 and 3 and Cracks 2 and 4 should provide identical results. It is seen that they do. These consistency checks were quite important in making sure the FEAM procedure was providing good results. Mixed mode effects play a small, but not negligible, role here.

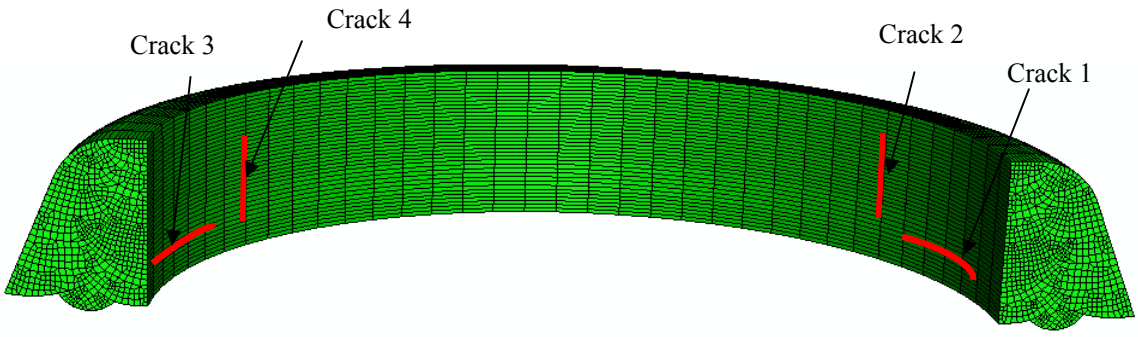

Figure 5-12 A general case of four surface crack locations

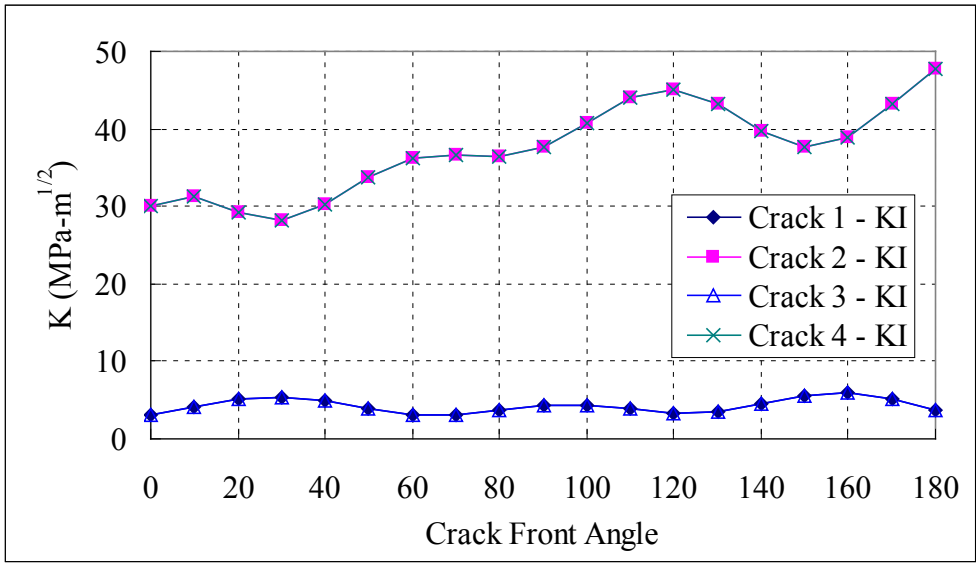

Figure 5-13 Stress intensity factors (K_I) for different crack front angles

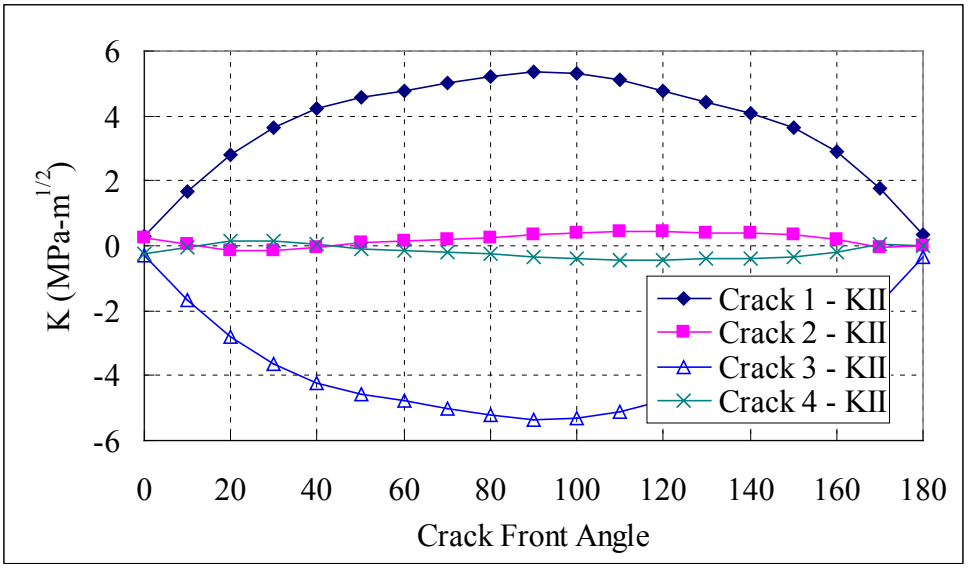

Figure 5-14 Stress intensity factors (K_{II}) for different crack front angles

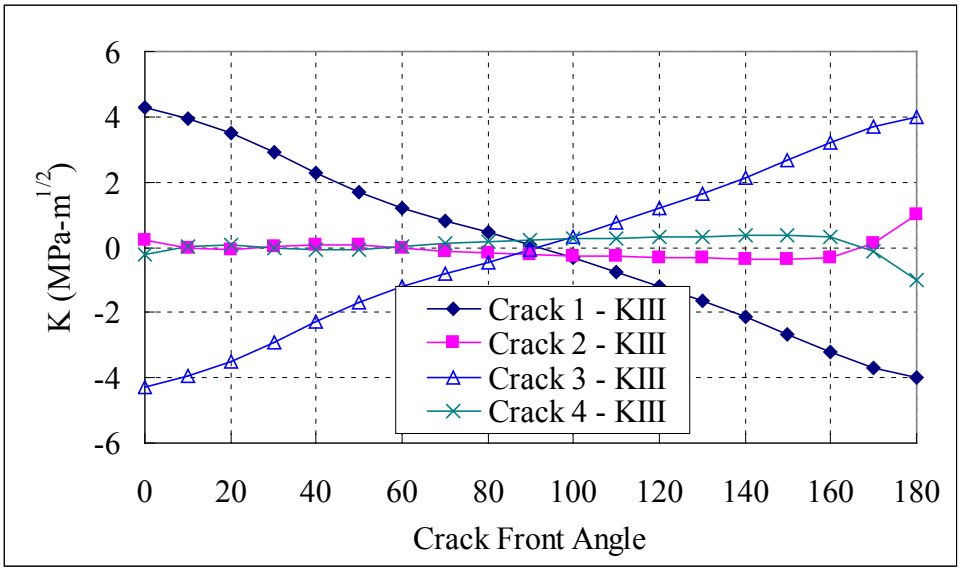

Figure 5-15 Stress intensity factors (K_{III}) for different crack front angles

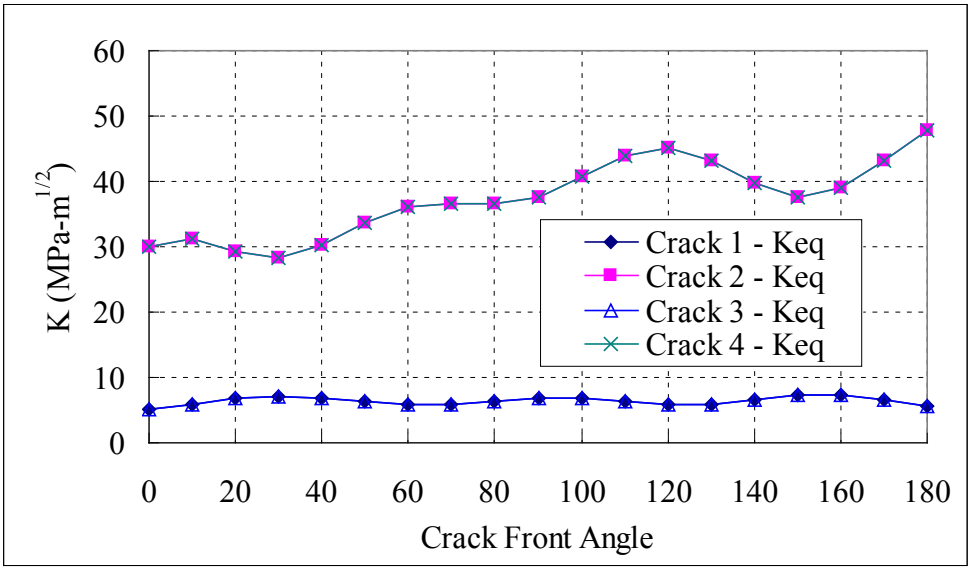

Figure 5-16 Stress intensity factors (K_{eq}) for different crack front angles

5.1.3 Mesh Density and Refinement Effects.

In the numerical simulations or the center-hole case, the mesh refinement sensitivity is a factor affecting solution accuracy. Since the ABAQUS code can generate three dimensional stresses for fracture analysis from an axis-symmetric weld analysis, it is convenient to use this model to examine mesh refinement needs so that FEAM results are accurate. This was examined by using

different mesh densities for the four crack problem, and an additional 5 crack problem. A new mesh shown in Figure 5-17 was generated. The model was generated using 25 2-degree divisions, 10 5-degree divisions and 8 10-degree divisions. The total number of nodes is 106,920; the total number of elements is 96,019 in this model. The four crack case (Figure 5-12) and a five crack case (not shown here) were revisited using this refined mesh. All the crack sizes and locations used are the same as reported above for the four crack case. The results of four crack cases are presented above. From the studies, all models gave similar results, though the mesh density is quite different. This suggests that quite accurate results can be obtained for meshes as coarse as 10-degree refinement in the 'theta' direction. For the cases considered next, 5-degree refinement is used for both the center-hole and 53-degree side-hill cases. Note that since the side-hill cases cannot be modeled with an axis-symmetric model, the mesh refinement for the weld modeling portion of the analysis had to use this same mesh refinement.

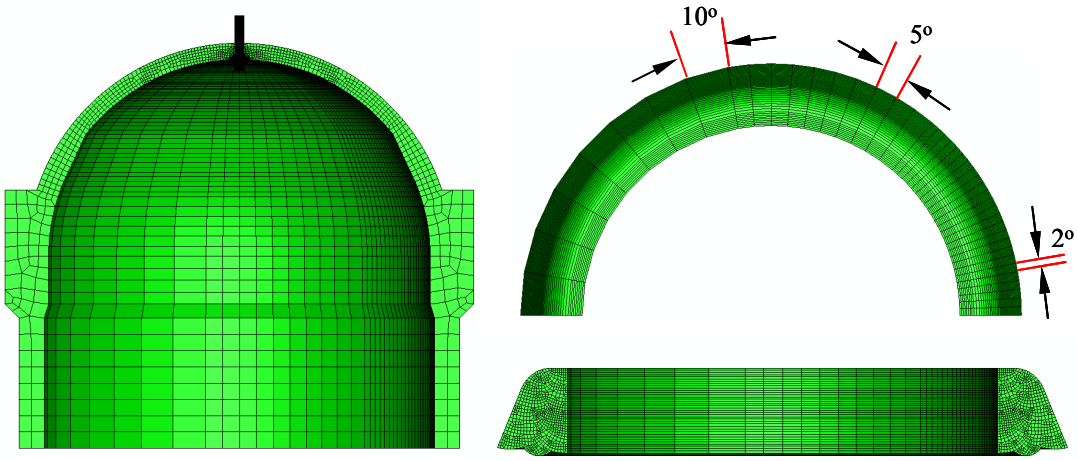

Figure 5-17 Center-hole model with different mesh densities in the hoop direction.

5.2 Center-Hole Case

As seen in Figure 1-1 and Figure 3-1, there are many penetrations in a reactor pressure vessel head. The center-hole case is an axis-symmetric case while the side-hill cases are for penetrations located at different locations away from the head centerline region. From the UT measurements of the replacement head penetration cracks, the center-hole had less cracking than did the side-hill penetrations. Figure 5-1 and Table 2 show a sketch of crack indications typical for one of the side-hill penetrations, labeled 'Penetration 59' here for reference. It is seen that most of the cracking occurs at the downhill or 0- and 360-degree locations in Figure 5-1, probably because welding with Alloy 52/152 is more difficult at these locations. Here, for the center-hole case, we will also assume a crack distribution for the side-hill case and examine the stress re-distributions and stress intensity factors for such cracking. All results are for operating temperature of 318 C and 17 MPa pressure applied.

A series of multiple crack analyses were performed by putting simulated cracks at different locations in the model and by varying the number of cracks. For brevity, only one example for center-hole nozzle is presented here. Two sets of results are shown in the next section for the side-hill case. The locations of the cracks are defined from UT measurements on a recent

replacement head plant. An example of the type of cracks found in heads is shown in Figure 5-1. The cracks shown are typical of what can be found and were used here to illustrate the effect. The cracks are numbered, with the 0- and 360-degree positions at the bottom of the penetration. Because of the symmetrical nature of FEA model, only the cracks in the range of 180 degree to 360 degree are considered, in which there are 12 cracks, i.e. Crack 7 to Crack 18 from Figure 5-1. This means that there were actually 23 cracks in the full model due to this assumption of symmetry (Crack 18 is an embedded symmetrical crack to the symmetry plane). The crack locations from measurements are for different types of nozzle configurations. The crack orientation is defined such that the circumferential crack is opened by axial stress and axial crack is opened by hoop stress. Some cracks are not ideally circumferential, i.e., a slight angle exists between the crack plane and the circumferential direction. However, for convenience sake, these cracks will be referred to as circumferential cracks, although they were placed in the model with the correct orientation. All cracks of Penetration 59 are circumferential cracks. Table 2 listed all the cracks and their locations. Among those: Crack 18, Crack 17, Crack 16 and Crack 15 are embedded cracks defined from 0 to 360 degrees. Crack 13, Crack 14, Crack 10, Crack 12, Crack 11, Crack 9, Crack 8, Crack 7 are referred to as circumferential cracks, defined from 0 to 180 degrees.

The stress components obtained from FEAM are the centroid values in every element. Figure 5-18 shows the stress S_{yy} (axial) contour plot. The stress units are MPa. It is seen in Figure 5-1 that most of the cracks are distributed around the center of the weld or above this point, where the axial stress (S_{yy}) is less tensile than those at bottom of the weld. From the contours, it is seen that all stresses redistribute around the crack location. Line stress plots are developed for the 25 degree and 65 degree locations. The line plot paths are defined in Figure 5-18(b), in which the solid line indicates the ID of the weld and the dashed line indicates the middle of weld at the same angle (right end is 0 degree and left end of the FEA model is 180 degree). Figure 5-19 shows the line plots of S_{yy} (axial stress) at the weld ID and middle of weld. Overall the stress trends are similar. The stress redistribution is not observed in the middle of the weld, where the stresses are almost identical, because the cracks do not penetrate at these locations. However due to stress redistribution around the crack locations, there are some fluctuations locally at weld ID. The magnitude of the local fluctuation is about 100 MPa according to the line plots shown in Figure 5-19.

Line plots at 0, 45, 90, 135 and 180 degrees at the weld ID are developed as shown in Figure 5-20. Dashed lines represent the results after cracks are added, while solid lines represent original welding residual stresses. In Figure 5-1, most cracks are distributed between 270 and 360 degrees (for FEA model, those locations are between 0 to 90 degrees). Therefore, the local stress fluctuations happen mostly between 0 to 90 degree locations. Stress changes are also visible at other angle locations, but they are minor. It is seen that the redistribution of stress after introduction of the cracks increases the stress state at some locations. Overall the stress trends are similar. However, due to the stress redistribution around the crack locations, there are some local stress fluctuations at the weld ID. The magnitude of the local stress fluctuation is about 100 MPa according to the line plots from Figure 5-20. Finally, the stress intensity factors for the center-hole case with 23 cracks were quite small in general for the cracks that were introduced. The largest values are for Crack 16 and are shown in Figure 5-21.

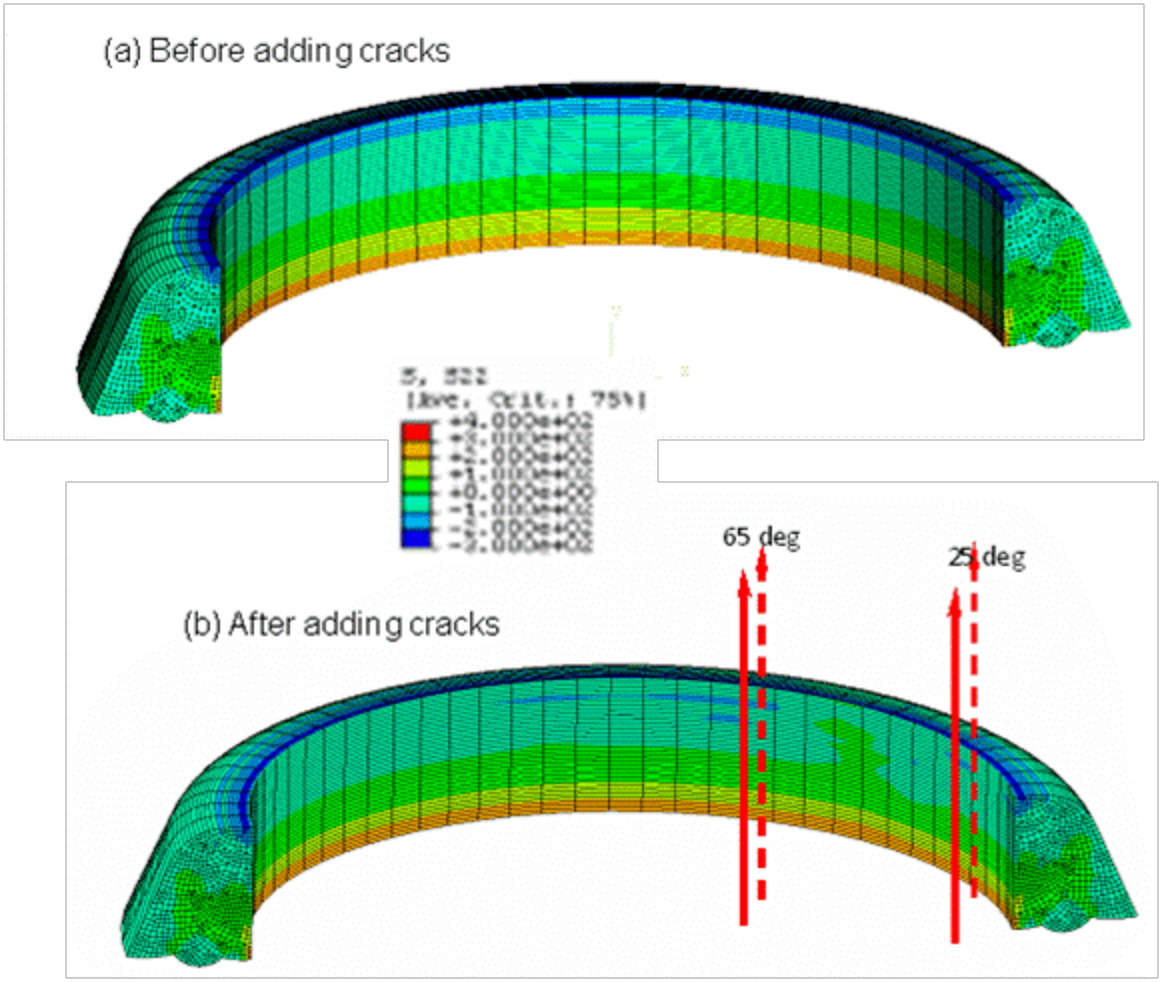

Figure 5-18 Center-hole case – axial stress contours (MPa) before and after adding cracks.

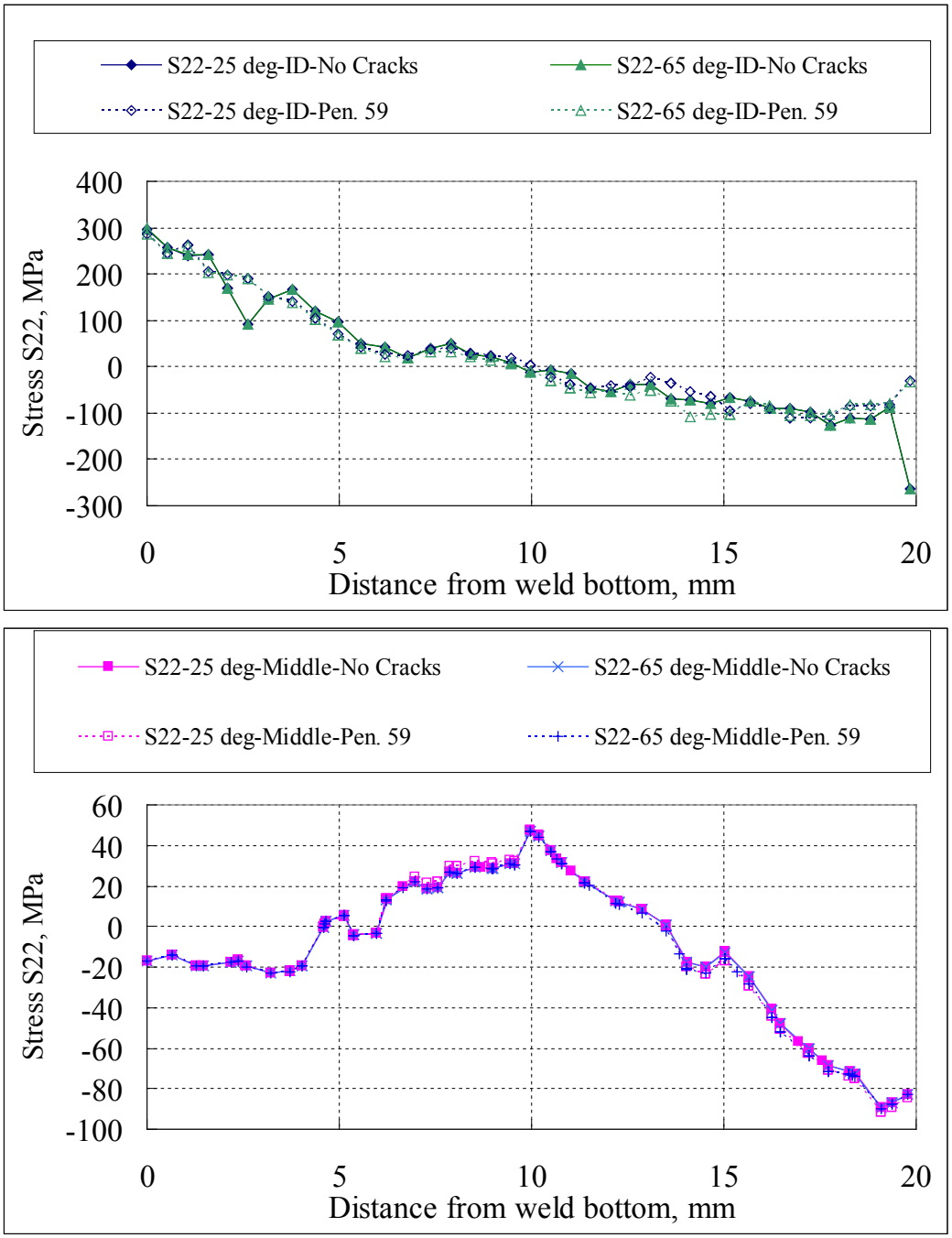

Figure 5-19 Line plots for S_{yy} (axial stress) at 25 and 65 degrees for Penetration 59 cracks.

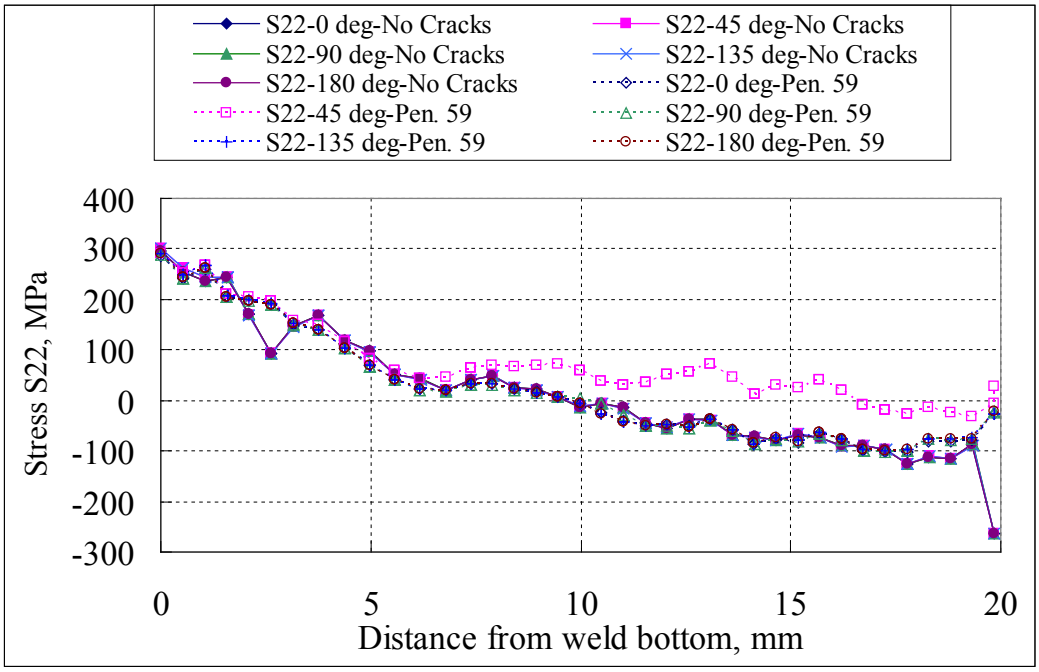

Figure 5-20 Axial stress line plots at different locations before and after crack introduction.

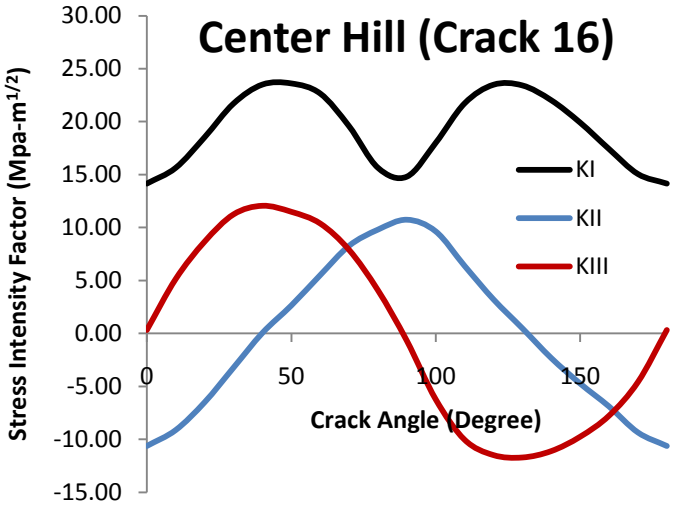

Figure 5-21 Stress intensity factors Penetration 59, Crack 16.

5.3 Side-hill Case

Figure 3-15 shows the FEA model and magnified view of the weld and tube for the 53-degree side-hill case. The tube inner diameter (ID) and outer diameter (OD) are shown along with the welds on the uphill and downhill sides of the tube. Multiple crack analyses were conducted for different cases: Penetration 59 (see Figure 5-1 and Table 2) and for Penetration 67 (Figure 5-34, and Table 3) illustrate the crack sizes, shapes, and locations. It is emphasized that these are typical for the crack measurements of two of the side-hill penetration cases which had indications identified via UT. They do not represent exact measurements, but are typical of what was seen. Moreover, the welding process for replacement heads using Alloy 52M/152 today is better, resulting in fewer cracks with today's processes. However, the effect of the possible cracks needs to be examined.

5.3.1 Case of Penetration 59.

The locations of the cracks are defined from Figure 5-1 and Table 2, with the cracks colored and numbered. The designation of 'Penetration 59' is arbitrary, but represents a side-hill case. Because of the symmetrical nature of FEA model, only the cracks in the range of 180 degrees to 360 degrees are considered, in which there are 12 cracks, i.e. Crack 7 to Crack 18. This means that there were actually 23 cracks in the full model due to this assumption of symmetry (Crack 18 is an embedded symmetrical crack in the symmetry plane.)

The crack orientation is defined such that the circumferential cracks are opened by axial stresses and axial cracks are opened by hoop stress. Some cracks are not ideally circumferential, i.e., a slight angle exists between the crack plane and the circumferential direction. However, for convenience sake, these cracks will be referred to as circumferential cracks even though the FEAM model included the correct orientation. These slanted cracks tend to produce more mixed mode stress intensity factors. All cracks of Penetration 59 are circumferential cracks. Table 2 lists all the cracks and their locations. Among these cracks, Crack 18, Crack 17, Crack 16 and Crack 15 are embedded cracks. Embedded cracks are defined from 0 to 360 degrees since stress intensity factors result along the entire 360-degree crack front. Crack 13, Crack 14, Crack 10, Crack 12, Crack 11, Crack 9, Crack 8, and Crack 7 are referred to as circumferential cracks, defined from 0 to 180 degrees since they do not penetrate the tube. Figure 5-22 (left) shows the schematic of different crack locations and Figure 5-22 (right) describes the path definitions for stress line plots that will be reported later from FEAM analyses.

The stress components obtained from FEAM analysis are the centroid values in every element. Figure 5-23 shows the von Mises stress contour plots before and after introduction of the cracks. Note that there is stress redistribution mainly in the crack region, but some of the stress redistribution does occur away from the cracks. Figure 5-24, Figure 5-25, and Figure 5-26 show the axial, hoop, and radial stress contour plots before and after introduction of the cracks. Note that hoop stresses do not redistribute much after addition of the cracks since all cracks were axial. The stress units in this study are MPa and the plots on the left show results with no cracks while plots on the right provide results with cracks added. It is seen from Figure 5-1 that most of the cracks are distributed around the center of the weld or above, where the axial stress is less tensile than those at the bottom of the weld. From the contours, it is clear that stress redistribution occurs. Among these cracks, the stress intensity factors of Crack 18, Crack 16 and

Crack 7 are presented because the stress intensity factors are positive, i.e., opening, while the rest of the cracks experienced closing. This is an important observation since the cracks were introduced during the welding process (not due to PWSCC in a tensile weld residual stress field). Figure 5-27, Figure 5-28, and Figure 5-29 show the K_I, K_{II}, and K_{III} plots for Cracks 18, 16, and 7. It appears that Mode II and Mode III are dominant for these three cracks. The shear modes are invoked due to both crack interaction and shear stresses in the models. For Mode I PWSCC crack growth, which is what all growth laws are based on, crack growth tends to occur for values of K_I on the order of 20 MPa-in$^{1/2}$. This suggests that the cracks should not grow much, if at all in Alloy 52 even if there was a fluid path to these cracks.

Line plots of axial, hoop, radial, and von Mises stress are presented in Figure 5-30, Figure 5-31, Figure 5-32, and Figure 5-33. The paths are defined in Figure 5-22 (right). Path A1, starting from tube OD towards the outside, is located at about 1/3 of the weld height. Path A2 passes through Crack 18. Path A3, starts from the middle point of the weld top and moves towards the weld bottom. Overall the stress trends are similar to those before adding cracks. Cracks introduce more local fluctuations of stress in the weld. The magnitude of these local fluctuations is around 70 MPa. Hence, for PWSCC assessment of a dominant crack (where many cracks link), modifications to the applied residual stress fields may be necessary.

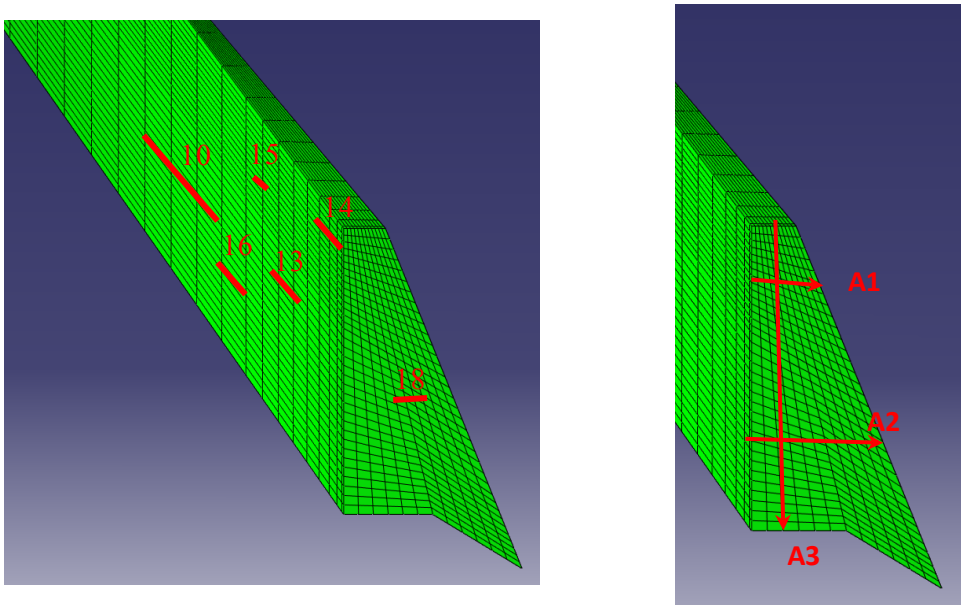

Figure 5-22 Schematic of crack locations and path definition for line plots

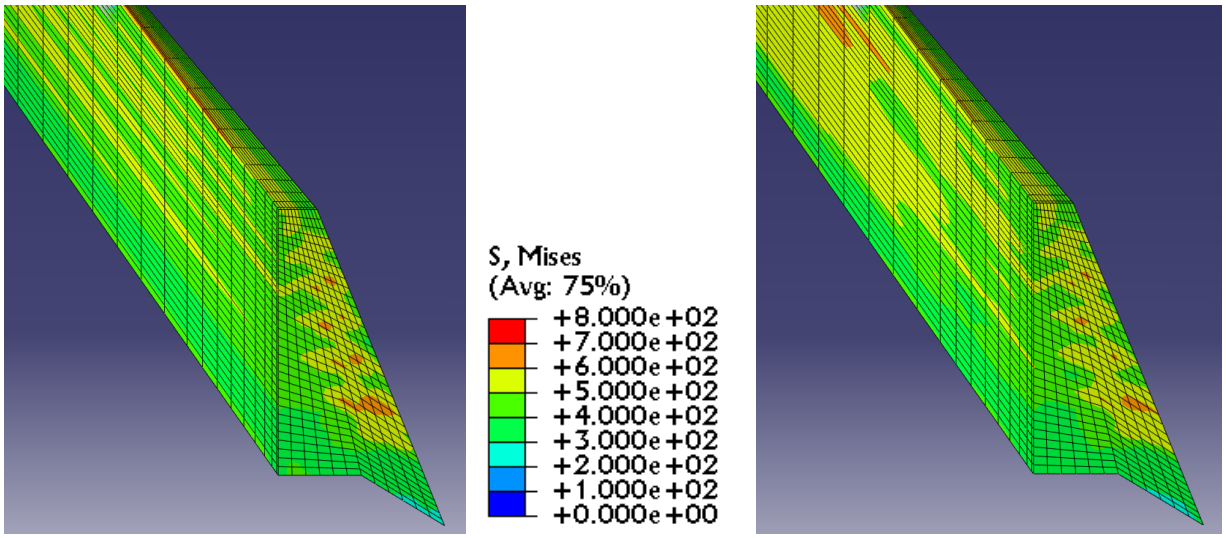

Figure 5-23 Von Mises stress (MPa) (a) before adding cracks, left (b) after adding cracks, right

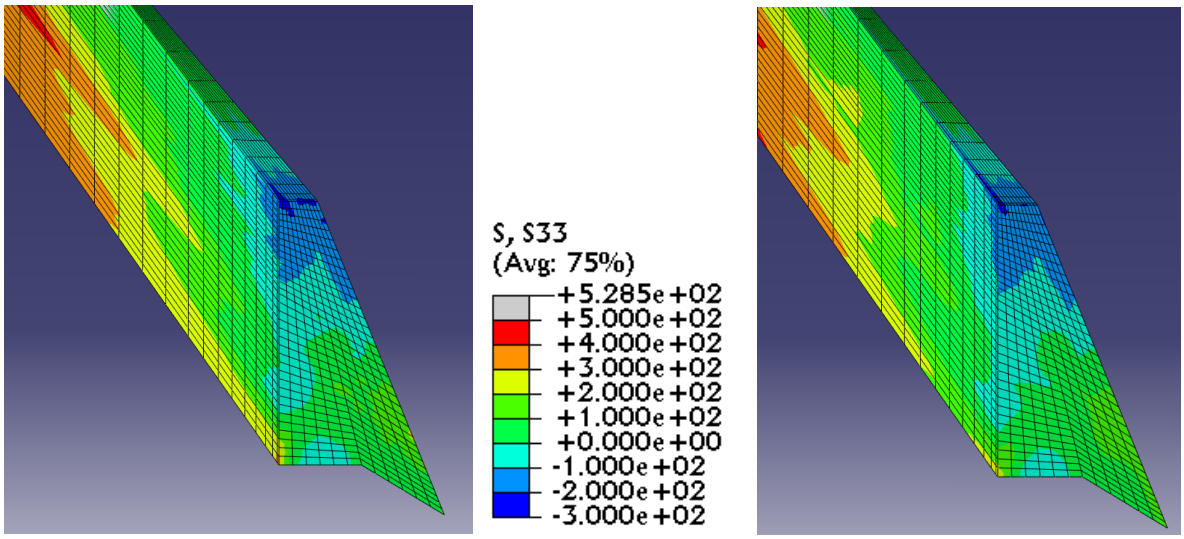

Figure 5-24 Axial stress (MPa) (a) before adding cracks, left (b) after adding cracks, right

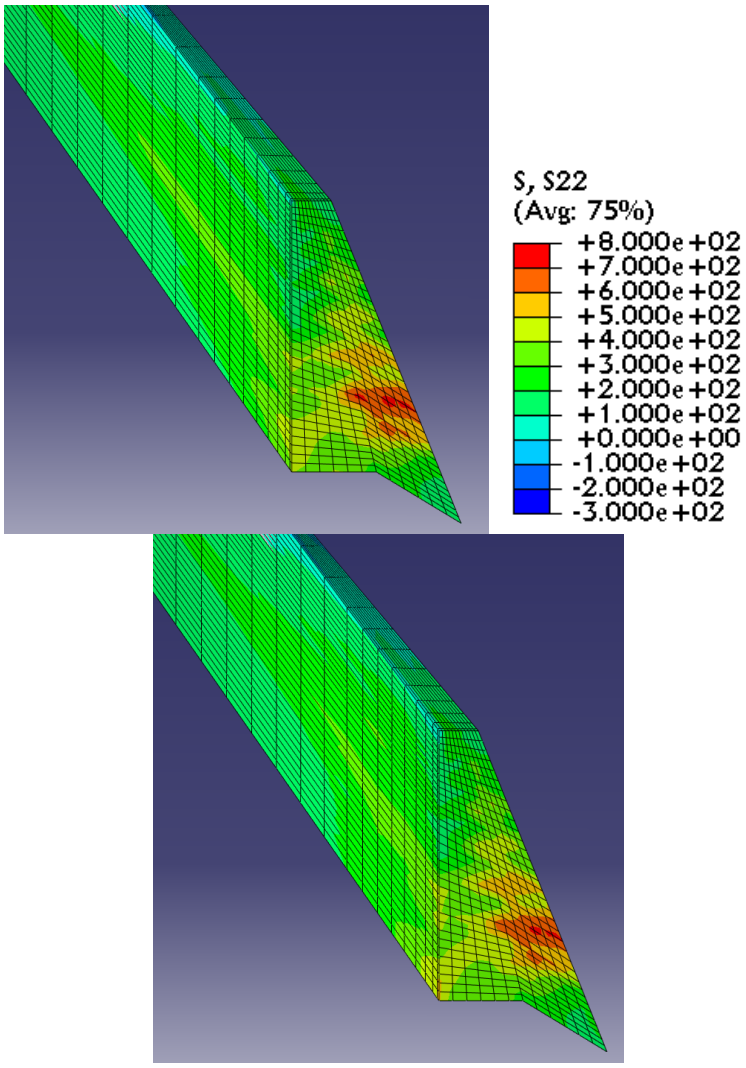

Figure 5-25 Hoop stress (MPa) (a) before adding cracks, left (b) after adding cracks, right

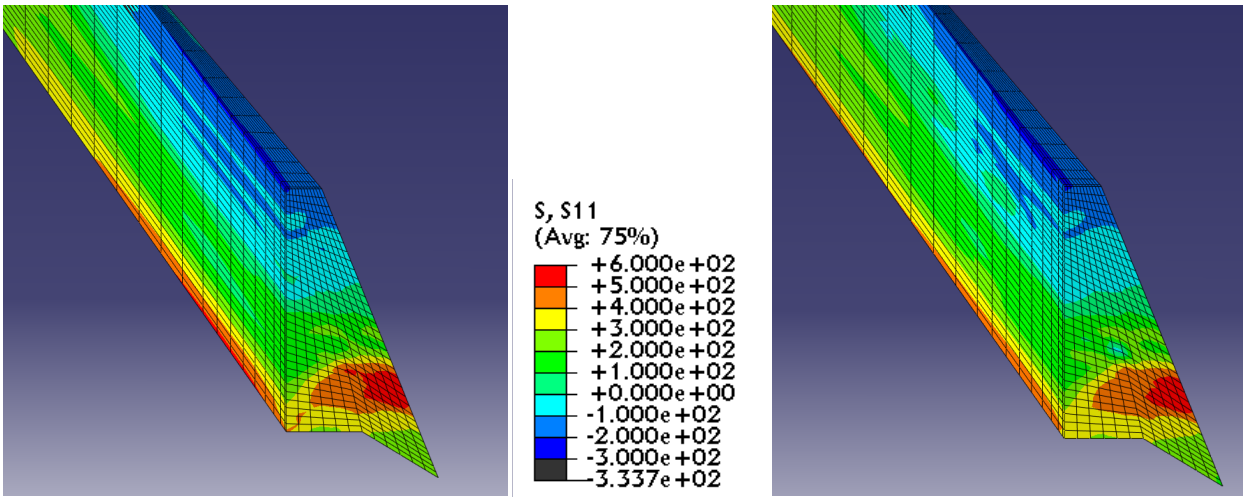

Figure 5-26 Radial stress (MPa) (a) before adding cracks, left (b) after adding cracks, right

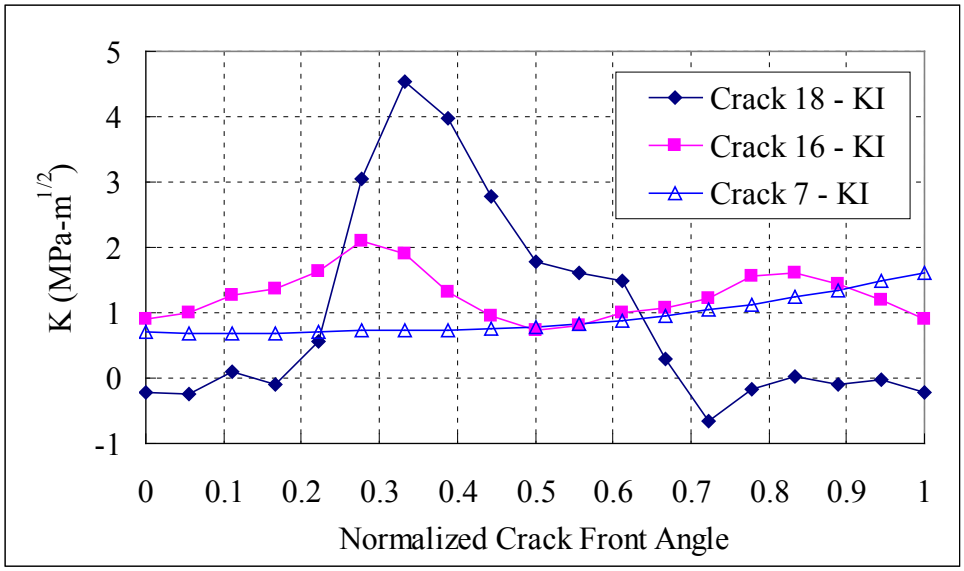

Figure 5-27 Stress intensity factor (K_I) of different cracks

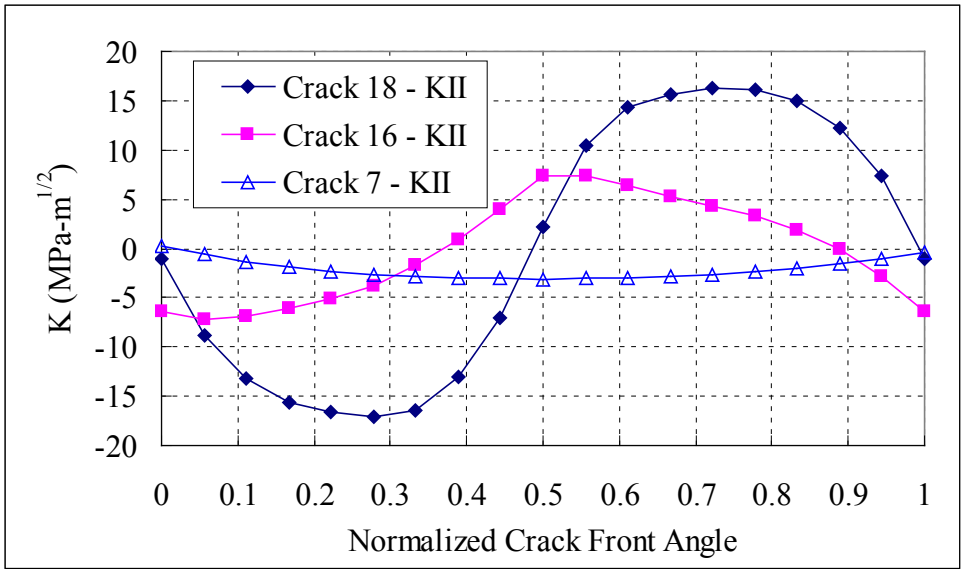

Figure 5-28 Stress intensity factor (K_{II}) of different cracks

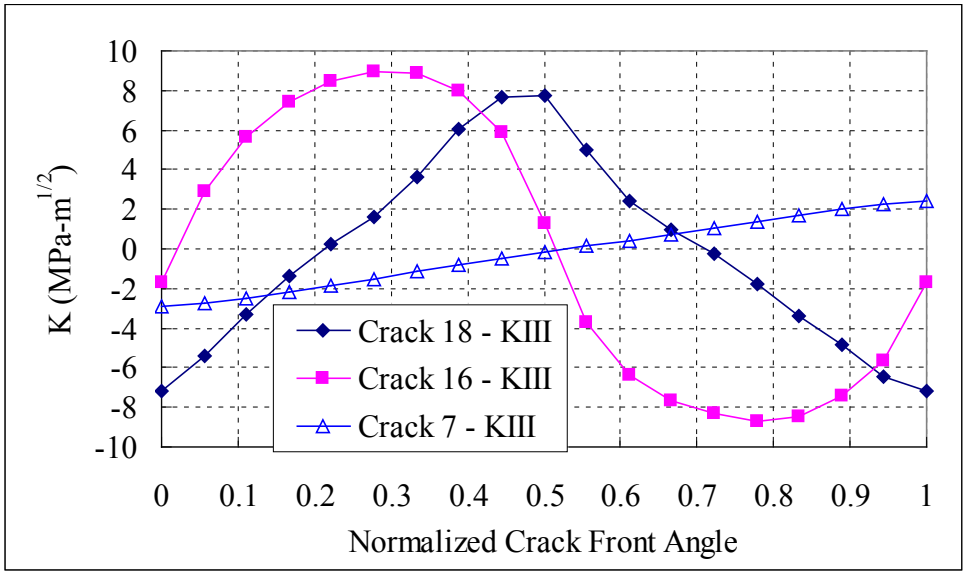

Figure 5-29 Stress intensity factor (K_{III}) of different cracks

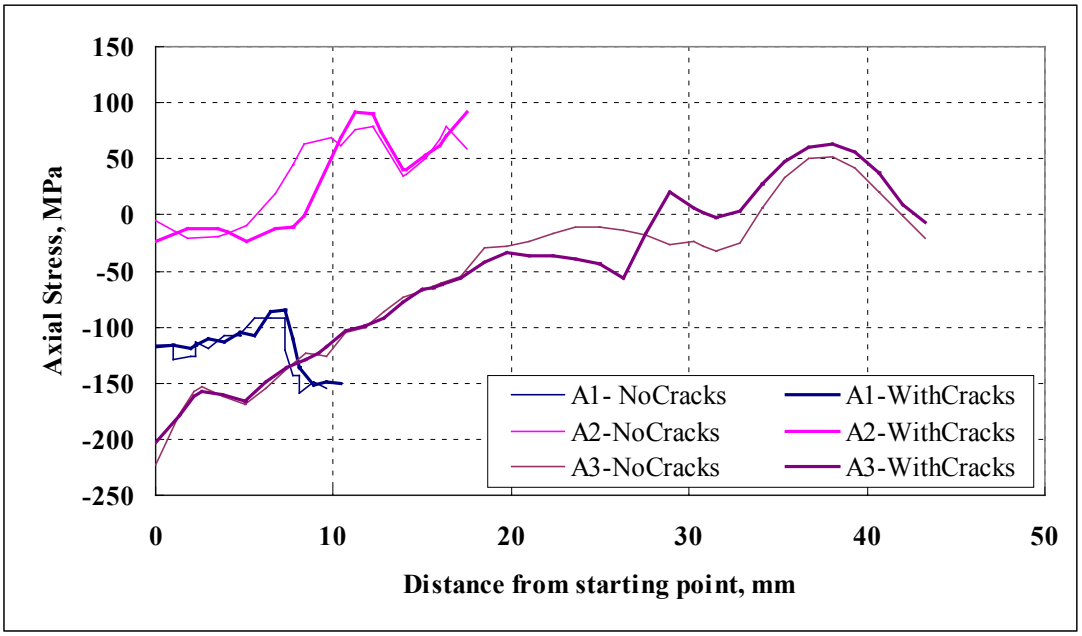

Figure 5-30 Line plots for axial stress at given paths defined in Figure 5-22

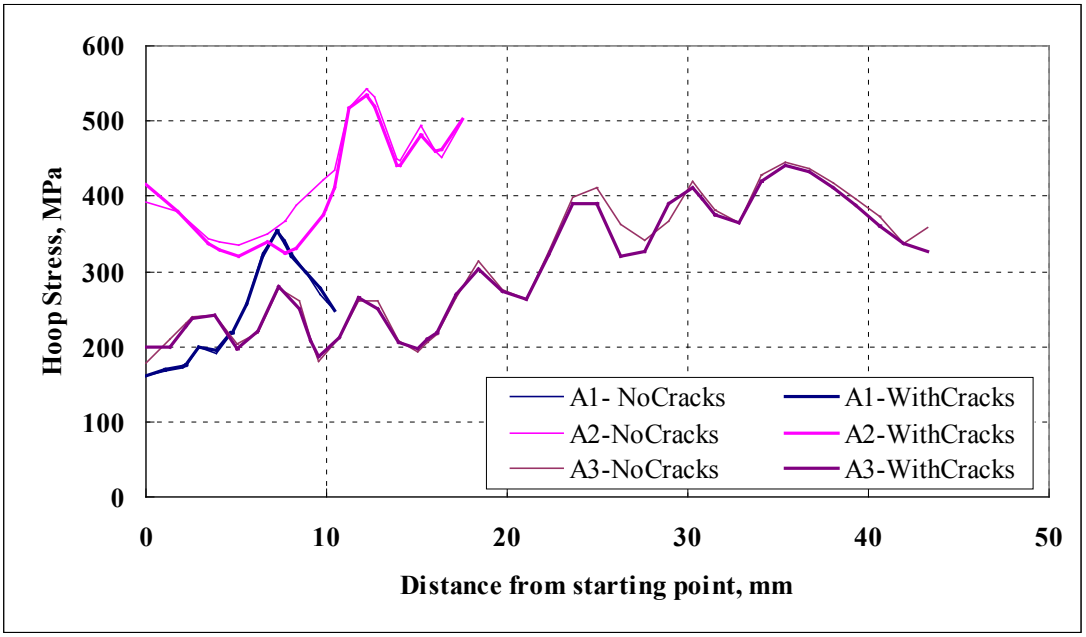

Figure 5-31 Line plots for hoop stress at given paths defined in Figure 5-22

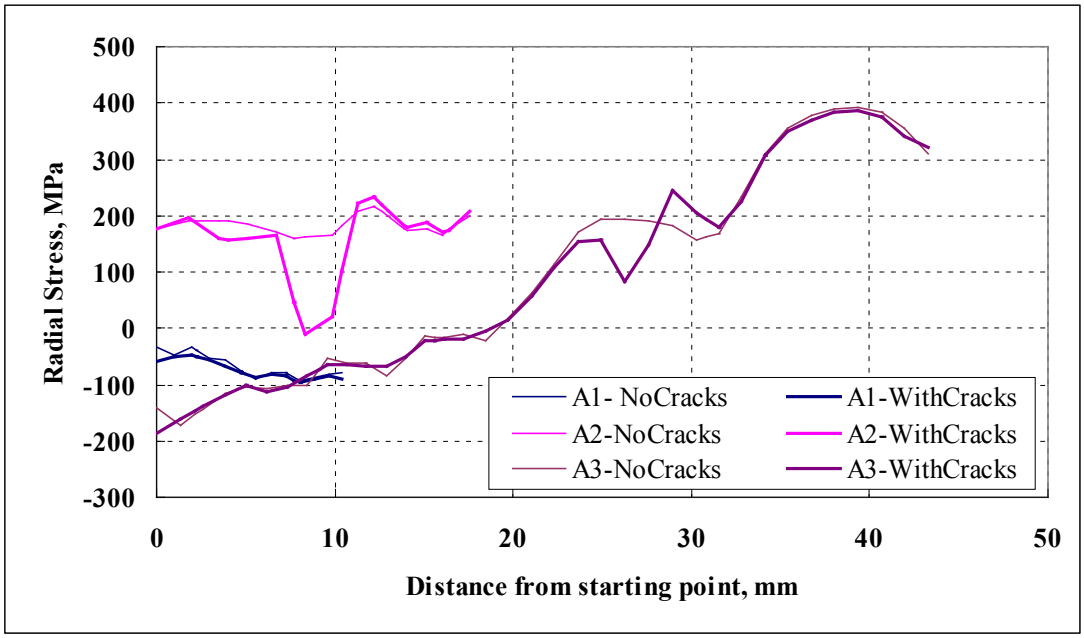

Figure 5-32 Line plots for radial stress at given paths defined in Figure 5-22

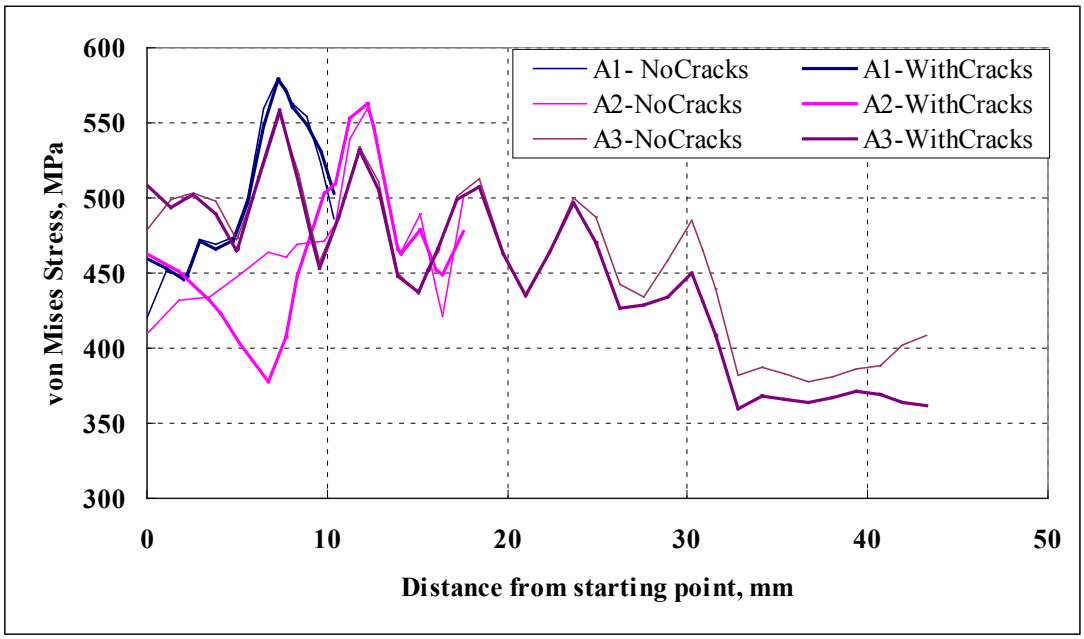

Figure 5-33 Line plots for von Mises stress at given paths defined in Figure 5-22

5.3.2 Case of Penetration 67

Here we look at another set of cracks that were measured in the same CRDM replacement head. This is a 12 crack case in the half model (24 cracks in full model). The measured crack arrangement is shown in Figure 5-34. Compared to the cracks observed in Penetration 59 (Figure 5-1) more cracks in Penetration 67 appear near the bottom of the weld where residual stresses are tensile. Because of the symmetrical nature of the FEA model, only the cracks in the range of 180 degree to 360 degree are considered, in which there are 12 cracks, i.e. Crack 11 to Crack 22, and a total of 24 total cracks in the full model. Again, the designation 'Penetration 67' is an arbitrary designation and the measured crack profile is typical for this type of side-hill penetration.

Table 3 lists all the cracks and locations. As discussed above with regard to Penetration 59, the crack locations are for different types of nozzle configurations. Most cracks of Penetration 67 are circumferential cracks except Crack 13 which is an embedded axial crack. Crack 22, Crack 15, Crack 14, Crack 13, Crack 12, and Crack 11 are embedded cracks defined from 0 to 360 degrees. Crack 16, Crack 21, Crack 20, Crack 19, Crack 18, and Crack 17 are referred to as circumferential surface cracks, defined from 0 to 180 degrees. The surface cracks start at the tube OD and project into the weld metal.

The stress components obtained from FEAM are the centroid values in every element. Figure 5-35 shows the von Mises stress contour plot with and without the addition of the cracks. Figure 5-36, Figure 5-37, and Figure 5-38 show the axial, hoop and radial stress contour plots before and after the introduction of the cracks. The stress unit in this study is MPa and the plots on the left are the results with no cracks added while plots on the right are the results with cracks added. It is seen in both Figure 5-1 and Figure 5-34 (as well as in general) that most of the cracks are distributed near the downhill side for the side-hill case. From the contours, stress redistribution was observed. Among these cracks, the stress intensity factors of Crack 21, Crack 15, Crack 13, and Crack 12 are presented because these stress intensity factors are positive, i.e., opening while the rest of the cracks experienced closing since they are in compressive weld residual stress fields. Figure 5-39, Figure 5-40, and Figure 5-41 show the K_I, K_{II} and K_{III} stress intensity factors. In terms of magnitude, mixed mode effects are as important as Mode I opening for the multiple crack case which is not surprising. However, the magnitudes are low; suggesting that even in the case where a fluid path to the cracks exists, it is unlikely that PWSCC growth will occur very fast, especially for Alloy 52/152 replacement weld material.

Line plots of axial, hoop, radial and von Mises stress are presented in Figure 5-42, Figure 5-43, Figure 5-44, and Figure 5-45, respectively. The paths are defined in Figure 5-22 (right). Overall the stress trends are similar to those before adding cracks. Cracks introduce more local fluctuations of stress in the weld region. The magnitude of local fluctuation is around 70 MPa. Hence, as for Penetration 59, for PWSCC assessment of a dominant crack (where many cracks link), a modification of the applied residual stress fields may be necessary.

Table 3 Crack distribution of Penetration 67

Crack #	Crack length (mm)	Crack depth (mm)	Type	Crack center position	
				Disp. from weld bottom (mm)	**Disp. from weld ID (mm)**
22	20.16	4.0	Circ. (embed)	12.49	4.24
21	22.07	5.4	Circ.	9.94	0
20	4.49	1.0	Circ.	22.49	0
19	11.02	2.0	Circ.	40.17	0
18	21.56	1.6	Circ.	31.13	0
17	21.56	1.6	Circ.	39.51	0
16	21.39	2.0	Circ.	12.49	0
15	9.2	2.4	Circ. (embed)	3.91	1.5
14	2.72	2.4	Circ. (embed)	4.97	11.44
13	10.21	2.0	Axial(embed)	21.55	1.70
12	3.56	2.0	Circ. (embed)	4.82	1.52
11	21.09	2.4	Circ. (embed)	30.5	2.69

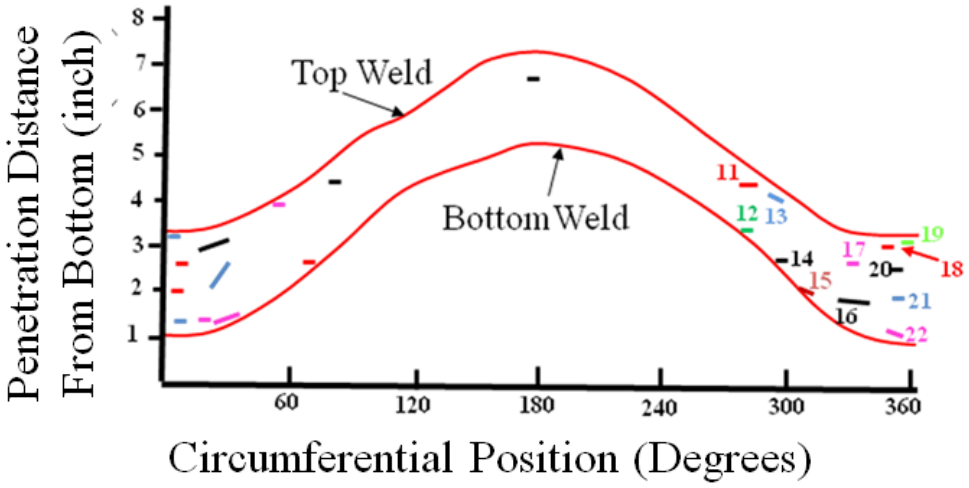

Figure 5-34 Weld profile and crack distribution of Penetration 67

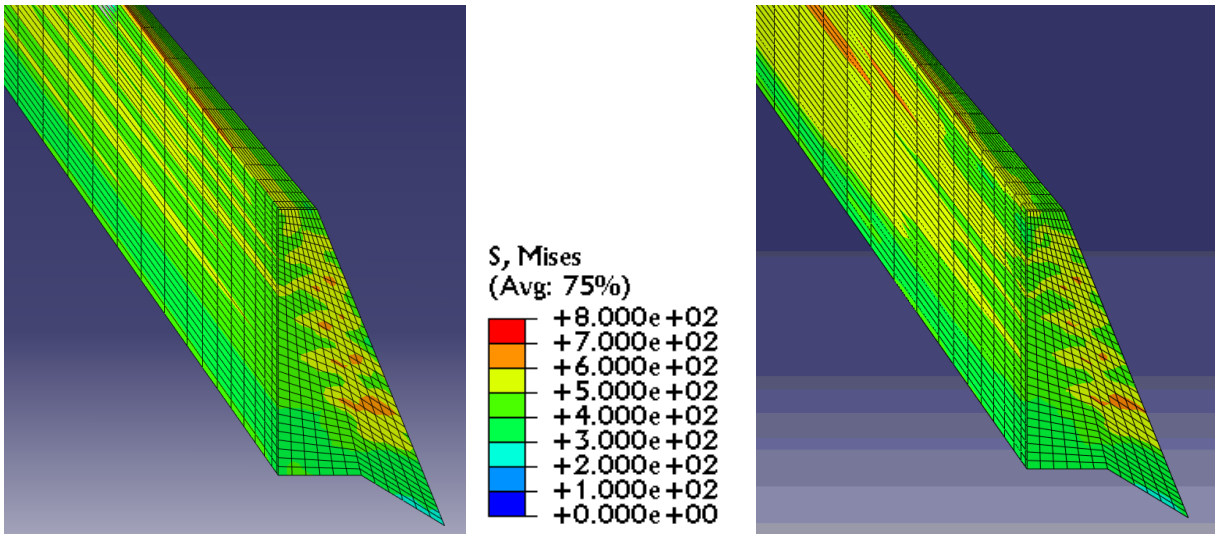

Figure 5-35 Von Mises stress (MPa) (a) before adding cracks, left (b) after adding cracks, right

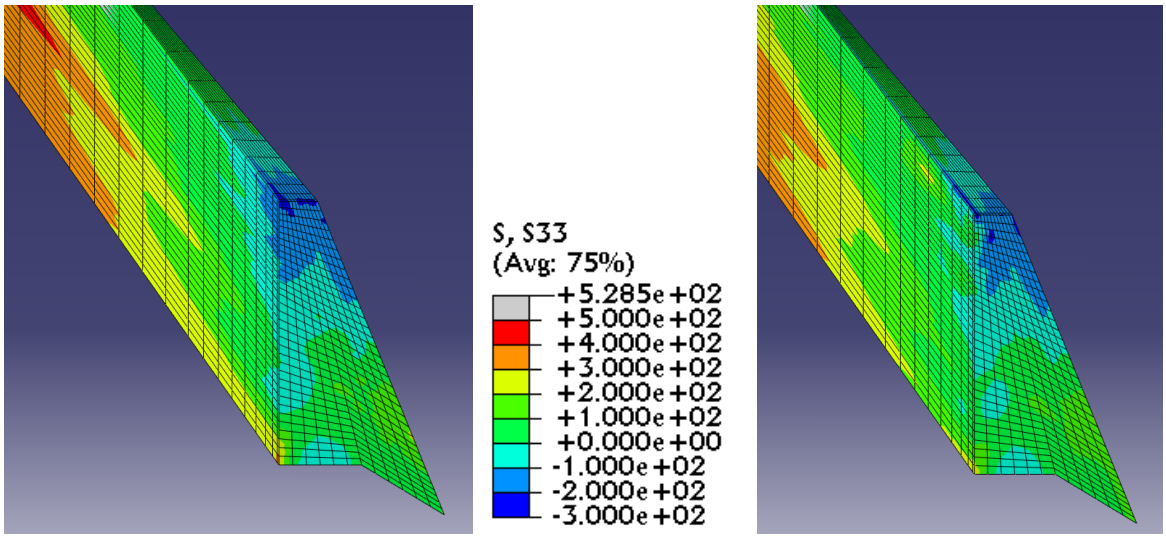

Figure 5-36 Axial stress (MPa) (a) before adding cracks, left (b) after adding cracks, right

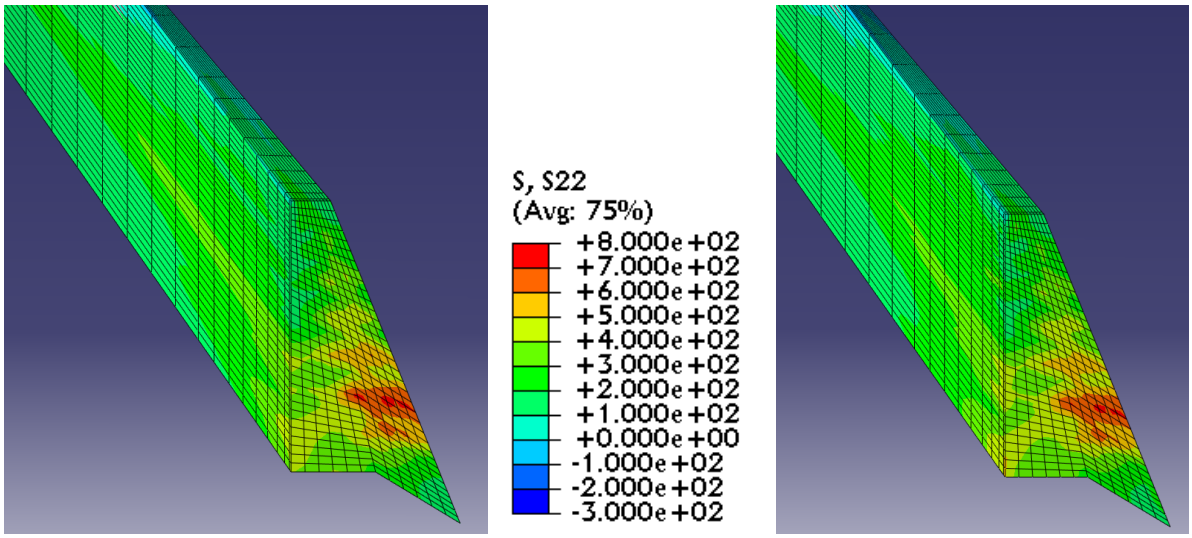

Figure 5-37 Hoop stress (MPa) (a) before adding cracks, left (b) after adding cracks, right

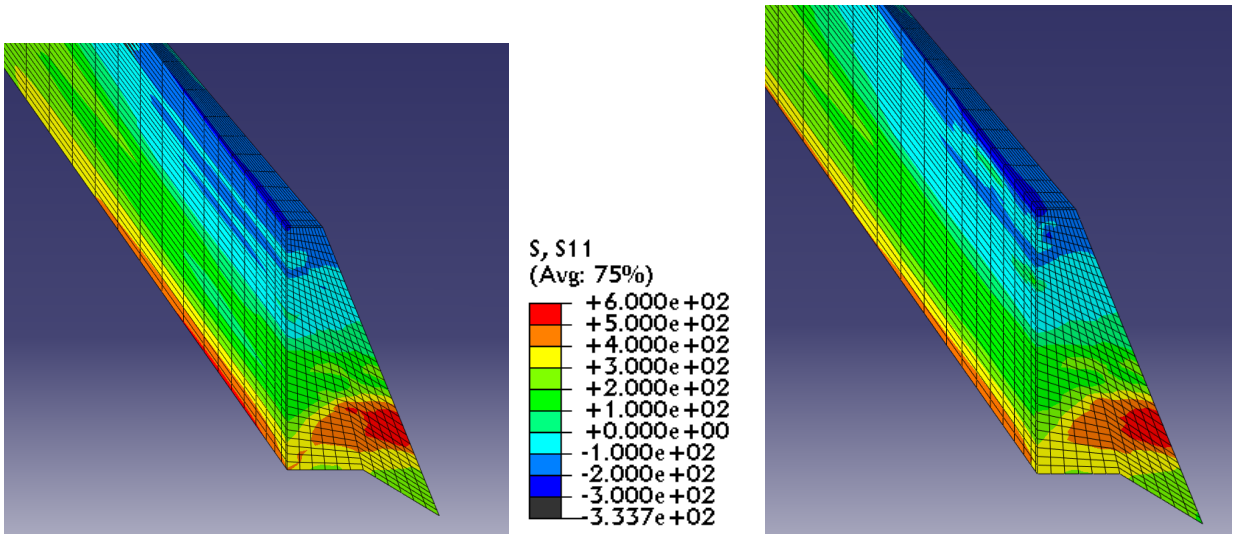

Figure 5-38 Radial stress (MPa) (a) before adding cracks, left (b) after adding cracks, right

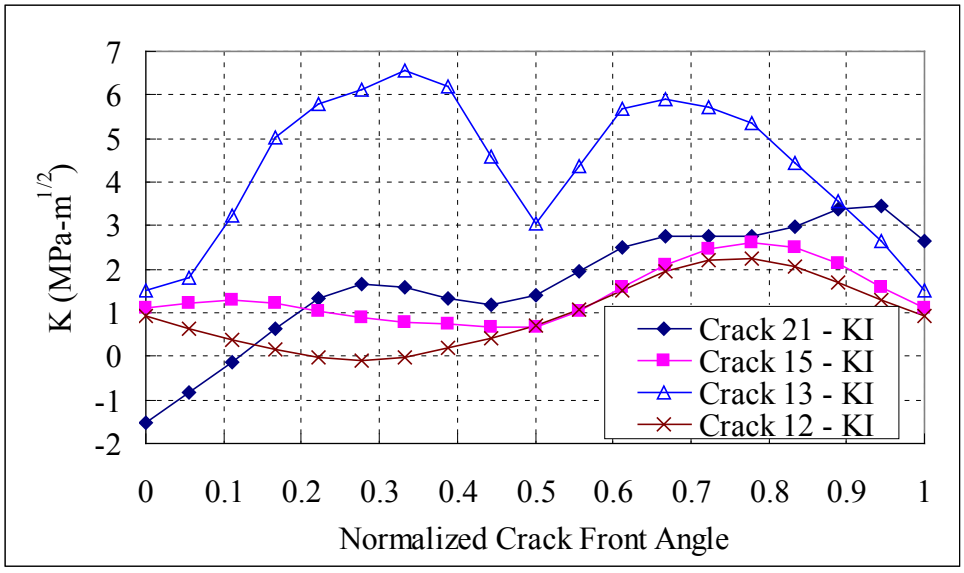

Figure 5-39 Stress intensity factor (K_I) of different cracks

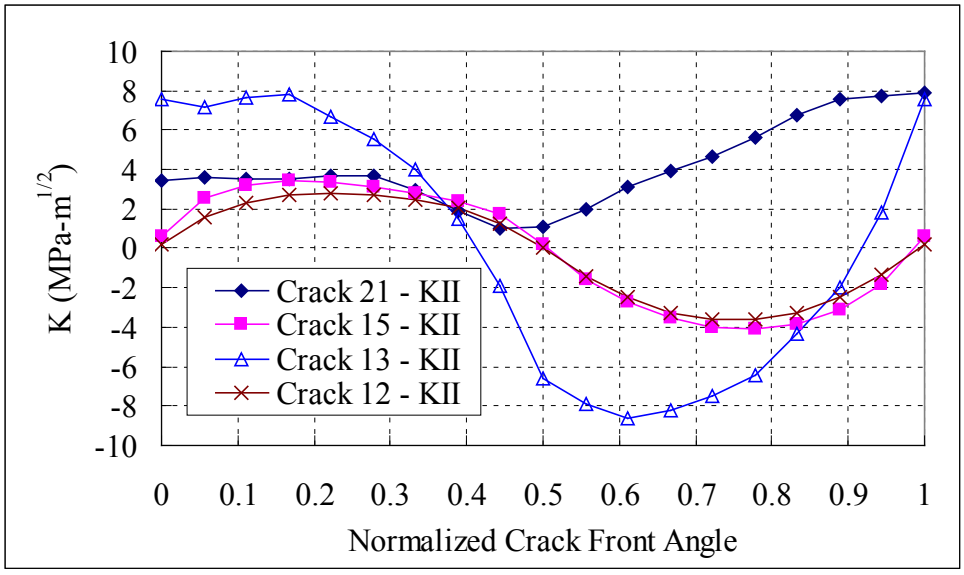

Figure 5-40 Stress intensity factor (K_{II}) of different cracks

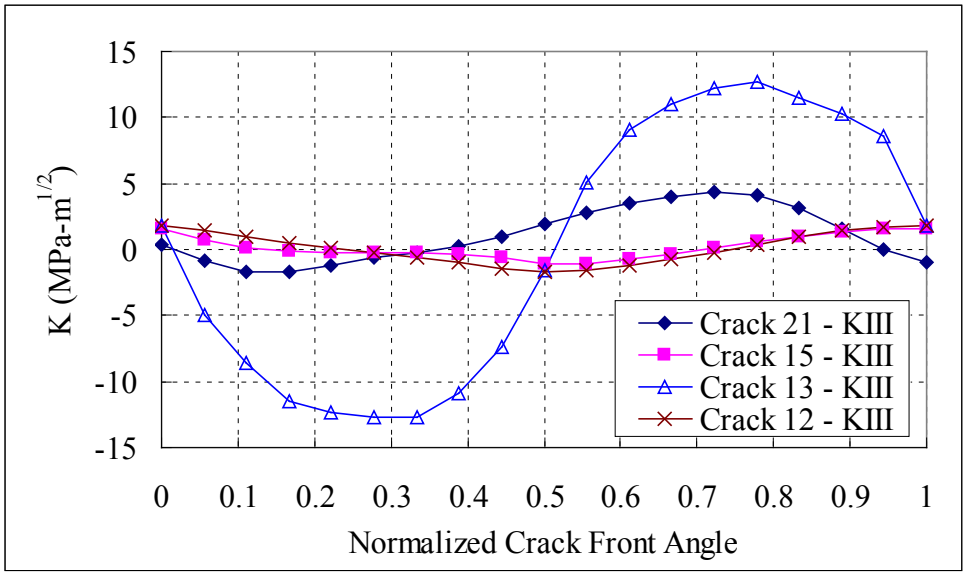

Figure 5-41 Stress intensity factor (K_{III}) of different cracks

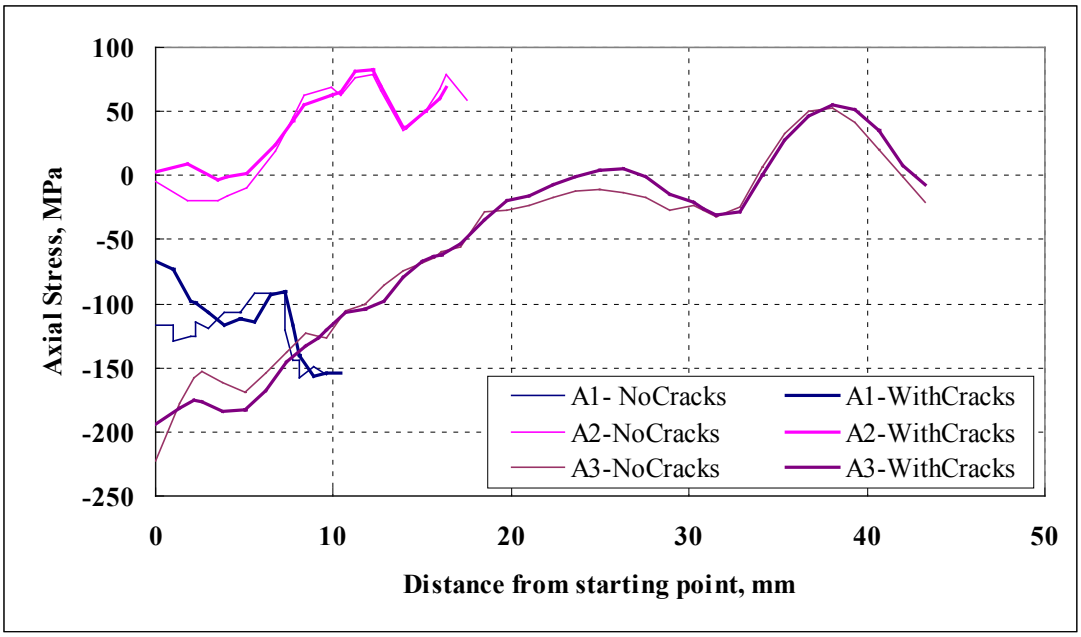

Figure 5-42 Line plots for axial stress at given paths defined in Figure 5-22

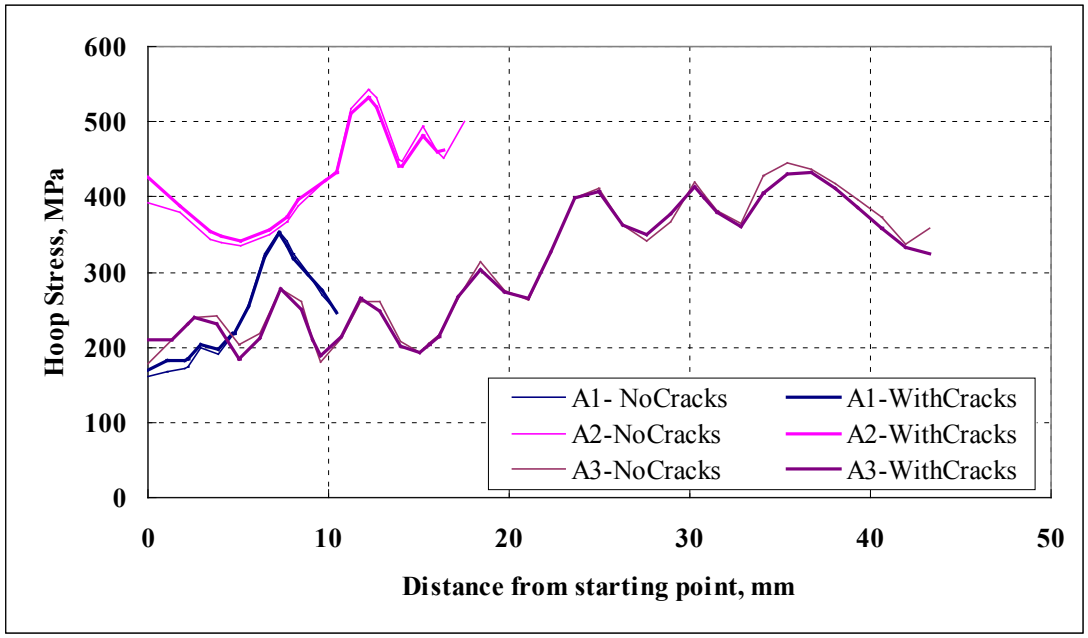

Figure 5-43 Line plots for hoop stress at given paths defined in Figure 5-22

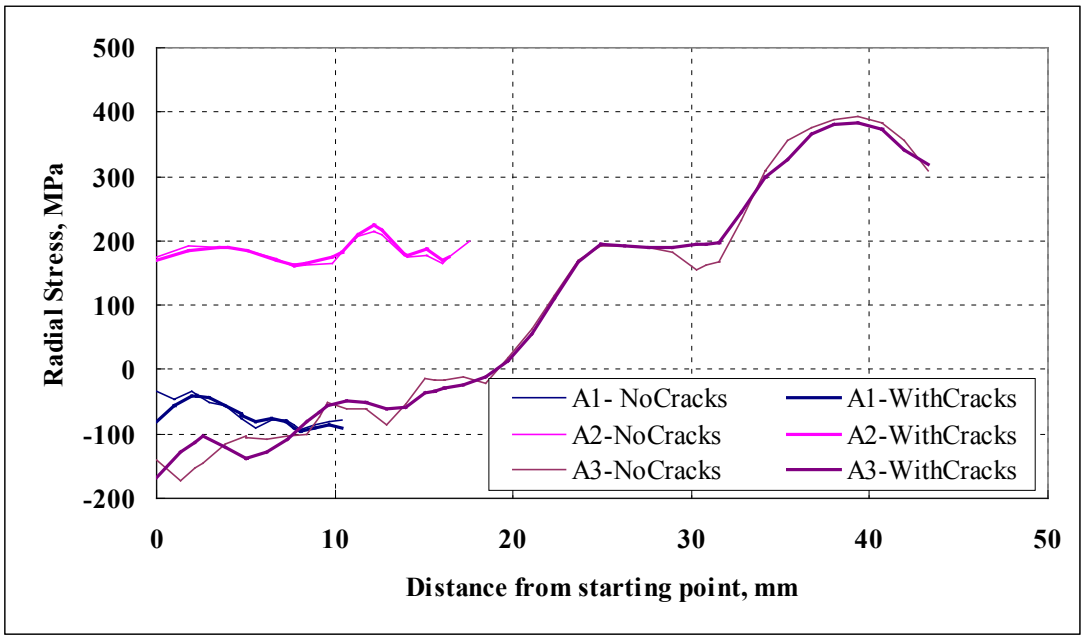

Figure 5-44 Line plots for radial stress at given paths defined in Figure 5-22

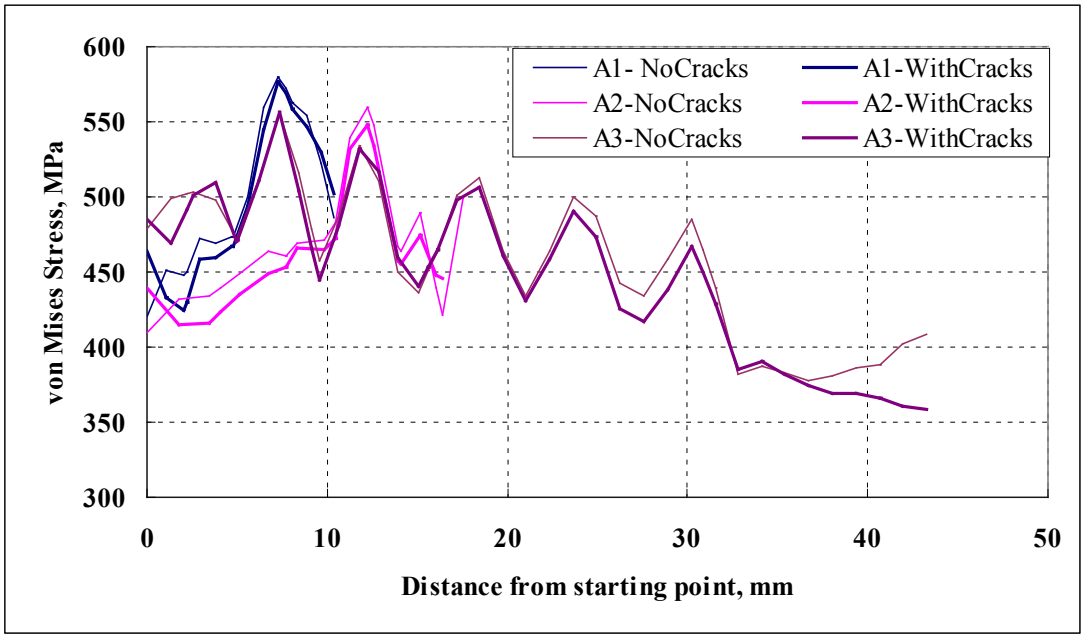

Figure 5-45 Line plots for von Mises stress at given paths defined in Figure 5-22

The residual stress magnitudes and locations for typical cracks found in the CRDM nozzles, along with service loads, are not critical. The stress intensity factors for most cracks are low. Since the replacement material is much more resistant to PWSCC growth, and there is not a likely fluid path to this weld metal, it does not appear that multiple hot cracks in replacement heads will be a problem. A limit load assessment is provided next to determine if imminent overload failure is possible.

6. Limit Load Analysis

This section provides an estimate of the overload margin for tube ejection if we assume that the fabrication indications result in reduced area of the weld, i.e. the indications are treated as removed weld material. This is a conservative assumption since the area where the indications occur is assumed to be removed. First a numerical limit load analysis is performed. Next, a simple code assessment is made to estimate margin.

6.1 Finite Element Limit Load Analysis

To complete the reactor pressure vessel head (RPVH) J-groove structural integrity analysis assessment, a limit load assessment is performed in this section. This limit load assessment considered the addition of multiple cracks in the model with up to 24 cracks being inserted. PWSCC may not be a concern in this analysis because the cracks are embedded. The mixed-mode stress-intensity factors were calculated along with the redistribution of weld residual stress caused by the multiple cracks. As discussed above, multiple fabrication induced indications,

modeled here as micro-cracks, tend to be introduced into the weld metal during deposition of Alloy 52/152 weld replacement heads. The purpose of this portion of the study is to examine the limit load of the head for a situation where many of the small cracks have linked to form a larger crack. The linking of cracks was based on conservative estimates of the measured cracking considered earlier. The cracks were not explicitly modeled. Rather elements were eliminated from the model (or voided out) and the limit analysis was performed.

Figure 6-1 is the finite element mesh of a 53-degree side-hill nozzle. Because of the symmetrical geometry, only half of the model was considered. The overall mesh is shown as Figure 6-1(a) and Figure 6-1(b) is the mesh of only the side-hill weld without the cracks. This limit load assessment considered the effect of multiple cracks in replacement and new head welds using Alloy 52/152 weld material. The cracks are introduced into the welds for these assessments by voiding-out weld the cracked region elements in the model to simulate loss of structural capacity between the weld and tube. The model has been generated by the ABAQUS element-removal technique for 53-degree side-hill nozzle. The area of removed elements was based on a conservative worst case conglomerate of indications found in the inspected nozzles. It was assumed that at locations of the indications that there the entire weld was missing at these regions. A similar region of removal was assumed in a proprietary industry report for worse case assessment.

There are two void-out regions in the chosen model; one is a 75-degree region and the other a 45-degree section. The voided regions were assumed to be the entire depth of the weld. The three-dimensional view is shown in Figure 6-2(a) and top view is described as Figure 6-2(b). The normal operating temperature is 591 K (318 C) and the design pressure inside the pressure vessel head is 17 MPa (2.5 ksi). The purpose of this effort is to examine the limit load with the operating temperature of 318 C with the void-out element region modeled. A series of limit analyses were carried out, i.e., Riks analysis in ABAQUS. With the voided-out elements shown in Figure 6-2, the limit load was obtained as 3.86 times the operating pressure, i.e., 66.5 MPa or 9.6 ksi. At limit status, the von Mises contour plot was shown in Figure 6-3. It is observed that there are stress concentration areas near the voided-out elements as expected. A separate analysis was performed based on constraint-based strain failure criteria, and produced results similar to the Riks analysis indicating that the Riks-based limit analysis is accurate.

Another analysis was performed with full weld included, i.e., without the cracking present and without element removal. The limit load was obtained as 5.32 times operating pressure, 91.7 MPa (13.3 ksi). It is seen that the high stress region is at the top part of the weld and is relatively uniformly distributed (Figure 6-4). The last sensitivity case involved removing a smaller portion of the weld. Figure 6-5 shows the mesh, which is about half of previous voided region. In this case, the limit load was obtained as 5.25 times the operating pressure, 90.5 MPa (13.1 ksi). The stress contour is shown in Figure 6-6 and the limit load is very similar to the case without element removal, but stress redistribution was still observed. Because of element removal, a high stress region in the middle of the weld exists between the void-out regions.

Limit-load analysis was studied for the 53-degree side-hill nozzle. By using void-out elements in a limit load assessment, the maximum limit load was decreased and stress was re-distributed. From maximum limit load point of view, the smaller void-out region has little influence. But the

stress redistribution and stress concentration region were observed. It is seen that significant margin exists even for a rather large region of damage in the head. This suggests that the replacement heads are quite safe and that tube ejection has very low probability.

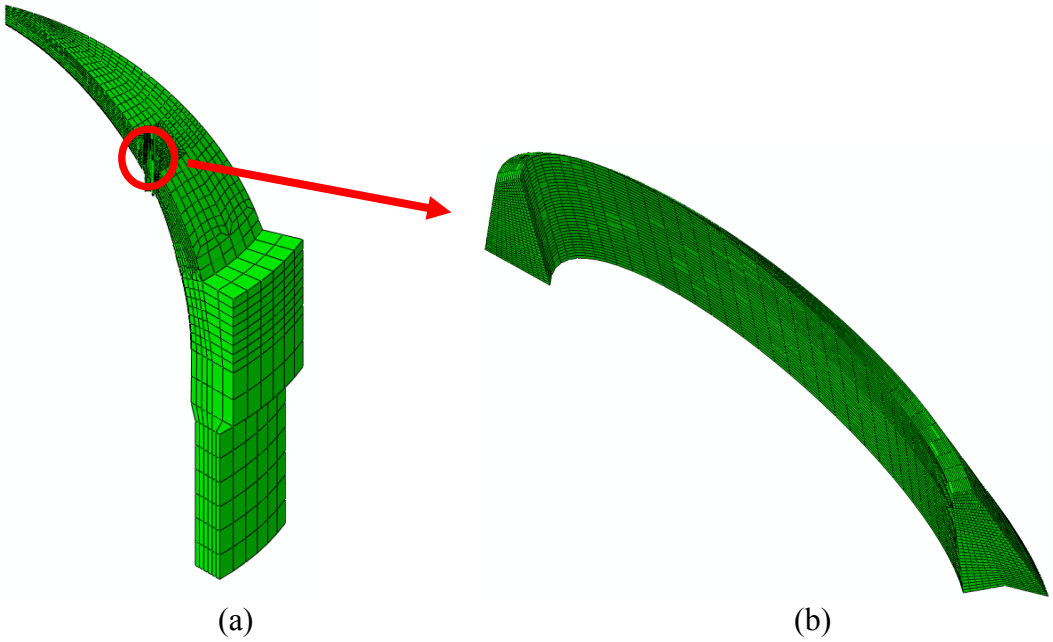

Figure 6-1 FEA model of a 53-degree side-hill nozzle (a) and weld (b)

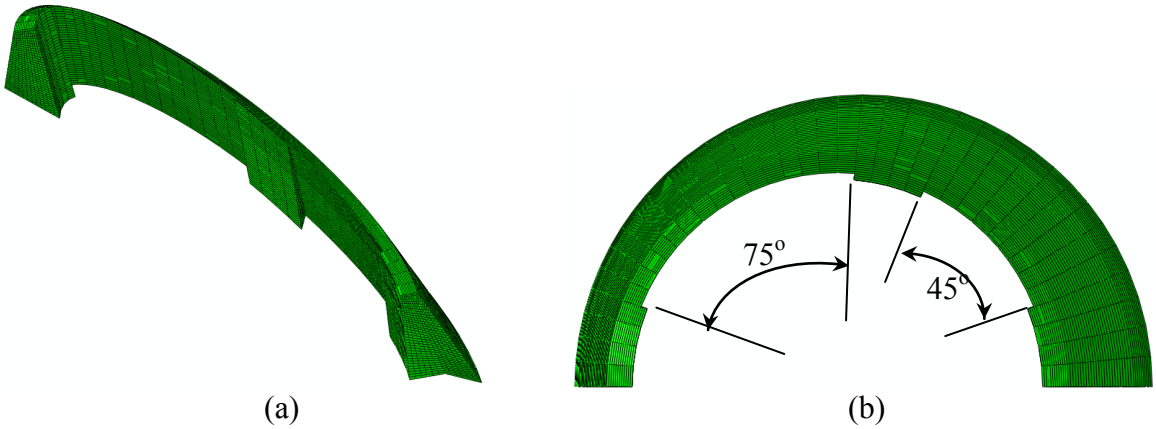

Figure 6-2 Weld mesh with void-out region (a) and top view (b)

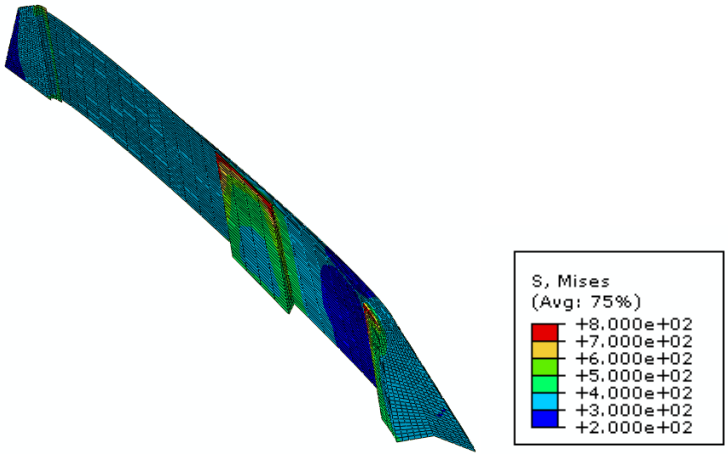

Figure 6-3 Von Mises stress (MPa) contour plot with voided-out elements

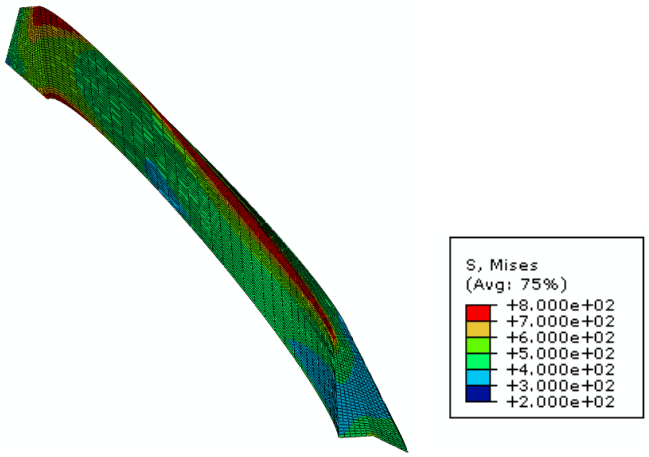

Figure 6-4 Von Mises stress (MPa) contour plot with all elements present

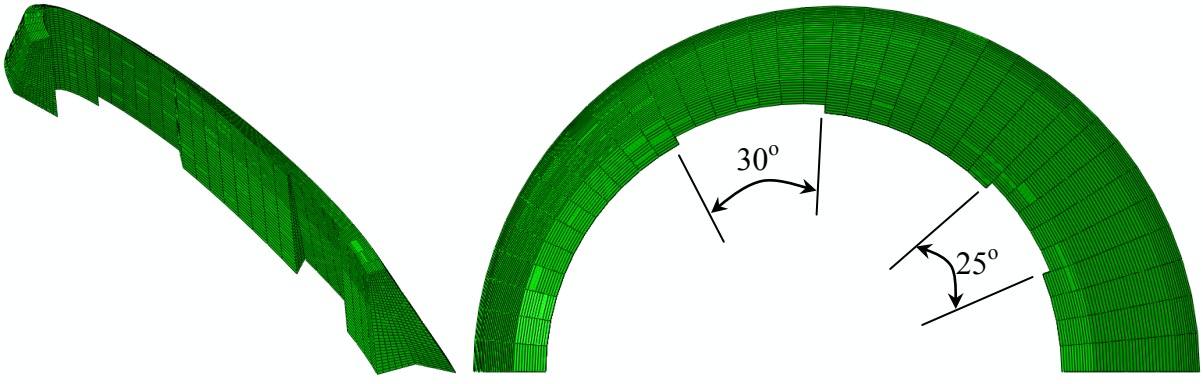

Figure 6-5 Weld mesh with small void-out region (a) and top view (b)

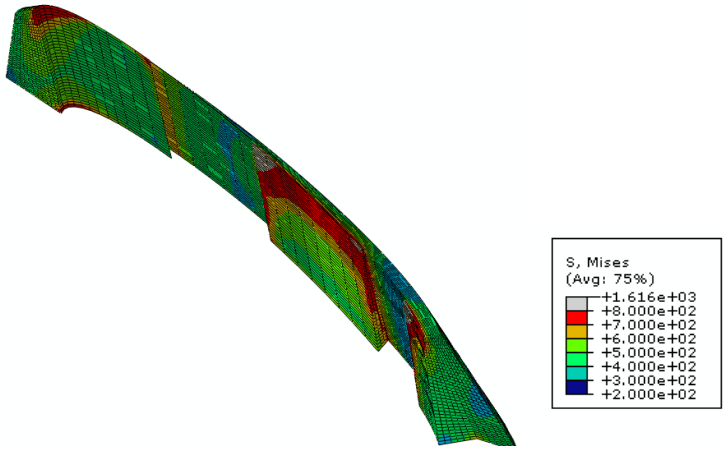

Figure 6-6 Von Mises stress (MPa) contour plot after small region of voided-out elements

6.2 Simplified Code Assessment

To complete this section we perform a simple code assessment to determine margins in order to complement the limit load calculations made above. For Alloy 690, the allowable stress (S_m) at the operating temperature of 318 C is 160.6 MPa (from ASME BPV Section II). To prevent tube ejection, the shear stress must satisfy the allowable Section II stress of $0.6S_m$, or 96.4 MPa. The remaining area of weld, after removing the area shown in Figure 6-2 (and neglecting the spiral nature of the weld/tube interface for the 53-degree nozzle) is 3660 mm^2. The shear stress in the remaining weld material from end cap loads on the tube (and operating pressure of 17 Mpa) is 20 MPa, which leads to a margin of 4.78 on allowable stress. Even with the very conservative assumption of material loss made here the tube satisfies ASME BPV section II stress allowable.

7. Summary and Conclusions

Welding residual stress analyses were conducted for Alloy 52/152 and comparison was made with Alloy 82/182. Alloy 82/182 was the material used in the original dissimilar metal welds for these heads. Results for both center-hole and side-hill nozzles show slight differences between Alloy 52/152 and Alloy 82/182. The second section discusses the assessment of flaws in the reactor pressure vessel head penetration nozzles. In common flaw analysis, representations of physical cracks need to be placed into the system model, which could result in prohibitive computational expense. In this report, finite element alternating method (FEAM) was used for calculating stress intensity factors for cases where multiple cracks exist. More than twenty cracks, which were all from practical measurements, are modeled in the analyses for both center-hole and side-hill nozzles. The stress intensity factors are in the range where PWSCC is possible in the Alloy 52/152, although at a low rate compared with Alloy 82/182 weld metal. It is observed that the overall stress trends are similar to the ones without adding cracks. However, cracks introduce more local fluctuations around indications. The magnitude of the local fluctuation could be around 100 MPa. Limit analysis was also conducted and resulted in a large

margin, even when conservatively considering the micro-cracks to be linked. Overall, it was found that replacement heads are resistant to CRDM ejection even if micro-cracks are introduced from the Alloy 52/152 weld metal deposition process.

A summary of the conclusions reached is presented below.

- Alloy 52/152 stress-strain properties are very close to Alloy 82/182 tensile properties at all temperatures except at room temperature where Alloy 52/152 was about 15% higher.
- Weld analyses performed here were made prior to obtaining the Alloy 52/152 tensile test data. Based on some data obtained from Specialty Metals, Inc., it was assumed that the Alloy 52/152 stresses were 20% higher than Alloy 82/182 for these analyses. With the higher tensile properties for Alloy 52/152, the weld residual stresses in the replacement heads were higher than the corresponding values using Alloy 82/182. However, this increase was not significant. Using the higher tensile properties, the crack analyses were conservative.
- The WRS analyses were performed on both center-hole and 53-degree side-hill penetrations. The center-hole case is less severe than the 53-degree side-hill case in terms of the magnitude of the weld residual stresses, the stress intensity factors calculated when introducing multiple cracks, and the WRS redistributions caused by the crack introductions.
- The stress intensity factors for the nozzles with different multiple cracks introduced were in the range where, if a fluid path existed to these cracks, it is possible that some PWSCC could occur. However, since the K-values are not large and Alloy 52/152 is more resistant to PWSCC compared with Alloy 82/182, crack growth is not anticipated to be significant.
- The introduction of multiple cracks does redistribute the WRS somewhat. However, this redistribution is not significant.
- A limit analysis of the RPVH assuming linkage of the cracks for a particular penetration showed a large margin on operating pressure of about 4.
- A simple, conservative estimate of the ASME stress allowable considering two thirds of the weld material removed results in compliance with Section II allowable stress.

8. References

1 1994 EPRI Workshop PWSCC of Alloy 600 in PWR's, Nov 15-17, 1994, Tampa, FL.

2 Rudland, D., and Wilkowski, G., "Development of Axial Surface Crack K-Solutions for Control Rod Drive Mechanism," Final report to U.S. NRC, January 16, 2004.

3 D. Rudland, G. Wilkowski Y.-Y. Wang, and W. Norris, "Analysis of Circumferential Through-Wall Crack K-solutions for CRDM Nozzles," *International Journal of Pressure Vessels and Piping*, 81 (2004) pp. 961-971.

4 Feng, Z., Wilkowski, G., Rudland, D., Wang, Y.-Y., and Wolterman, R., "Analysis of CRDM Nozzle-to-Vessel Weld Stresses," report by Engineering Mechanics Corporation of Columbus, March 5, 2003, for U.S. NRC, Office of Regulatory Research.

5 *Materials Reliability Program Probabilistic Fracture Mechanics Analysis of PWR Reactor Pressure Vessel Top Head Nozzle Cracking (MRP-105)*, EPRI, Palo Alto, CA: 2004,1007834.

6 S.N. Atluri, "Computational Methods in the Mechanics of Fracture", Amster-Adam: North Holland, also translated in Russian, Mir Publishers, Moscow.

7 Brust, F. W., Kim, D. S., "Mitigating Welding Residual Stress and Distortion", Chapter 8, in Processes and Mechanisms of Welding Residual Stress And Distortion, Ed. Z. Feng, Woodhead Publishing Limited, Cambridge, UK, 2005.
8 Chen, L., Zhang, Z., and Brust, F. W.., "Modeling Distortion and Residual Stress During Welding: Practical Applications", Chapter 7, in Processes and Mechanisms of Welding Residual Stress And Distortion, Ed. Z. Feng, Woodhead Publishing Limited, Cambridge, UK, 2005.
9 Y.-Y. Wang, Z. Feng, W. Cheng, and S. Liu, "Residual Stress Effects on Crack Driving Force in Multipass Welds," *Pressure Vessel and Piping (PVP) Conference*, San Diego, CA, July, 1998.
10 C. L. Tsai, S. C. Park, and W. Cheng, "Welding Distortion of a Thin-Plate Panel Structure," *Welding Journal*, Vol. 78 No. 5, May 1999, pp. 156s-165s.
11 Z. Feng, X. Wang, C. R. Hubbard, and S. Spooner, "A FE Model For Residual Stresses In Repair Welds," *Residual Stresses in Design, Fabrication, Assessment and Repair*, ASME PVP-Vol. 327, 119-125, 1996.
12 H.D. Hibbitt and P.V. Marcal, "A Numerical, Thermo-Mechanical Model for the Welding and Subsequent Loading of a Fabricated Structure, "*Computers & Structures*, Vol. 3, 1145-1174, 1973.
13 J. Goldak, A. Chakravarti, and M. Bibby, "A New Finite Element Model for Welding Heat Sources," *Metall. Trans.,* Vol. 15B, 299-305, 1984.
14 Engineering Mechanics Corporation of Columbus, Technical Progress Monthly Report to US NRC, Phase II – Alloy 600 Cracking, June, 2006.
15 T. Zhang, G. Wilkowski, D. Rudland, F. Brust, H. S. Mehta and D. V. Sommerville, Weld-Overlay Analyses – An Investigation of the Effect of Weld Sequencing, 2008 ASME Pressure Vessels and Piping Division Conference, July 27-31, 2008, Chicago, IL, USA.
16 D. Rudland, Y.Chen, T. Zhang, G. Wilkowski, J. Broussard and G. White, Comparison of Welding Residual Stress Solutions for Control Rod Drive Mechanism Nozzles, 2007 ASME Pressure Vessels and Piping Division Conference, July 22-26, 2007, San Antonio, TX, USA.
17 D. Rudland, T. Zhang, G. Wilkowski, and A. Csontos, Welding Residual Stress Solutions for Dissimilar Metal Surge Line Nozzles Welds, 2008 ASME Pressure Vessels and Piping Division Conference, July 27-31, 2008, Chicago, IL, USA.
18 ABAQUS 6.8-1, Dassault Simulia, 2008.
19 Y. Chen, D. Rudland, and G. Wilkowski, "Impact of Welding Sequence on the CRDM Nozzle-to-Vessel Weld Stress Analysis," Proceedings of ASME-PVP 2004: ASME/JSME Pressure Vessels And Piping Conference, Hyatt Regency, La Jolla at Aventine, San Diego, California, July 25 – 29, 2004.
20 Wang, L, F. Brust and S. Atluri, "The Elastic-Plastic Finite Element Alternating Method and the Prediction of Fracture Under WFD Conditions in Aircraft Structures – Part I Theory", *Computational Mechanics*, Vol. 19, No. 5, pp 356-369, 1997.
21 Wang, L., Brust, F. W., and Atluri (1995c), "Elastic-Plastic Finite Element Alternating Method and Prediction of Fracture, Part II: Fracture and The T*-Integral" *Computational Mechanics*, Vol. 19, No. 5, pp 370-379, 1997.
22 Wang, L., Brust, F. W. and Atluri, S. N., "The Elastic-plastic Finite Element Alternating Method (EPFEAM) and the Prediction of Fracture Under WFD Conditions in Aircraft

structures. Part III: Computational predictions of the NIST multiple site damage Experimental Results", *Computational Mechanics*, vol. 20, no. 3, pp. 199-212, 1997.
23 Schwarz, H. A., "Gesammelte Mathematische Abhandlungen", Vol. 2, pp. 133-143, circa 1865.
24 Neumann, C., "Zur Theorie des Logarithmischen and Newtonschen Potentials", Leipziger Berichte, vol. 22, pp. 264-321, 1870.
25 Nishioka, T. And Atluri, S. N., "Analytical Solutions for Embedded Elliptical Cracks, and Finite Element Alternating Method for Elliptical Surface Cracks, Subjected to Arbitrary Loadings,☐ Engineering Fracture Mechanics, Vol. 17, No. 3, pp. 247-268, 1983.
26 Nishioka, T. And Atluri, S. N., "Analysis of Surface Flaw in Pressure Vessels by a new 3 Dimensional Alternating Method", Journal of Pressure Vessel Technology, Vol. 104, pp. 299-307, November 1982.
27 Shah, R. C., and Kobayashi, A. S., "Stress Intensity Factor for an Elliptical Crack Under Arbitrary Normal Loading", Engineering Fracture Mechanics, Vol. 3, pp. 71-96, 1971.
28 Vijayakumar, K., and Atluri, S. N., "An Embedded Elliptical Crack, in an Infinite Solid, Subject to Arbitrary Crack-Face Traction's", Journal of Applied Mechanics, Vol. 103, No. 1, pp. 88-96, 1981
29 Kantorovich, L.V. and Krylov, V.I, Approximate Methods of Higher Analysis**,** P. Noordhoff, Ltd., Groningen, Netherlands, 1964.
30 User Manual of ALT3D, Engineering Mechanics Corporation, 2009.